UNIVERSITY of OULU

OULUN YLIOPISTO

The Mustajärvi orogenic gold occurrence, Central Lapland Greenstone Belt, northern Finland

Matthias Müller

Master's Thesis

Oulu Mining School

University of Oulu

2019

UNIVERSITY of OULU

Oulu Mining School

Major subject: Economic Geology

Maturity test for M.Sc.

(**Appendix for M.Sc. thesis**)

Author (surname, forename)

Mueller Matthias

Thesis's number of pages:

97 + 9

Title

The Mustajärvi orogenic gold occurrence, Central Lapland Greenstone Belt, northern Finland

Keywords: Gold, Orogenic Gold, Paleoproterozoic, Mustajärvi, Central Lapland Greenstone Belt, CLGB

Summary

The thesis gives the first description of the geological setting, alteration, mineralization style and structural control of the Mustajärvi gold occurrence in the Central Lapland Greenstone Belt, northern Finland. The applied methods mainly comprise drill core logging, bedrock mapping, thin section studies and microprobe analysis.

The Mustajärvi gold occurrence lies at the southern border of the Central Lapland Greenstone Belt, in proximity to the first-order transcrustal Venejoki thrust system. The occurrence is structurally controlled by the second-order Mustajärvi shear zone, which is located at the contact between Sodankylä Group siliciclastic metasediments and Savukoski Group mafic and ultramafic metavolcanic rocks. The outcropping gold-mineralized veins comprise a set of parallel quartz-tourmaline-pyrite veins that show typical pinch and swell features, with the vein widths ranging approx. from 0.15 to 1 m. At a depth of 90 m, a different mineralization style was recently discovered, comprising a 2-m-thick, quartz-poor, massive pyrite-mineralized zone grading 45.1 ppm Au. The geochemistry of both mineralization styles is typical for orogenic gold deposits, with strongly enriched elements comprising Au, B, Bi, C (CO_2), Te, and Se. Silver, As, Sb, and W are moderately elevated and positively correlate with gold. Atypical for orogenic gold deposits is the strong enrichment of Ni and Co. In unweathered rock, gold is hosted by Au- and Au-Bi-telluride micro-inclusions in pyrite, whereas strong weathering near the surface has caused a remobilization of gold, resulting in free gold, deposited mainly in the cracks of oxidized pyrite.

The thesis emphasizes the prospectivity for a more extensive gold mineralized system, especially at greater depths and encourages further exploration. Future research on the Mustajärvi occurrence could comprise mineralogical studies on the massive pyrite mineralization at depth, and age dating of the mineralization based on observed monazite within the mineralized veins.

Date: **14/04/2019** **Student's signature:** **M. Müller**

Table of Contents

Appendices

1. INTRODUCTION

The Paleoproterozoic Central Lapland Greenstone Belt (CLGB) has a total reported gold endowment of just over 10 Moz, but with most of this resource solely defined in the giant Suurikuusikko deposit and dozens of other prospective occurrences lacking detailed exploration.

One potentially promising target, the Mustajärvi orogenic gold occurrence, lies close to the southern border of the CLGB, in proximity to the first order Venejoki thrust zone. Exploration wise, the Venejoki thrust system has mostly been ignored, despite the fact that, regarding the time and direction of deformation, it shares many features with the nearby Sirkka thrust zone which is associated with the majority of the known gold occurrences in the Central Lapland Greenstone Belt. The Venejoki thrust zone can be traced to reach the mantle at a depth of approx. 42 km (Patison et al. 2006; Niiranen et al. 2014). Not many gold occurrences are known from the Venejoki thrust system, probably due to limited exploration activities and a generally poorer bedrock exposure. With this study, Mustajärvi is one of the few, if not the first, extensively studied gold occurrence along the Venejoki thrust system.

This thesis gives the first overview of the geological setting, alteration, style of mineralization and structural control of the Mustajärvi occurrence and furthermore emphasizes the prospectivity for a more extensive gold mineralized system, especially at greater depths. Some of the presented characteristics of the Mustajärvi mineralization are atypical for gold occurrences in the CLGB and for orogenic gold systems in general. These features might represent a distinct mineralization style, characteristic for gold occurrences along the Venejoki thrust zone.

2. GEOLOGICAL SETTING

2.1 Regional geology of the Central Lapland Greenstone Belt

The Fennoscandian Shield forms the northwestern part of the East European craton and comprises most of Finland, Sweden, Russian Karelia and the Kola Peninsula (Fig. 1) (Eilu & Niiranen, 2013). In the northern part of the Fennoscandian Shield, the Archean basement is covered by a belt of Paleoproterozoic supracrustal rocks, extending from northern Norway through Finnish Lapland into Russia. The Finnish part of this belt is called the Central Lapland Greenstone Belt (CLGB) (Hanski & Huhma, 2005) (Fig. 3).

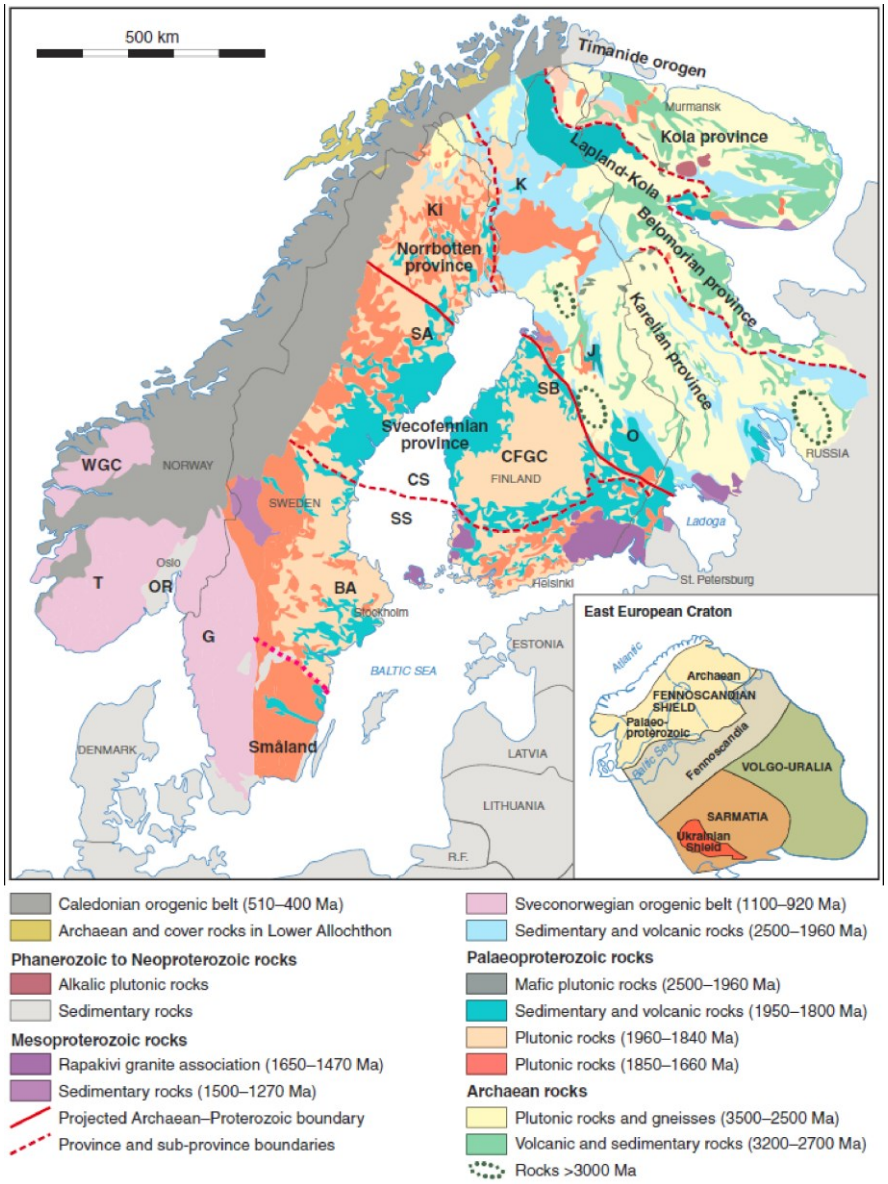

Fig. 1. The Fennoscandian Shield and its position within the East European Craton. Subareas: CS – Central Svecofennia, SS - Southern Svecofennia, BA – Bergslagen Area, G – Gothian Terranes, J – Jormua, K – Kittilä, Ki –

Kiruna, O – Outokumpu, OR – Oslo rift, SA – Skellefte Area, SB – Savo Belt, T – Telemarkian Terranes, WGC – Western Gneiss Complex (Lahtinen, 2012).

The Paleoproterozoic rocks of the CLGB were deposited on the Archean basement gneisses of the Karelian craton, beginning at ca. 2.45 Ga. Approximately 400 million years of intracratonic to cratonic margin rifting led to deposition of a series of autochthonous volcanic and sedimentary rocks during the early Paleoproterozoic, which were later deformed in the 1.93-1.77 Ga Svecofennian orogeny (Lehtonen et al., 1998; Hanski & Huhma, 2005).

The CLGB is bordered by the Central Lapland Granite Complex in the south and the arc-shaped Lapland Granulite Belt in the northeast (Hanski & Huhma, 2005). The most recent interpretation of the CLGB stratigraphy divides the rocks into seven lithostratigraphic groups of metavolcanic and metasedimentary rocks: Vuojärvi, Salla, Kuusamo, Sodankylä, Savukoski, Kittilä, and Kumpu (Figs. 2 and 4) (Niiranen et al., 2015). The first lithostratigraphic model of the CLGB by Lehtonen et al. (1998) did not include the Vuojärvi Group, distinguished a separate Lainio Group, which is now part of the Kumpu Group, and listed the Kuusamo Group as the Onkamo Group.

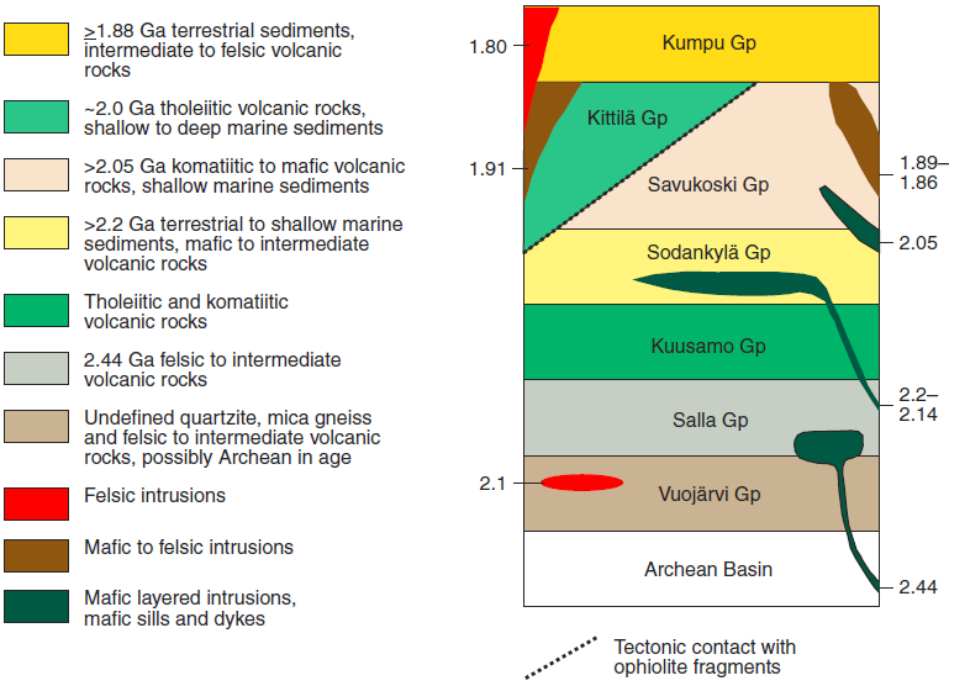

Fig. 2. Stratigraphy of the CLGB with descriptions of the lithostratigraphic units (mod. after Eilu & Niiranen, 2013).

Vuojärvi Group

The Vuojärvi Group, being only recently distinguished as a lithostratigraphic group, is dominant at the southern margin of the CLGB (Fig. 3) (Niiranen et al., 2015). Its quartz-feldspar and quartz-sericite schists may represent metamorphosed clastic sedimentary rocks and/or felsic metavolcanic rocks (Eilu & Nykänen, 2011). While Vuojärvi Group rocks are thought to overlie the Archaean basement, the exact age and stratigraphic position of this new group is still not well understood.

Salla Group

Salla Group rocks occur in the eastern parts of the CLGB. They also directly overlie the Archean basement and due to the lack of clear field observations the exact stratigraphic relation between the Vuojärvi and Salla Group is uncertain (Eilu & Nykänen, 2011). The supracrustal rocks of the Salla Group mainly comprise subaerial calc-alkaline intermediate to felsic metavolcanic rocks including volcanic conglomerates and andesitic, dacitic and rhyolitic pillow lavas and pyroclastics (Lehtonen et al., 1998; Hanski & Huhma, 2005). The eruptional environment, chemical compositions of the metavolcanic rocks with a strong crustal signature, and the stratigraphic position of the metavolcanic rocks indicate that Salla Group volcanism was related to the initial stage of rifting of the Archean craton (Lehtonen et al., 1998).

Kuusamo Group

Kuusamo Group rocks (formerly described as Onkamo Group by Lehtonen et al., 1998) are dominated by subaerial komatiitic to tholeiitic volcanic rocks, which were erupted on top of the Salla Group, the Archean basement, and possibly the Vuojärvi Group. They generally differ from Salla Group metavolcanic rocks in being more primitive with overall higher Mg, Cr and Ni concentrations and lower TiO_2 contents (Lehtonen et al., 1998). As with the Salla Group, the Kuusamo Group metavolcanic rocks show clear evidence of a sialic crustal contamination (Lehtonen, 1998).

Sodankylä Group

The abundant rift-related magmatic activity of the Salla and Kuusamo Groups was followed by the deposition of a thick and wide-spread, epiclastic sedimentary sequence on top of the older units of the CLGB and Archean basement gneisses (Lehtonen et al., 1998; Hanski & Huhma, 2005). This sedimentary sequence is represented by the terrestrial to shallow marine orthoquartzites, sericite quartzites, mica schists and minor

carbonate rocks of the Sodankylä Group with additional tholeiitic basalts and basaltic andesites. The prominent abundance and distribution of quartzites suggest a great widening of the depositional basin from a relatively narrow rift basin after the cessation of Salla and Kuusamo magmatism. A minimum age of the sedimentary sequence is estimated by sills cutting the quartzites at around 2.22 Ga but not reaching into the overlying lithostratigraphic units (Hanski & Huhma, 2005). The Sodankylä Group rocks are the oldest currently known gold-hosting rocks in the CLGB.

The Sodankylä Group is subdivided into the Virttiövaara Formation (ViF) and the Honkavaara Formation (HvF). The direct stratigraphic relation between these formations is not known except for gravimetric data showing that the ViF is dipping under the HvF (Lehtonen, 1998). Virttiövaara Formation rocks are mainly composed of orthoquartzites, sericite schists and sericite quartzites with locally high amounts of fuchsite, coloring the rocks green. Several sedimentary structures can be observed in the ViF, such as cross bedding, graded bedding, herringbone structures, and mud cracks, indicating sedimentation in a tidal environment (Nikula, 1985). The Honkavaara Formation is composed of quartzites, siltstones, carbonate rocks and additional felsic, intermediate and mafic metavolcanic rocks (Lehtonen et al., 1998). All rock units are strongly albitized. The mafic metavolcanic rocks are tholeiitic basalts, and the felsic and intermediate metavolcanic rocks are trachytes, trachyandesites and rhyolites (Lehtonen et al., 1998). Trace and rare earth element contents show that the mafic and felsic rocks did not evolve from the same parental magma (Lehtonen et al., 1998). Th/TiO_2 values of the HvF mafic metavolcanic rocks suggest a rather low degree of sialic contamination compared to the older Salla and Kuusamo Group magmas (Lehtonen et al., 1998).

Savukoski Group

The transition between the Sodankylä and Savukoski Group is gradual and associated with a continual deepening of the depositional rift basins, resulting in sedimentation of more and more fine-grained sediments (Lehtonen et al., 1998). The deposition of Sodankylä quartzites gave way to the formation of the phyllite-tuffite-black schist assemblages of the lower Savukoski Group. Similar units were also formed in the Kuusamo and Peräpohja belts (Lehtonen et al., 1998; Rastas et al., 2001). These graphite- and sulphide-bearing, fine-grained sediments may be important sources for S and Au in some locations, assuming a metamorphic model for orogenic gold occurrences in the

CLGB. A minimum age for the pelitic metasediments is provided by the crosscutting ca. 2.06 Ga Keivitsa intrusion (Mutanen & Huhma, 2001).

The upper part of the Savukoski Group is characterized by a reactivation of magmatic activity and the filling of the basin with mafic and ultramafic rocks, such as tholeiitic and picritic basalts and komatiites (Lehtonen et al., 1998). These mantle-derived, high-temperature komatiitic and picritic rocks are suggested to represent plume-related volcanism (Hanski et al., 2001) that is coeval with a major rifting event at ca. 2.1 Ga (Perttunen & Vaasjoki, 2001; Rastas et al., 2001; Väänänen & Lehtonen, 2001; Kyläkoski et al., 2012). The metavolcanics have preserved their original chemical composition well, without any intense sialic contamination (Lehtonen et al., 1998). The ultramafic volcanic rocks were subsequently altered to serpentinite-chlorite ± talc ± amphibole rocks or to more intense carbonate ± talc assemblages either during seafloor events or during regional greenschist facies metamorphism. Especially the ultramafic rocks are important gold targets along the regional "Sirkka line" thrust fault, as they act as sites of major deformation adjacent to many gold occurrences in the CLGB, but only host some gold themselves, with the exception of the currently second largest gold occurrence in the CLGB, the Pahtavaara deposit which is hosted by komatiites of the upper Savukoski Group.

Kittilä Group

Rifting culminated at ca. 1.97 Ga resulting in the formation of oceanic crust (Eilu & Niiranen, 2013) consisting of a ca. 6 km-thick pile of mafic and minor ultramafic metavolcanic rocks, with interbeds of greywacke, phyllite, graphite- and sulphide-bearing schists, and minor carbonates and banded iron formations (Lehtonen et al., 1998). Similarly to the sedimentary rocks of the Savukoski rocks, the deep marine pelitic graphite- and sulphide- bearing units of the Kittilä Group possibly represent suitable sources for S, creating bisulphide complexes for transporting gold. Consequently, Kittilä Group rocks have a large potential for Au deposits, which is represented, for example, by the >6 Moz Suurikuusikko orogenic gold deposit, currently being the biggest gold mine in Europe (Agnico Eagle, 2017). The Kittilä Group is bound against the surrounding sequences by tectonic contacts (Niiranen et al., 2015), which are thought to represent thrusting of the submarine Kittilä Group rocks over the older more subaerial autochthonous lithostratigraphic groups of the CLGB at ca. 1910 Ma (Hanski & Huhma, 2005). The age for the Kittilä Group has been obtained from cross-cutting felsic

porphyries that are coeval with the associated mafic metavolcanic rocks and have yielded a U-Pb zircon age of ca. 2015 Ma (Lehtonen et al., 1998).

Kumpu Group

The Kumpu Group is the youngest stratigraphic unit of the CLGB and represents a major stratigraphic break, showing a drastic change from volcanic- to sedimentary-dominated facies. The Kumpu Group sediments comprise coarse-clastic, non-mature, molasse-type arkoses, conglomerates, and siltstones, with sedimentological features suggesting deposition in a fluvial environment, such as alluvial fans and braided river systems, directly on top of the older volcano-sedimentary sequences of the CLGB (Kortelainen, 1983). The Kumpu Group metasediments commonly display a characteristic red-brown to purplish color, which is caused by the presence of abundant hematite (Lehtonen et al., 1998).

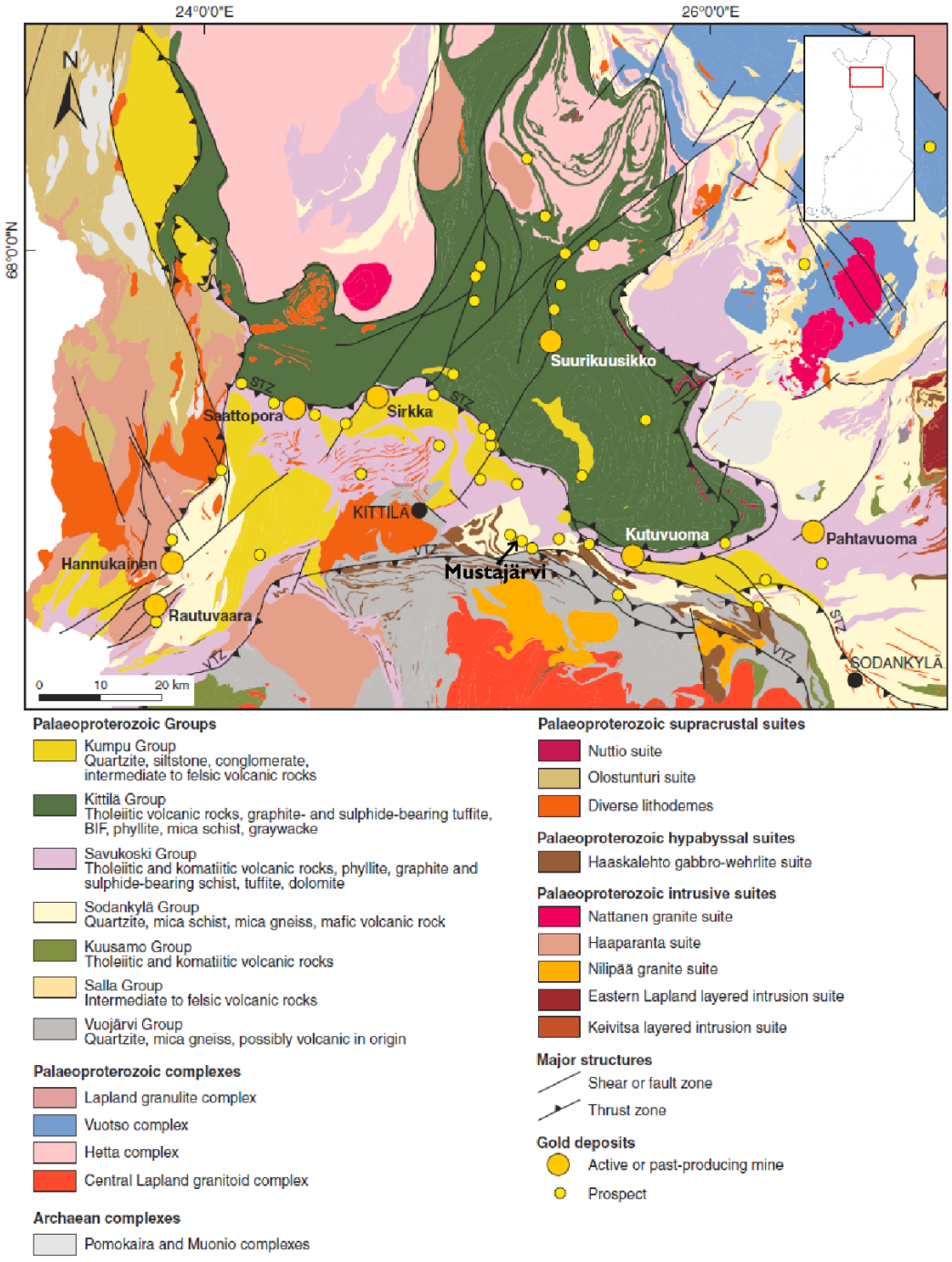

Fig. 3. Geological map of the Central Lapland Greenstone Belt and its known gold occurrences (modified after Eilu & Niiranen, 2013).

2.2 Deformation history

The Paleoproterozoic rocks of the Central Lapland Greenstone Belt have undergone several phases of deformation and metamorphism (Hölttä et al., 2007; Niiranen, 2015; Molnar et al., 2017). The general metamorphic grade throughout the CLGB is mid- to

upper greenschist facies, only reaching mid- to upper amphibolite facies along the southern (south of the Venejoki thrust zone), western and northeastern (locally reaching granulite facies in the northeasternmost corner in the Vuotso area) boundaries and in the vicinity of granitoid intrusions.

The deformation history of the CLGB is typically divided into three ductile deformation events D_1, D_2, D_3, followed by brittle stages (Hölttä et al., 2007; Patison, 2007; Niiranen, 2015). The main deformation stages D_1 and D_2 relate to thrusting events at the margins of the CLGB (Hölttä et al., 2007; Patison, 2007). In the north-eastern margins of the CLGB, high-grade rocks of the Lapland Granulite Belt and adjacent Vuotso complex rocks were thrust to the S-SW onto CLGB successions during D_1, driven by the collision of the Kola and Karelian cratons (Patison, 2007; Niiranen, 2015). In the southern margin, north to north-east thrusting occurred along the Sirkka and Venejoki thrust zones (D_2), driven by the early stages of the Svecofennian orogeny (Patison, 2007; Eilu & Niiranen, 2013; Niiranen, 2015). Due to a lack of distinct overprinting relationships and clear geochronology, these early events cannot be clearly discriminated and might also be roughly synchronous (Patison, 2007; Niiranen, 2015). However, indirect evidence shows D_1 ages of around 1.91 Ga, and estimations for D_2 ranging between 1.89-1.86Ga (Niiranen personal communication, 2017; Niiranen, 2015) (Fig. 4).

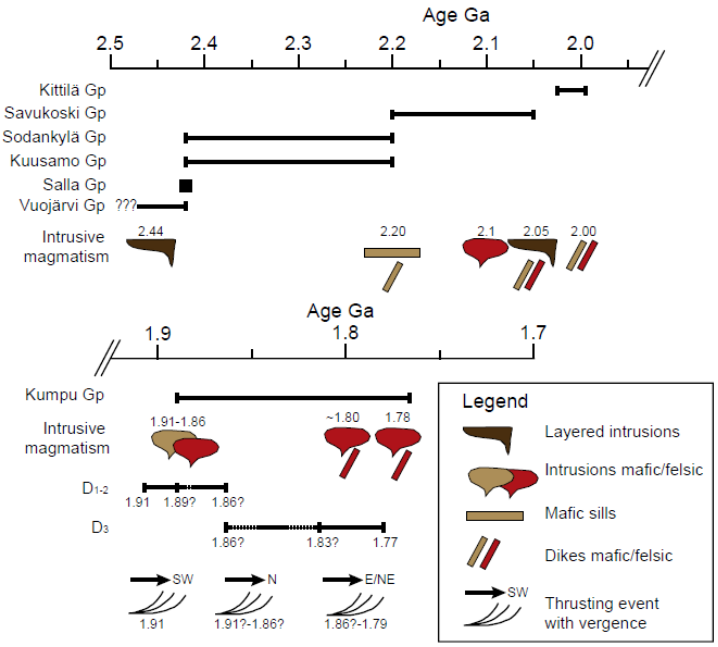

Fig. 4. Stratigraphy and deformation events of the CLGB (Wyche et al., 2015).

D_1 and D_2 faults represent mainly ductile thrust fault systems striking roughly E-W, whereby some features could be reflected by reactivation of pre-D_1 extensional features

related to the Paleoproterozoic rifting. The D_2 thrust systems include the Venejoki thrust zone and the Sirkka thrust zone in the southern part of the Kittilä terrane (Fig. 5) (Niiranen, 2015), which act as the main rheological boundaries within the CLGB. Especially the Sirkka line comprises a series of E-W to SE-NW, closely-spaced, subparallel ~40° south-dipping thrust- and shear zones and segments (Hölttä et al., 2007; Patison, 2007;). Some segments along this zone were displaced and reoriented by later D_3 strike-slip shear zones. The Sirkka line is not a straight thrust system, but curves in the east to the southeast. Representing a major stratigraphic and litho-geochemical boundary, the Sirkka line controls many of the Au occurrences in the CLGB (Patison, 2007). South of the Sirkka line, the Venejoki fault may reflect overthrusting to the north by units of the Central Granitoid Complex. The Venejoki fault system is not well defined, however, a set of roughly E-W striking, subparallel, ca. 40° south-dipping thrust zones similar to the Sirkka thrust system is assumed to be a likely scenario (Niiranen, personal communication, 2018) (Fig. 5). An impact on Au mineralization similar to the Sirkka line has not yet been observed from the Venejoki fault system.

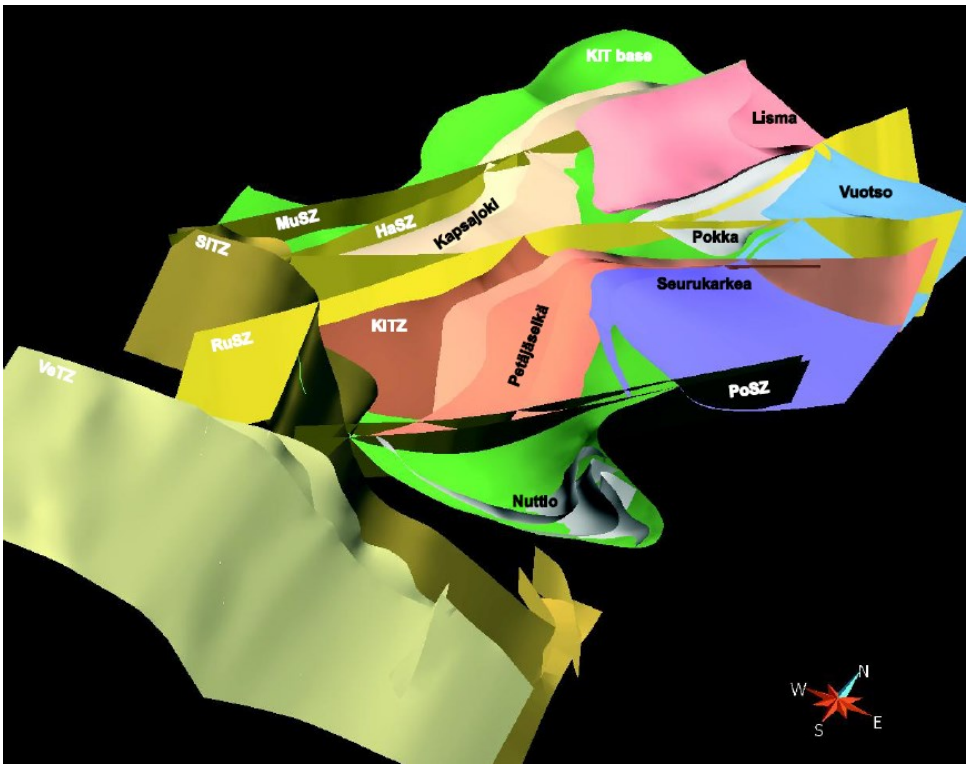

Fig. 5. Major structures in the CLGB seen from the SSW. The Venejoki- (VeTZ) and Sirkka (SiTZ) thrust faults appear as E-W trending, ~40° S dipping major fault zones with multiple segments. Other faults are: HaSZ-Hanhimaa shear zone; KiTZ-Kiistala thrust zone; MuSZ-Muusa shear zone; PoSZ-Porkonen shear zone; RuSZ-Ruoppapalo shear zone (Niiranen, 2015).

A shift in the regional stress regime resulted in a D_3 convergence from the western and southwestern margin of the CLGB. The D_3 deformation involved the development of NW-N-NE-striking strike-slip shear zones that displace and/or reactivate D_1/D_2 thrust zones (Patison 2007; Hölttä et al., 2007). The timing and the cause of the D_3 stress regime shift are not clearly understood. Age estimations range from 1.89 Ga to a minimum age of 1.77 Ga (whereby 1.83-1.80 Ga is assumed to be the most precise age) (Sorjonen-Ward et al., 1997; Lehtonen et al., 1998; Väisanen, 2002; Patison, 2007). Some of the D_3 N-S shear zones are thought to have been either initiated as a compensating response to the opposing compression during D_1/D_2 (Patison 2007), or that they may have utilized transfer shear zones formed during pre-D_1 rift-related volcanism (Ward et al., 1989). However, it is clear, that the orientation of D_3 features is strongly influenced at a local scale by pre-existing structures, especially south of the Sirkka line (Patison, 2007). The Suurikuusikko deposit is situated along the Kiistala D_3 northeast-trending strike-slip fault (Fig. 3), expressing the important correlation between gold mineralization and D_3 shearing which is observable throughout the CLGB.

The D_4 deformation consists of small-scale brittle faulting, jointing and discontinuous brittle shear zones that overprint all structures within the CLGB. The maximum age for D4 deformation is 1.77Ga (Väisanen, 2002; Patison, 2007). Therefore, D_4 features are post-orogenic and perhaps post-gold mineralization.

3. METHODS

The thesis methods comprise a combination of practical field work and analytical research. The practical part consists of a ground magnetometer survey including its interpretation, geological mapping of the wider study area, geological mapping of the artisanal mining pit and re-logging of the available historical drill core. The analytical research comprises thin section studies with subsequent microprobe analysis, and modelling the mineralization with a 3D software.

Field work

The ground magnetic survey at the Mustajärvi study area spanned a total of 40.4 km of measured distance. A spacing of 50 m with a total of 28.15 km measured distance was applied for a more regional testing, whereas a spacing of 25 m with a total of 12.23 km measured distance was applied in the area of the known mineralization. The survey lines were oriented N-S, based on the historically assumed approx. E-W strike of the known occurrence. Other field work comprised mapping the geology of the study area, mostly consisting of a glacial erratic boulder survey since a generally thick till cover results in a scarcity of outcrops. However, a small artisanal mining pit exposes outcrop, which includes the contact between both rock formations that host outcropping auriferous quartz-tourmaline-pyrite veins. As part of the study, the pit was mapped in great detail including a full structural analysis. During the mapping, a total of 30 boulder and outcrop samples were taken from the study area for thin section and geochemical analysis.

During 1991 and 1992, Outokumpu drilled 12 holes at Mustajärvi. As part of the thesis, all available drill core was re-logged, with the resulting geological data acting as a base for a consequent 3D model, which was created to better understand the spatial extent of the gold mineralization. A total of 30 samples was taken from the drill core for geochemical analysis and for thin sections to study the petrography and alteration. Geochemical analysis was performed by *ALS* and consisted of a four-acid digestion with an ICP-MS finish (code *ME-MS61*) and fire assay for gold concentrations (code *Au-AA24*). The results included a wide array of elements, however, neither B, Hg nor Si was part of the analysis. With B being a major constituent of tourmaline, Hg being commonly enriched in orogenic gold deposits, and Si being crucial for geochemical calculations, these elements would have been beneficial for the study.

Research

A total of 60 thin sections were prepared and studied with transmitted and reflected light microscopes for the general petrography of the host rocks, alteration processes and gold distribution. A microprobe study with quantitative WDS analysis was later conducted to further investigate the mineralogy of the gold occurrence. All measurements were made at the University of Oulu, utilizing a Jeol JXA-8200 superprobe. As measurement parameters, a 15 kV accelerating voltage and a 15 nA probe current with a tungsten filament were used. The spot size diameter was kept under 1 µm due to the small grain sizes of the gold associated minerals. All measured elements with their relating measurement parameters can be found in Tables 1 and 2.

Table 1. Measurement parameter of the quantitative WDS analysis.

Element	Std name	X-ray	Crystal	CH	Acc.V	Peak	Peak s	Back s
Se	Se	La	TAP	1	15	97.40	10.0	5.0
S	FeS2	Ka	PETJ	2	15	172.10	10.0	5.0
Co	Co	Ka	LIFH	4	15	124.78	10.0	5.0
Au	Au15	Ma	PETH	5	15	187.08	30.0	15.0
As	GaAs	La	TAP	1	15	104.89	10.0	5.0
Fe	FeS2	Ka	LIF	2	15	134.65	10.0	5.0
Ni	Ni	Ka	LIFH	4	15	115.65	10.0	5.0
Bi	Bi	Ma	PETH	5	15	163.90	10.0	5.0
W	W	La	LIFH	4	15	102.89	10.0	5.0
Ag	Ag	La	PETH	5	15	133.09	10.0	5.0
Sb	Sb	La	PETH	5	15	110.20	10.0	5.0
Te	Hg-Te	La	PETH	5	15	105.39	10.0	5.0

Table 2. Distribution of the elements over the measurement channels for the quantitative WDS analysis.

Channel	1	2	3	4	5
	Se1T	S		Co4LH	Au5PH
	As1T	Fe2L		Ni4LH	Bi5PH
				W4LH	Ag5PH
					Sb5PH
					Te5PH

Furthermore, a 3D model was created in Leapfrog to visualize the extent of the gold mineralization (Fig. 10).

4. MUSTAJÄRVI STUDY AREA

4.1 Geographical overview

The Mustajärvi study area spans roughly 200 hectares and is situated approx. 15 km ESE of the Kittilä town (centered location at 427720E 7500270N: EUREF_FIN_TM35FIN). The site is easily accessible by the Highway 80, which cuts through the northern part of the study site and connects the towns of Kittilä and Sodankylä (Fig. 6). A high-voltage power line passes through the area, which might prove favorable for any potential mining operations. The Mustajärvi site is almost entirely covered by an open pine and birch forest (Fig. 7). The study site is flanked to the southwest, south and east by marshy wetlands, which belong to the Natura 2000 environmental protection network (Fig. 6). The area is nearly flat with elevations ranging between 195 and 210 above sea level, whereby the elevation gradually increases from the south to the north. The till cover at the study site is on average 3.5 m thick, ranging between 0.5 and 10 m (Fig. 8). The till thickness increases towards the south, where glacial deposition is interpreted based on field observations and digital elevation models. There are no outcrops at the Mustajärvi study site, except for a small-scale artisanal mining pit exposing roughly 5 m x 10 m of bedrock.

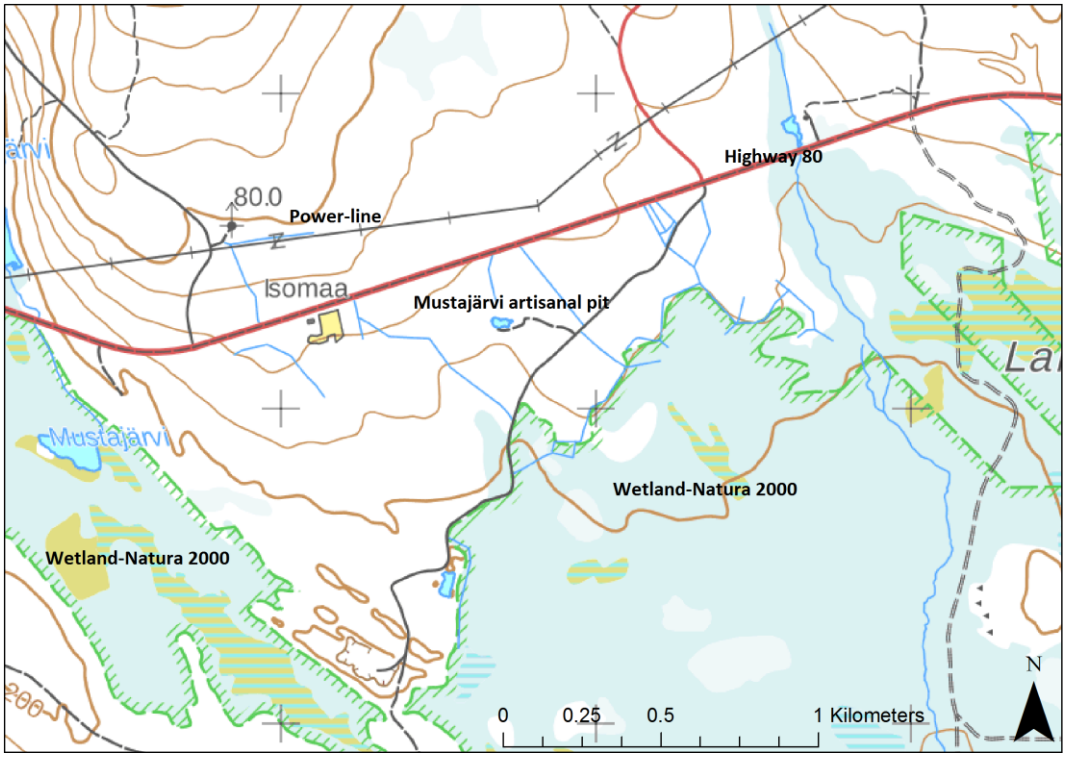

Fig. 6. Geographic overview of the Mustajärvi study with features of interest.

Fig. 7. Orthophotograph of the Mustajärvi study area. Clearly recognizable are the Highway 80 connecting Kittilä with Sodankylä, a high-voltage power-line, the Natura-2000 wetlands in the SW, S and E, the artisanal mining pit, and 2 houses.

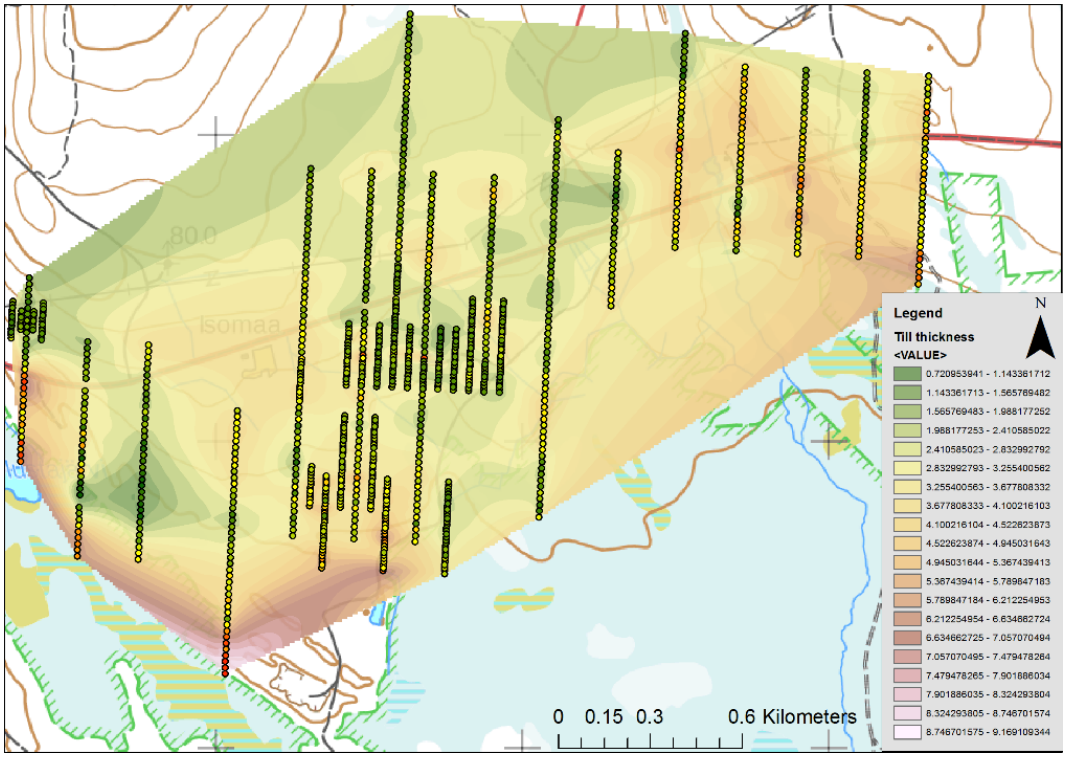

Fig. 8. Till thickness at Mustajärvi. The thickness is interpolated based on the sample depth of Outokumpu Bottom-of-till (BoT) samples.

4.2 Exploration history

Anomalous gold values at Mustajärvi were first discovered in a GTK regional till survey in the late 1980s (Eilu and Nykänen, 2011). Subsequently, Outokumpu Oy investigated this anomaly in 1990-1991 with multiple N-S oriented bottom of till (BoT) survey lines using a 10 m sample spacing in areas with high Au anomalies and a 20 m sample spacing for a more regional exploration. The sampling lines were generally 50 m apart, however also larger spacings were applied for more regional work (for sample points see Fig. 8). Clearly anomalous gold values were recognized in 10 consecutive lines (Hugg, 1996). In 1991, Outokumpu followed up on these anomalies with excavating seven trenches of 72.5 m combined length. They reported short intervals containing a few tens of ppm of Au in the best cases (Hugg, 1996). Shortly after, they carried out an additional heavy mineral till survey and conducted a small ground magnetic- and IP survey (Hugg, 1996). Between December 1991 and December 1992, Outokumpu drilled 12 holes totaling 706 m in length. The holes were short, with an average length of 59 m and a maximum length of 72.4 m (Table 3). The holes were oriented towards 315° with a dip of 50° and were spaced 20 or 40 m apart along eight parallel sections (Fig. 12). All but one drill hole intersected mineralization exceeding 1 ppm Au, with the best intervals being 2.7 m at 14.6 ppm Au, 12 m at 2.68 ppm Au, and 1 m at 18.8 ppm Au (Table 3) (Anttonen, 1993). Moreover, reported core losses of up to 50 % in the mineralized zones likely undervalue many gold intercepts. Drilling was terminated due to a poor understanding of the gold occurrence with an apparent "poor correlation" between the holes, resulting in an evaluation of the mineralization as an "uneconomic gold occurrence" (Hugg, 1996). Consequently, the tenement was given up by Outokumpu in 1996.

From 2002-2010 and 2013-2016, Mustajärvi was subject of small-scale artisanal mining by the company *Gold Mine Siitonen & Saiho AY*. The company exclusively mined heavily weathered outcropping mineralization, in which gold occurs in a native form and is easily extractable, whereas no unweathered ore was mined. As part of the artisanal mining activity, they excavated a 2 to 5 m deep pit, spanning 20 x 70 m, along the outcropping mineralized veins. Grades from tens of ppm of Au up to 100 ppm Au have been reported by *Gold Mine Siitonen & Saiho AY* (H. Siitonen, pers. comm., 2018). These gold concentrations were confirmed through channel sampling of the mined vein by *FireFox Gold Corp* in 2018. Channel samples yielded gold concentrations up to 140.5 ppm Au with visible gold along the vein.

Table. 3. Outokumpu drill holes at Mustajärvi from 1991-1992 with the best gold intersects (data after Anttonen, 1993).

Hole Nr.	Azimuth [°]	Dip [°]	Hole length [m]	Best mineralized interval [m]	Length [m]	Au [ppm]
MJ-1	315	50	56.50	20.7-23.4	2.7	14.6
MJ-2	315	50	50.00	22.0-23.0	1.0	12.2
MJ-3	315	50	57.70	9.6-23.0	13.4	0.52
MJ-3				29.3-31.7	2.4	1.03
MJ-4	315	50	44.40	21.0-33.0	12.0	2.68
MJ-5	315	50	63.05	43.0-44.0	1.0	1.42
MJ-5				53.0-54.0	1.0	1.92
MJ-6	315	50	68.20	27.85-29.05	1.2	5.45
MJ-7	315	50	49.75	23.5-24.9	1.4	6.02
MJ-8	315	50	72.40	45.0-45.8	0.8	0.42
MJ-9	315	50	68.45	6.0-7.0	1.0	4.78
MJ-9				52.0-54.0	2.0	1.2
MJ-10	315	50	58.15	41.0-42.0	1.0	18.8
MJ-11	315	50	60.20	34.8-36.5	1.7	1.8
MJ-12	315	50	57.20	48.1-49.4	1.3	1.08

4.3 Geological overview

The rock package at Mustajärvi can be divided into two major lithological units: 1) siliciclastic metasediments consisting of banded arkose quartzites, intermediate tuffites and mafic tuffites and 2) metavolcanic rocks comprising ultramafic lavas and tuffs, komatiitic basalts, mafic lavas and tuffs, and rare graphitic cherts (Table 4). The siliciclastic metasediments most likely belong to the Sodankylä Group with a minimum age of ca. 2.22 Ga which is given by the Haaskalehto gabbro intrusions (Lehtonen et al., 1998; Hanski et al., 2010). The metasediments are characterized by a low magnetic response (Fig. 11A) and a relatively low apparent resistivity (Fig. 11B). The metavolcanic rocks are likely part of the ca. 2.06 Ga (Hanski et al., 2001) Savukoski Group. They are characterized by a high magnetic response and a relatively high apparent resistivity. Gabbro intrusions of an unknown formation are present in the SW of the study area (Fig. 9). A 3D geological model of the Mustajärvi area is shown in Fig. 10. Ground magnetic data and BoT Cr-concentrations (Fig. 11D) indicate that both the siliciclastic metasediments and the metavolcanic rocks are intruded by gabbro intrusions. Lehtonen et al. (1988) list these mafic intrusions with an age of 2.0 Ga, which fits into the model of the host rock formation ages.

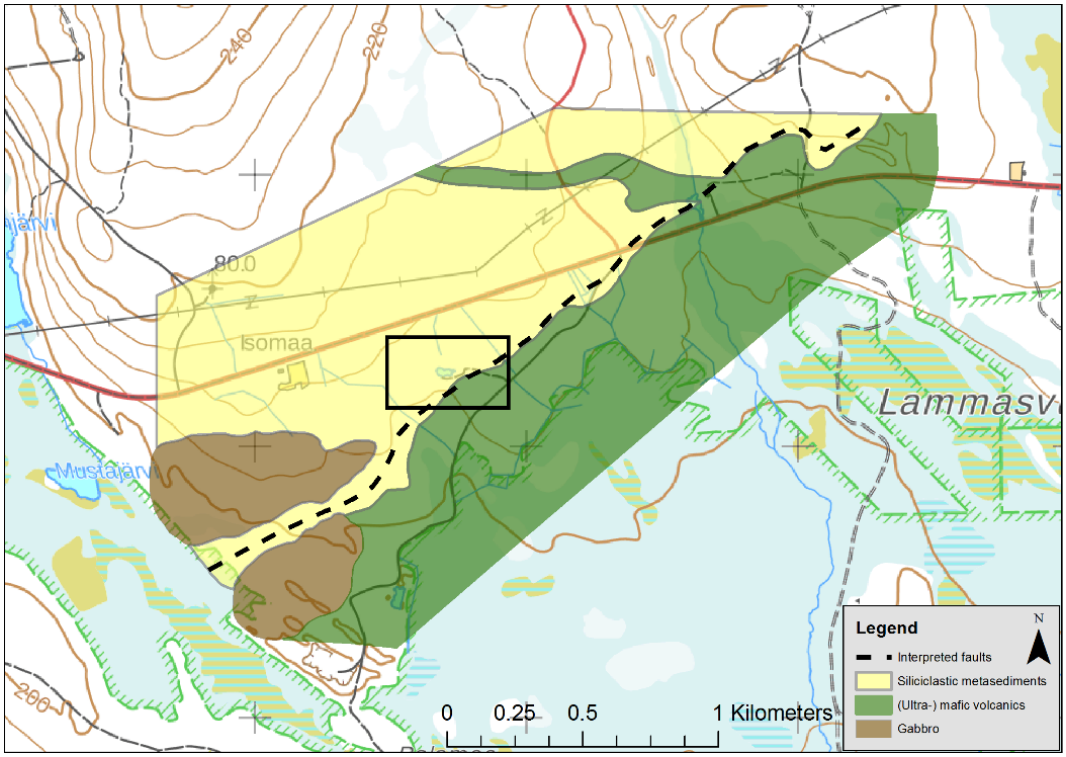

Fig. 9. Geological map of the Mustajärvi study site. Highlighted by a black rectangle is the area of the known gold occurrence (see Fig. 12 for a close-up view; and Fig. 10 for 3D geological model for the area indicated by the black rectangle).

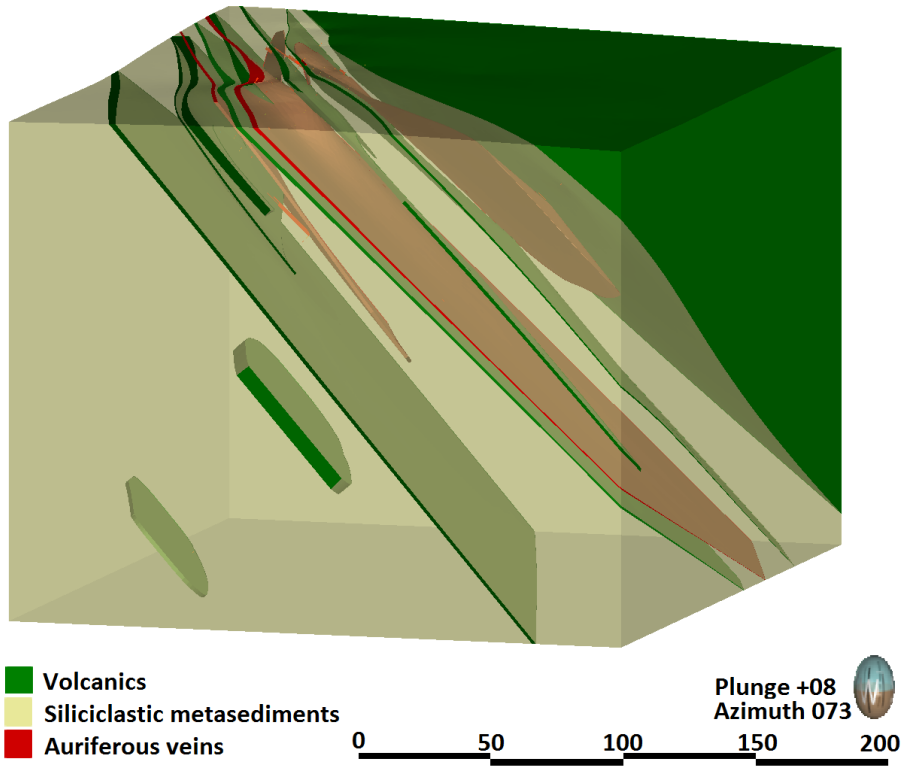

Fig. 10. 3D geological model of the area of the known gold mineralization at Mustajärvi. The 3D model covers roughly the area that is indicated by the black rectangle in Fig. 9. The Mustajärvi shear zone, located at the main contact between the rock units, is not modelled. The view is from WSW.

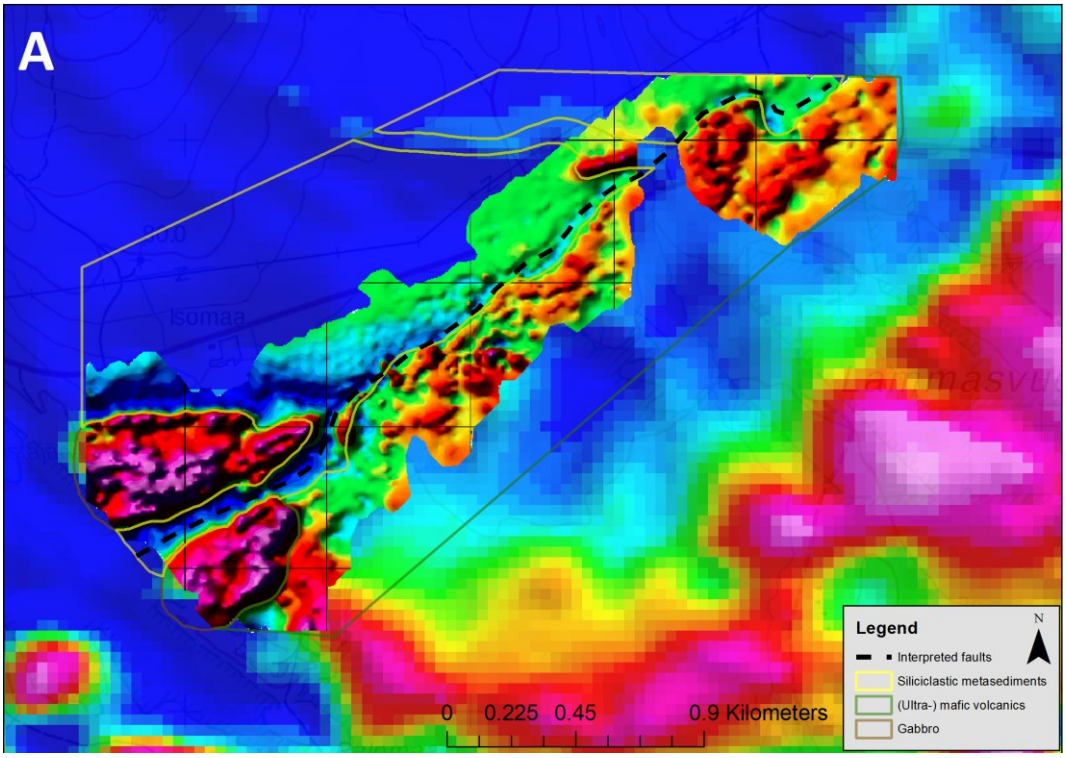
A
Isomaa
0 0.225 0.45 0.9 Kilometers
Legend
N
Interpreted faults
Siliciclastic metasediments
(Ultra-) mafic volcanics
Gabbro

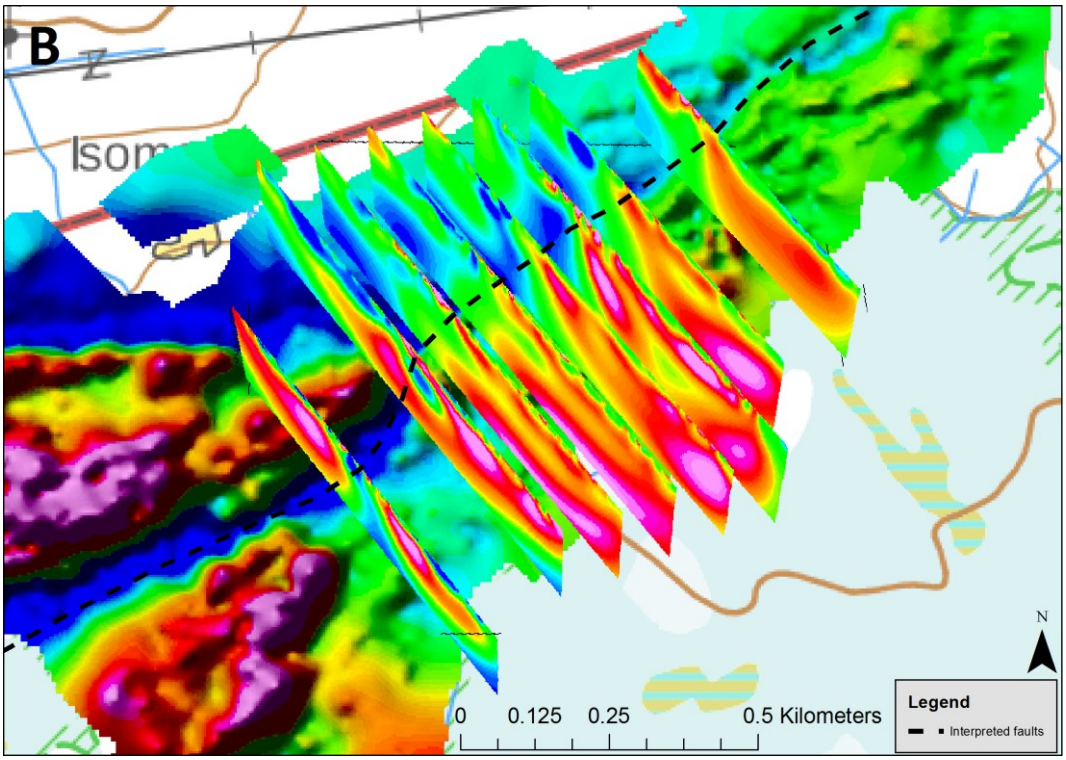
B
Isom
0 0.125 0.25 0.5 Kilometers
N
Legend
Interpreted faults

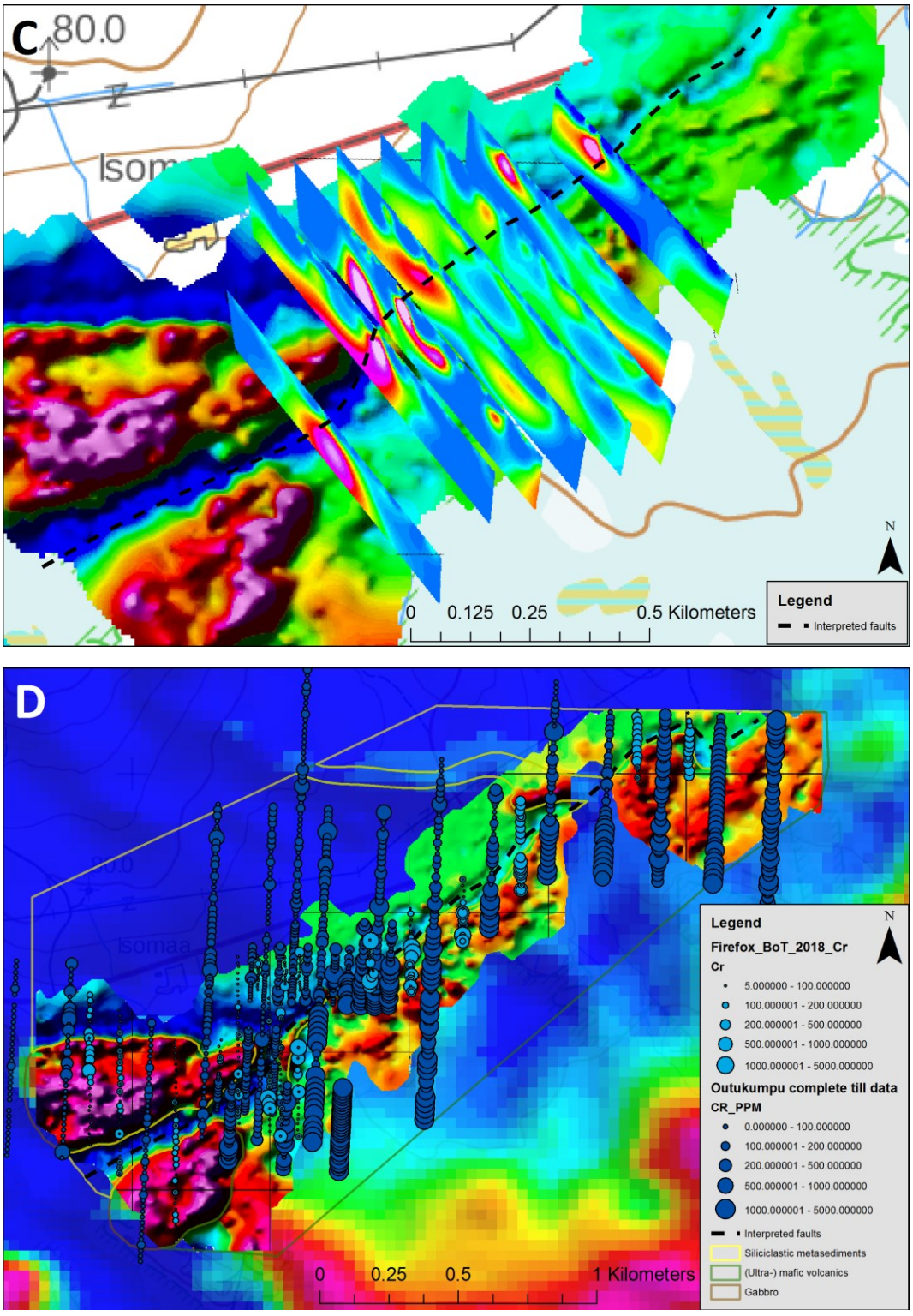

Fig. 11. Geophysical data and BoT Cr-concentrations visualizing the lithological units at Mustajärvi. (A) Ground magnetic survey with less detailed aero magnetics in the background. The data clearly shows all three existing lithologies: high values in the SW associated with gabbro intrusions, relatively high values SE of the fault zone (dashed line) associated with the metavolcanic rocks and relatively low values for the siliciclastic metasediments. Also, a demagnetized zone is visible along the fault zone. (B) IP apparent resistivity pseudo sections with ground magnetics in the background. The data allows to distinguish between the low resistive metasediments and the more resistive volcanics. The fault zone appears as a low resistivity zone dipping to the SE with ~45. (C) IP chargeability pseudo sections. The interpreted fault zone inhibits a high chargeability along the full extent. Also, the parts of the siliciclastic

metasediments that host the mineralization show elevated chargeabilities, in accordance to the low the resistivity values. (D) Outokumpu and FireFox Gold BoT samples with Cr-concentrations visualizing the extent of the ultramafic rocks mostly south of the interpreted Mustajärvi fault zone.

The Mustajärvi fault zone is interpreted to occur along the general contact zone between the host rocks, likely formed due to the competency contrast of the rock types. The fault is indicated by several fault zone-typical geophysical features: demagnetization in ground magnetic surveys (Fig. 11A), a low apparent resistivity (Fig. 11B), and a high chargeability anomaly (Fig. 11C). Interpreted from geophysical data, the fault zone has a similar orientation to the host rocks, dipping to the SE with an angle of ~45 °.

Based on geophysical data, BoT geochemistry data, and field and drill core observations, the siliciclastic metasediments dominantly occur on the NW side of the fault zone and the metavolcanic rocks dominantly on the SE side. The contact between the rock units is conform and rather gradual, with increasing interlayering between the rock types in proximity to the contact zone (Fig. 10), where also graphitic cherts have been observed to be interlayered with altered mafic tuff as part of the volcanic group.

The known gold mineralization is hosted by a set of quartz-pyrite-tourmaline veins that show typical pinch and swell features. The mineralization is not strongly host rock controlled as it has been observed to be hosted by both the siliciclastic metasediments and the metavolcanic rocks, as well as by the contact of both units. However, the mineralized veins appear generally structurally controlled, with the main mineralization trend being parallel to the Mustajärvi fault zone (Fig. 10). A second mineralization trend, which is semi-exposed in the artisanal pit, runs perpendicular to the main trend. Additionally, BoT Au anomalies outside of the known gold occurrence are also spatially related with the interpreted fault zone (Fig. 13) further suggesting a strong structural control.

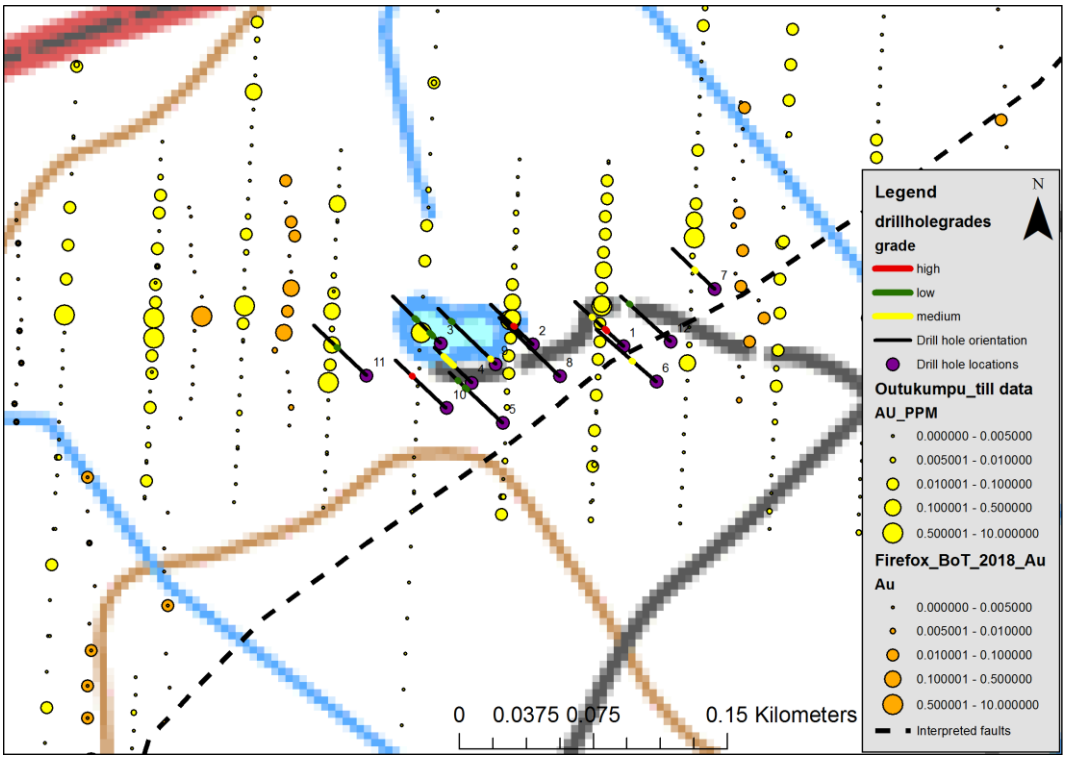

Fig. 12. Close up view of Fig. 9. Historical Outokumpu drill holes and BoT gold anomalies showing the extent of the mineralized veins. The artisanal mining pit is visible in the center. A set of parallel NE striking veins is proposed to be the main host for the gold mineralization (Fig. 10).

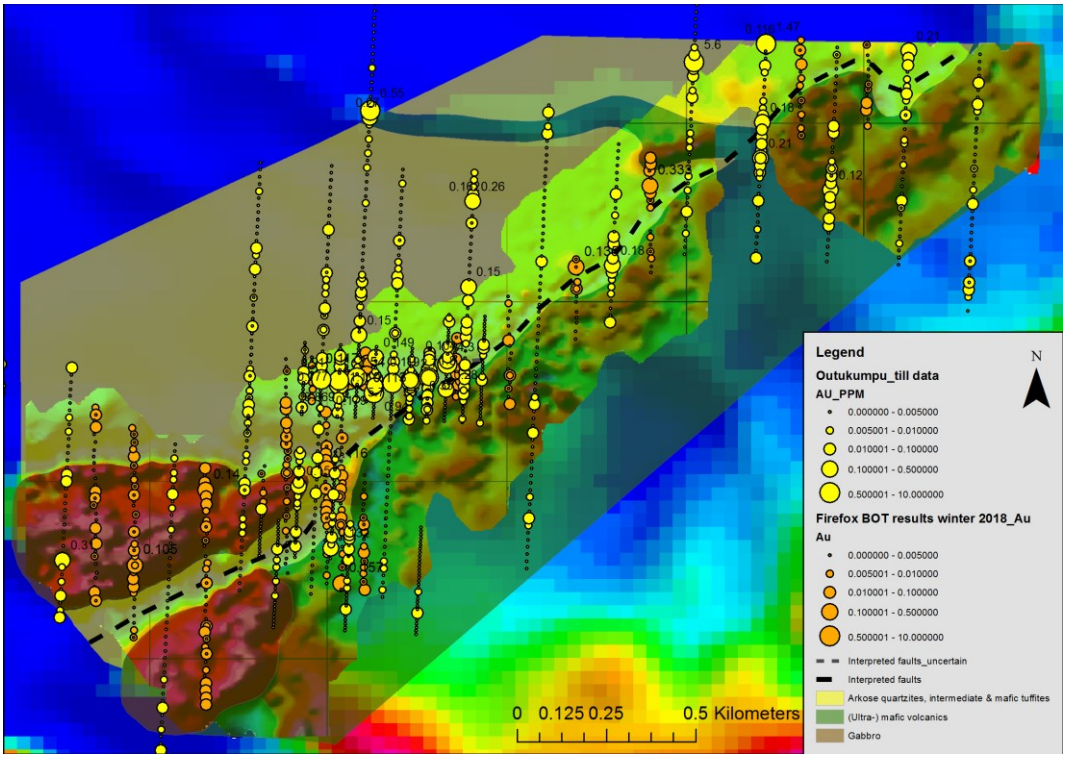

Fig. 13. Outokumpu and FireFox Gold BoT samples with Au concentrations over the extent of the entire study area. High-grade gold anomalies are strongly associated with the interpreted Mustajärvi fault zone outside of the area of known gold occurrence.

5. HOST ROCKS

5.1 Petrography of the host rocks

5.1.1 Petrography of the siliciclastic metasediments

The siliciclastic metasedimentary rock unit consists of banded arkose quartzite (felsic tuffite), intermediate tuffite and mafic tuffite. In most cases, no clear boundaries between the rocks can be drawn (Fig. 14) as most contacts are gradual, with the rock types being strongly interlayered on a meter to centimeter scale, commonly resulting in a strong layering typical for tuffs or tuffites (Figs. 15, 16 and 17). Observed strong banding, felsic clasts in a mafic matrix, an occasional gradual bedding suggest a volcaniclastic sedimentation. The entire metasedimentary unit could be generally described as tuffite with variations both in the amount of volcaniclastic sedimentary input, and variations in the geochemistry of the primary sedimentary input. However, the lack of porphyritic clasts in the arkose quartzites and the generally strong albitization and carbonatization make the general definition of the arkose quartzites as tuffites difficult and hence the general term of siliciclastic metasediments was preferred for the rock unit.

Table 4. Overview of the rock types and their petrographic features at Mustajärvi.

Rock type	Mineral assemblage	Grain size	Color	Textures
Siliciclastic metasediments:				
Arkose quartzite	Qtz + Ab + Cb + Ms + Ser ± Bt, Py, Hem, Mag, Rt, Zrn	medium-fine	beige	banded-bedded
Intermediate tuffite	Qtz + Ab + Ms + Cb + Bt + Ser ± Chl, Hem, Mag, Py, Rt,	medium-fine	beige-grey	banded-bedded
Mafic tuffite	Qtz + Ab + Chl + Bt + Ms + Cb + Ser ± Hem, Mag, Py, Rt, Ccp	fine	dark grey	banded-bedded, massive
Volcanic rocks:				
Ultramafic lava	Tr + Chl + Tlc + Mag + Chr ± Ttn, Py, Ccp	fine	dark green	massive
Ultramafic tuff	n/a	fine	dark	schistose
Komatiitic basalt	Act + Chl + Ep + Ab + Bt + Mag ± Ttn, Py, Ccp	fine	dark	massive
Mafic lava	n/a	fine	black	massive
Mafic tuff	n/a	fine	dark	schistose
Graphitic chert	n/a	fine	dark grey-greenish	bedded

Based on thin section studies, the main mineral assemblages of the siliciclastic metasediments are:

Banded arkose quartzite: quartz + albite + carbonate + muscovite + sericite ± biotite ± pyrite ± hematite ± magnetite ± rutile ± zircon

Intermediate tuffite: quartz + albite + muscovite + carbonate + biotite +sericite ± chlorite ± hematite ± magnetite ± pyrite ± rutile

Mafic tuffite: quartz + chlorite + biotite + muscovite + albite+ carbonate + sericite ± hematite ± magnetite ± pyrite ± rutile ± chalcopyrite

Fig. 14. Drill core showing least altered metasedimentary rock. The amount of mica is strongly varying in the rock package and changes gradually or sharply. Drill core MJ-5, depth 24.7 m.

Fig. 15. Drill core showing 0.5-cm-thick parallel interlayers of mafic tuffites and arkose quartzites indicating a volcaniclastic sedimentation. Drill core MJ-5, depth 8 m.

Fig. 16. Drill core showing porphyritic volcaniclastic sedimentation features in the top row, with felsic clasts in a mafic matrix. In the bottom row, strongly banded, deformed tuffite with bands of mafic/intermediate and felsic composition. Drill core 18MUS002, depth 5m.

Fig. 17. Drill core showing a ~5 cm thick arkose quartzite interlayer in an intermediate tuffite. Drill core 18MUS013, depth 168 m.

Arkose quartzite

Arkose quartzites make up the largest part (~50 vol. %) of the metasedimentary rock package. The rock is psammitic, typically weakly foliated, blastoclastic to granoblastic with rare lepidoblastic parts. Unless strongly altered or brecciated, the rock macroscopically shows primary bedding features including common bands of white mica-rich layers which have a grey-greenish color (Fig. 18B). The color of the rock is generally beige-grey (Figs. 14 and 17) with a pinkish tint due to the common moderate to strong albitization, and occasionally reddish due to silicification with enclosed Fe-oxides. In strongly albitized and carbonated parts, the rock has a strong beige to almost orange color (Fig. 18).

The main mineral assemblage consists of quartz, albite, carbonate, muscovite, sericite ± biotite and accessory minerals. Accessory minerals are most commonly pyrite, hematite and magnetite, rutile, whereas zircon is rare. The amount of accessory minerals varies over the rock package, but they never exceed 10 vol. % of the rock. Hematite commonly rims magnetite and forms hematite pseudomorphs after magnetite. The accessory minerals usually occur disseminated in the matrix but are locally also related to veins.

Quartz is the main matrix constituent, making up ~45 vol. % of the matrix. The quartz grains are subhedral and have average sizes of 100-200 µm (Fig. 19). Locally, quartz and albite show signs of dynamic recrystallization with a resulting decrease in the grain size (50-100 µm) and the formation of a weak foliation in the rock (Fig. 20). Albite is the other main constituent of the matrix with an average volume of 35 %. The ratio between quartz and albite is mostly homogenous with an average of 60:40, but it can also rarely vary

from 80:20 to 40:60 within one thin section, representing the heterogeneity of the arkose quartzite. The grain size of albite is similar to quartz with an average of 100-200 µm (Fig. 19). Albite grains are generally subhedral with clear polysynthetic twinning and show an omnipresent overprint of fine-grained sericite. The overprint ranges from very weak to very strong. In near-surface samples, albite is occasionally kaolinized. No other feldspar mineral than albite was observed in the rock package.

Disseminated carbonate makes up roughly 10% of the matrix. Carbonate is usually smaller than quartz and plagioclase with average grain sizes of 50-100 µm. The disseminated carbonate grains are subhedral to anhedral, mainly growing in the grain boundaries of quartz and albite crystals (Fig. 19). Carbonate generally also shows an overprint by fine-grained sericite.

Muscovite is commonly present in the entire metasedimentary rock package. In the purely quartzitic parts it has average concentrations of 1-5 vol. % and in the banded, mica-rich parts with ambiguous boundaries to intermediate tuffites, muscovite makes up 30 vol. % of the rock, together with accessory biotite contents. The grain size of the mostly subhedral muscovite ranges between 50 and 150 µm. Muscovite occurs mainly in parallel bands, which define foliation in the rock.

Sericite is present in the entire rock package of the metasediments and is unrelated to biotite and muscovite. It occurs as a weak overprint on albite and occasionally on carbonate and as <30 µm sized grains disseminated in the grain boundaries of quartz and albite. The intensity of the sericite overprint varies drastically over the rock package and increases in the vicinity to veining, especially quartz-pyrite veining.

Fig. 18. Arkose quartzite grab samples. (Left) Grab sample MJ-22 from the Mustajärvi artisanal pit. Albitized arkose quartzite without substantial amounts of mica. (Right) Grab sample MJ-37 from the Mustajärvi study area. Banded

arkose quartzite with primary bedding features of purely quartzitic parts and muscovite rich parts. The muscovite rich parts act as displacement planes for the visible quartz vein.

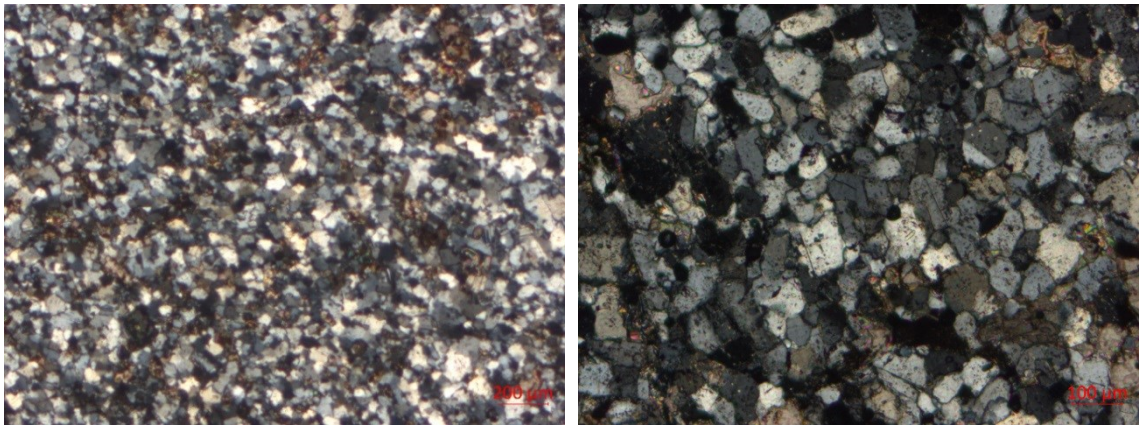

Fig. 19. Photomicrographs of homogenous quartz and albite rich matrix of the arkose quartzite. (Left) Arkose quartzite; crossed polarizers; field of view ~2,4 mm. (Right) Arkose quartzite; crossed polarizers; field of view ~1.2 mm. Additional to quartz and albite, carbonate in the grain boundaries and a weak sericite overprint of albite are visible.

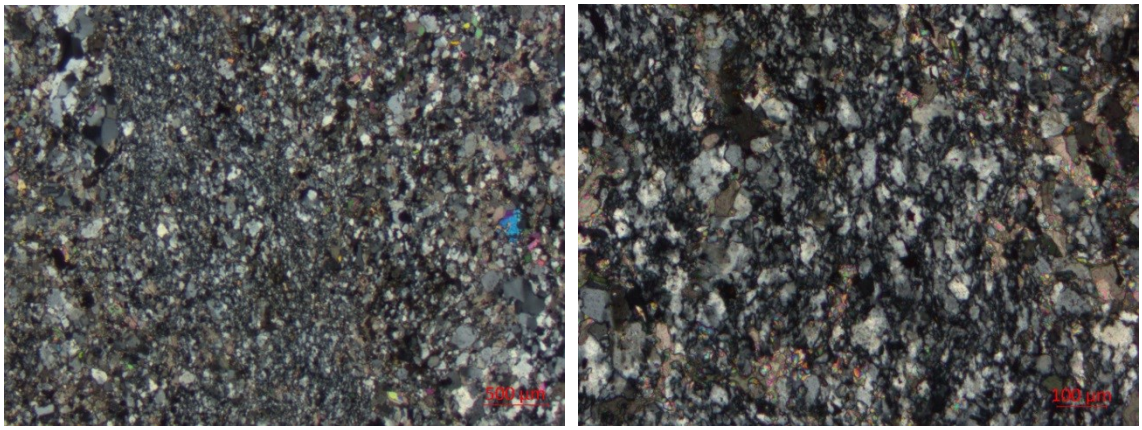

Fig. 20. Photomicrographs of dynamic recrystallization of quartz with associated grain size reduction. Recrystallization has formed a slight foliation in the rock. Also visible are disseminated muscovite and abundant carbonate in the matrix. (Left) Arkose quartzite; crossed polarizers; field of view ~6 mm. (Right) Arkose quartzite, crossed polarizers, field of view ~1.2 mm.

Intermediate tuffites

Intermediate tuffite is the second most common rock type in the metasedimentary rock unit, comprising approx. 40 vol. % of it. The transition from banded arkose quartzites is mostly gradual, with both rocks being strongly interlayered making it often impossible to draw a boundary between the rock types. However, more rarely the contact can also be sharp and distinct (Fig. 17). Moreover, in the intermediate tuffite, quartz and albitized feldspar clasts rarely resemble pyroclasts in a mafic matrix that, together with a graded bedding, suggest a sedimentation influenced by volcanic rocks (Figs. 16, 22 and 23).

Whereas the arkose quartzites contain none to only accessory biotite, intermediate tuffites can have substantial amounts of biotite of up to 20 vol. %, with an average of 10 vol. %. However, in most cases, muscovite still dominates over biotite, with white mica contents of up to 50 vol. % (Fig. 25) and an average of 20 vol. %. Biotite concentrations of over 10 vol. % cause the rock to appear dark (Figs. 21 and 22), making it often difficult to macroscopically distinguish between intermediate tuffites and mafic tuffites, however, intermediate tuffites are commonly less strongly foliated than mafic tuffites. Biotite occurs both as thin foliated bands forming a weak foliation (Fig. 24) and disseminated in the matrix between quartz and albite (Fig. 23). Associated with biotite is occasional chlorite, usually in the vicinity of carbonate. However, chlorite does not exceed 5 vol. % of the rock package. Muscovite commonly occurs in strongly foliated bands that are often associated with hematite (Fig. 25). The grain sizes of biotite and muscovite are similar, with average grain sizes ranging between 50 and 150 µm. The mineral characteristics of quartz, albite and carbonate are similar to what has been described in the arkose quartzite rock.

Fig. 21. Drill core showing least altered intermediate tuffite with biotite rich bands. Drill core 18MUS013, depth 184 m.

Fig. 22. Drill core sample showing intermediate tuffite (sample MJ-6-3374). Rare graded bedding features in a biotite rich matrix. See Fig. 23 for thin section pictures of the matrix.

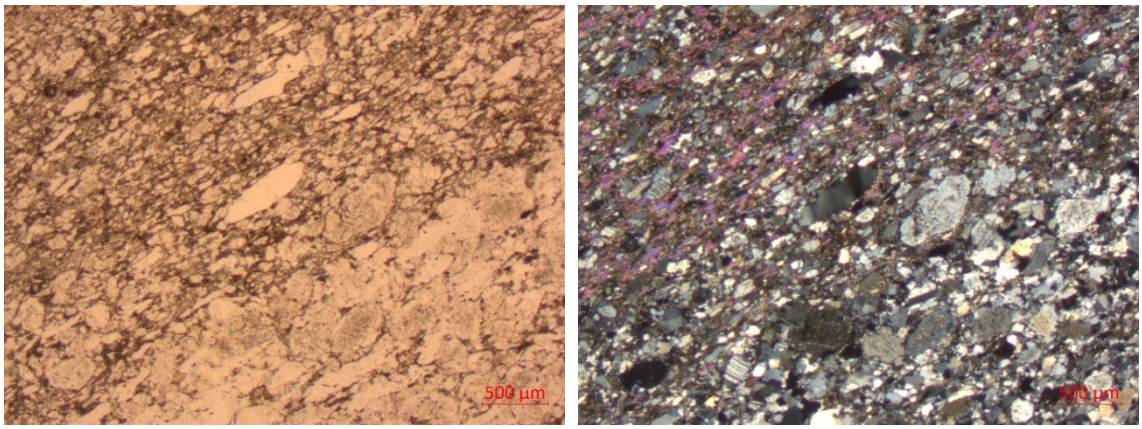

Fig. 23. Photomicrographs of intermediate tuffite; drill hole sample MJ-6-3374m. Graded bedding and albitized feldspar clasts in a biotite rich matrix are indicating a volcaniclastic sedimentation. (Left) Arkose quartzite; linear polarizers; field of view ~6 mm. (Right) Arkose quartzite; crossed polarizers; field of view ~6 mm.

Fig. 24. Photomicrograph of intermediate tuffite. Thin biotite bands (brown) form a weak foliation in the rock. Linear polarizers; field of view ~6 mm.

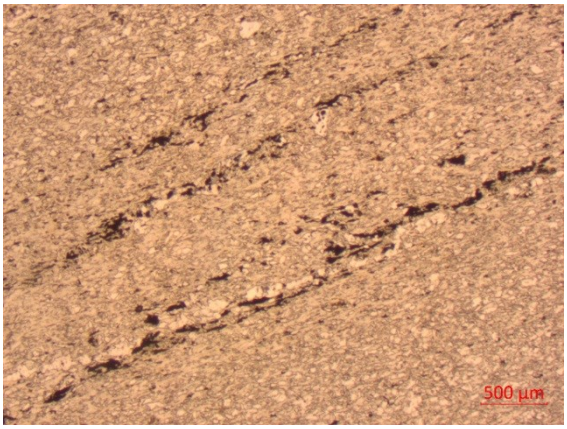

Fig. 25. Photomicrograph of intermediate tuffite. Muscovite rich layer associated with abundant hematite, also forming a foliation in the rock. Linear polarizers, field of view ~6 mm.

Mafic tuffite

Mafic tuffite forms about 10 vol. % of the siliciclastic metasediment pile. They mostly comprise 0.1-to 1-m-thick interlayers, but also rare massive layers with thicknesses of up to 7 m. The transition from intermediate tuffite is mostly gradual. Mafic tuffites can be distinguished from mafic lavas by their hardness caused by the high quartz content, and their foliation due to the layering of quartz with biotite-chlorite bands (Figs. 28 and 29). Least altered mafic tuffites are weakly to moderately foliated (Figs. 26 and 27) with the texture locally being either granoblastic or lepidoblastic. In biotite-rich lepidoblastic parts, the rock locally shows a weak crenulation cleavage (Fig. 29). Similar to the intermediate tuffite, biotite- or chlorite-rich parts are usually associated with abundant hematite which follows the lepidoblastic texture (Fig. 29). The main difference to intermediate tuffite is the higher chlorite and biotite content usually clearly dominating

over muscovite, and the slightly higher Fe-oxide content. Mafic tuffites have chlorite or biotite concentrations of at least 30 %, whereby either chlorite or biotite is clearly dominating. Both minerals show overprinting reactions between each other, with biotite mostly getting chloritized in the vicinity of carbonate. The grain size of biotite varies between 50-150 µm with an average of ~100 µm, the grain size of chlorite is slightly larger. The grain shapes of both minerals are mainly subhedral and only rarely euhedral due to veining related recrystallization (Fig. 29). For quartz, albite and carbonate, the same mineral characteristics apply that have been described in the arkose quartzites.

Fig. 26. Drill core showing weakly altered mafic tuffite with concordant albite-carbonate-(quartz) veining along the foliation. Drill core 18MUS013, depth 72 m.

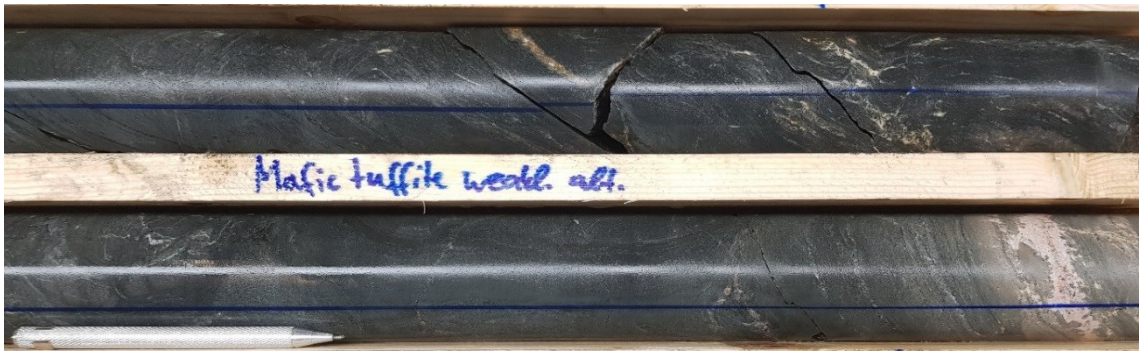

Fig. 27. Drill core showing least altered mafic tuffite. Drill core 18MUS013, depth 180 m.

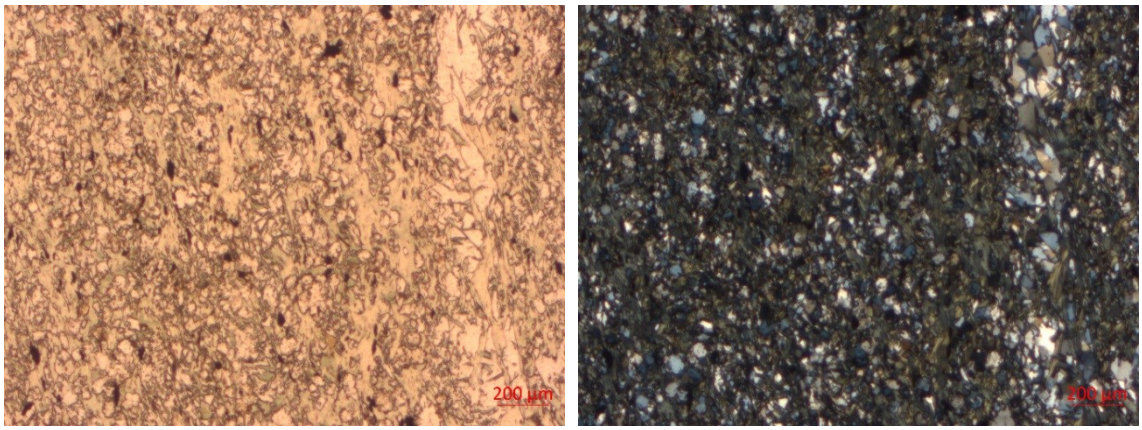

Fig. 28. Photomicrographs of mafic tuffite. In this sample, the matrix is dominated by abundant chlorite and quartz and some albite. (Left) Linear polarizers; field of view ~2.4 mm. (Right) Crossed polarizers; field of view ~2.4 mm.

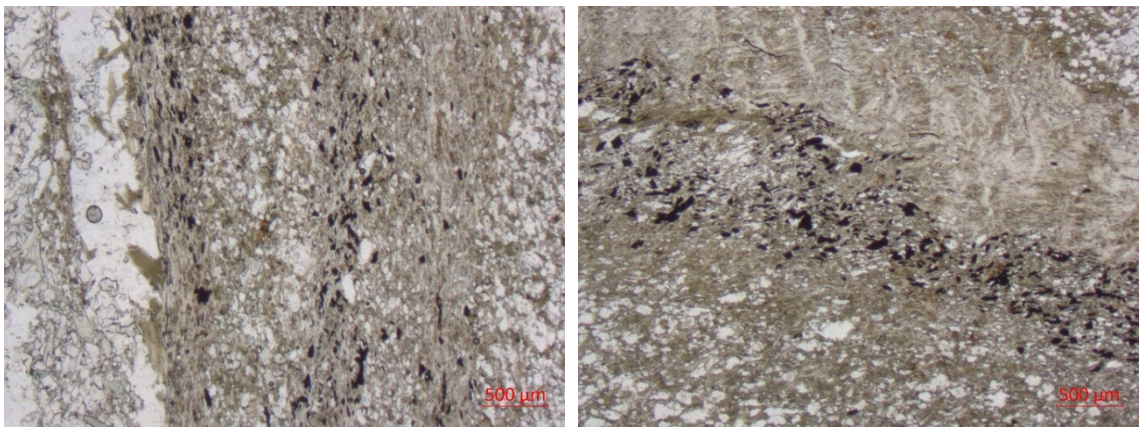

Fig. 29. Photomicrographs of the matrix of the least altered mafic tuffites. Biotite (brown) forms a foliation in the rock. Associated with the biotite rich layers is hematite (opaque). (Left) Mafic tuffite; linear polarizers, field of view ~6 mm. The contact to a quartz veinlet, parallel to the foliation, is characterized by coarse grained more euhedral biotite. (Right) Mafic tuffite; linear polarizers, field of view ~6 mm. Thick biotite-muscovite layer with a starting formation of a crenulation cleavage.

5.1.2 Petrography of the metavolcanic rocks

The volcanic rock unit at Mustajärvi consists of ultramafic lavas (komatiites) and tuffs, komatiitic basalts, mafic lavas (tholeiites) and tuffs, and graphitic cherts. Alteration commonly makes it difficult to locally differentiate between the individual rock types. At the known mineralization, the volcanic unit occurs as 0.5-to 3-m-thick interlayers in the metasedimentary unit. With increasing proximity to the fault zone, which likely represents the general contact of volcanics and siliciclastic metasediments, layers of the volcanic unit get gradually thicker. The different rock types of the volcanic unit are interlayered with individual layers being 0.1 to 25 m in thickness, whereas more thicker layers are usually lavas and thinner layers are tuffs. During the first drilling campaign of FireFox Gold in the end of 2018, graphitic cherts have been observed to be tightly interbedded with altered mafic metavolcanic rocks near the interpreted overall contact zone of volcanic rocks and siliciclastic metasediments. The graphitic chert - mafic volcanic interlayering has a thickness of about 7 m and was observed in only one drill core. The graphitic cherts were not subject of further research in this thesis since the observation was made after the research part of the thesis work.

Based on thin section studies, the main mineral associations of the volcanic rocks are:

Komatiite: Tremolite + chlorite + talc + magnetite + chromite ± albite ± biotite ± calcite, rutile ± pyrite ± chalcopyrite ± pyrrhotite

Komatiitic basalts: Actinolite + Chlorite + Epidote + albite+ biotite + magnetite ± titanite ± pyrite ± chalcopyrite

Ultramafic metavolcanic rocks

Ultramafic metavolcanic rocks comprise komatiite lavas and ultramafic tuffs. The ultramafic tuffs occur as 0.1-to 1-m-thick interlayers both in (ultra) mafic lavas (Fig. 30) and in siliciclastic metasediments. The tuffs show a strong schistosity and are commonly strongly veined with quartz-albite-carbonate veins parallel to the schistosity (Fig. 31). The color of the ultramafic tuffs is generally distinctively darker than that of the ultramafic lavas. Unfortunately, the ultramafic tuffs have not been part of thin section studies since no representative sample was found during the initial thin section sampling.

The ultramafic lavas have a komatiitic geochemistry and occur as massive layers in the rock package with individual thicknesses up to 25 m. The texture is lepidoblastic with a

distinct foliation. The rock is dark in color with a distinct greenish tint (Fig. 32). The matrix is dominated by fine-grained subhedral to rarely euhedral tremolite (on average 45 vol. %) with an average grain size of 250 µm (Figs. 33 and 39) and abundant chlorite (35 vol. % on average) with slightly smaller grain sizes and subhedral to euhedral grain shapes (Figs. 33-35). Chlorite partly forms bands in the matrix causing a weak foliation (Fig. 33). With an increasing chlorite and talc concentration, the rock inhabits a moderate to strong schistosity. In some more primitive komatiites that resemble talc-chlorite schists chlorite dominates and forms a distinct schistosity. Occasionally, chlorite forms nest-like accumulations that may represent textures after primary olivine cumulates (Fig. 34). Pseudomorphic olivine cumulus grains can also rarely be observed macroscopically as dark clusters in the rock. Chlorite occasionally shows an overprint by biotite (Fig. 35). Magnetite occurs as thin veinlets that follow the direction of the foliation and are commonly accompanied by carbonate (Fig. 33). Carbonate makes up 5-10 % of the rock. There are also coarser-grained and more disseminated magnetite crystals that often show chromite remnants in their core (Fig. 36).

Different sulphide minerals occur as accessory minerals in the ultramafic rock. The most common sulphide is pyrite, which occurs both in early-stage calcite veining that follows the foliation, and more coarse-grained disseminated in the matrix, seemingly unrelated to carbonate veining. Enclosed in the latter larger pyrite grains that have average grain sizes of 1 mm are common chalcopyrite and rare pyrrhotite (Fig. 37). Chalcopyrite also occurs more rarely as individual grains in carbonate and quartz-albite veins together with pyrite. Early-stage carbonate veinlets are commonly completely overprinted by tremolite (Fig. 39), which is slightly coarser-grained than the matrix tremolite. Later stage carbonate veins are characterized by a richness of coarser-grained recrystallized matrix chlorite in the contact between veins and matrix.

Fig. 30. Drill core showing a 1-m-thick ultramafic tuff layer (bottom row) in a massive ultramafic lava. Drill core 18MJ013, depth 9-13 m.

Fig. 31. Drill core showing ultramafic tuff with a strong schistosity and intensive parallel quartz-albite-carbonate veining. Drill core 18MUS013, depth 12 m.

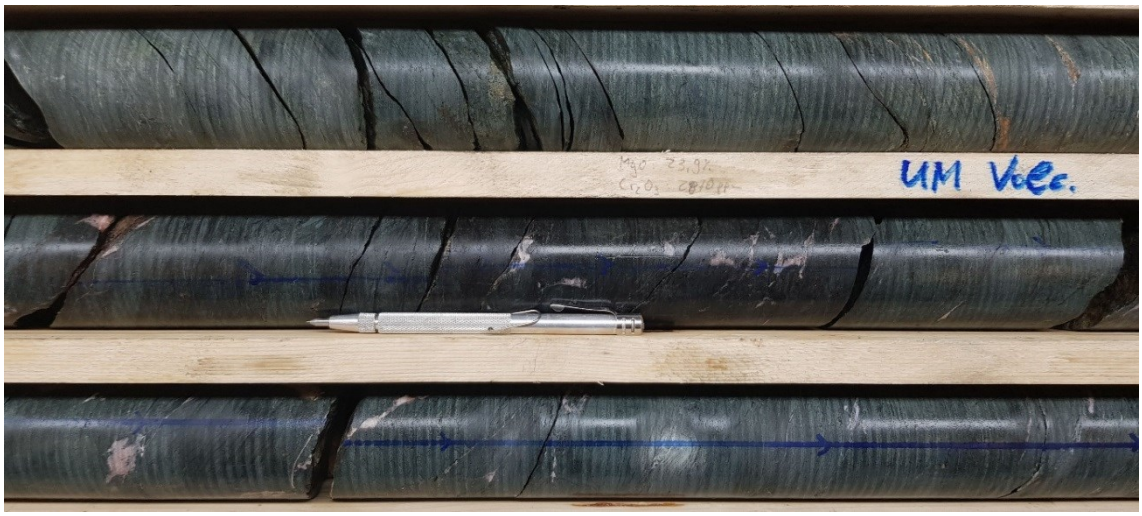

Fig. 32. Drill core showing massive ultramafic lava. The slightly darker interval in the center of the figure has a komatiitic basalt geochemical composition. Drill core 18MUS013, depth 24 m.

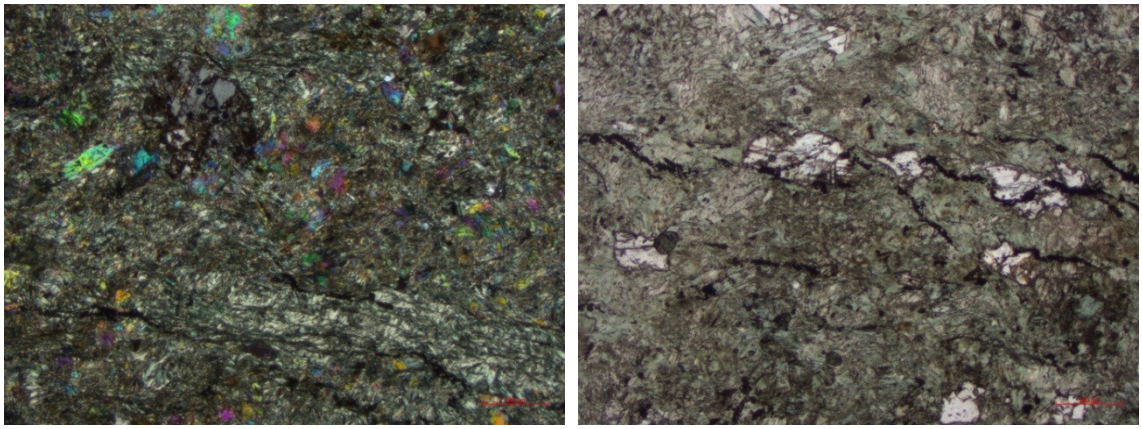

Fig. 33. Photomicrographs of ultramafic volcanic rock. Tremolite is dominating the matrix. Chlorite bands form a weak foliation in the rock, often accompanied by magnetite bands. Around large calcite grains grow more euhedral tremolite crystals. Thin magnetite bands occur along the foliation together with carbonate and chlorite. (Left) Crossed polarizers, field of view ~6 mm. (Right) Linear polarizers, field of view ~6 mm.

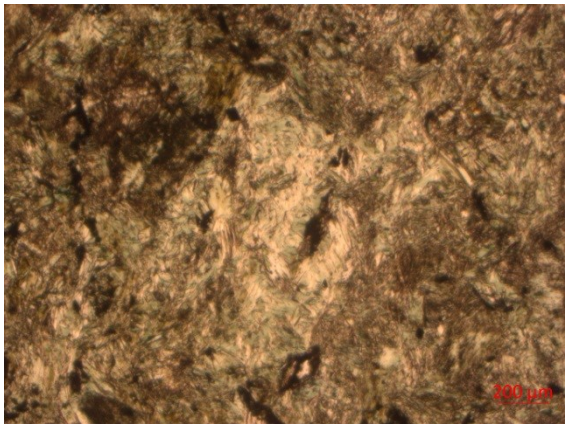

Fig. 34. Photomicrograph of ultramafic volcanic rock. Accumulations of nest-like chlorite might represent pseudomorphs after primary olivine clusters. Parallel polarizers, field of view ~2.4 mm.

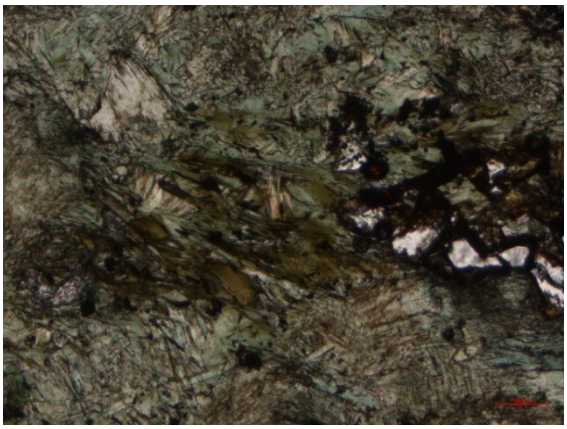

Fig. 35 Photomicrograph of ultramafic volcanic rock. Biotite overprint of Chlorite. Abundant rutile appears to be related to the biotite overprint. Parallel polarizers; field of view ~1.2 mm.

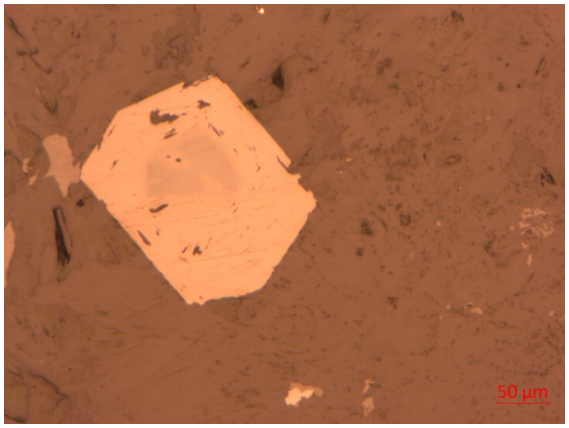

Fig. 36. Photomicrograph of ultramafic volcanic rock. Euhedral magnetite crystal with a core consisting of chromite. The magnetite grains are disseminated in the matrix. Reflected light, field of view ~0.6 mm.

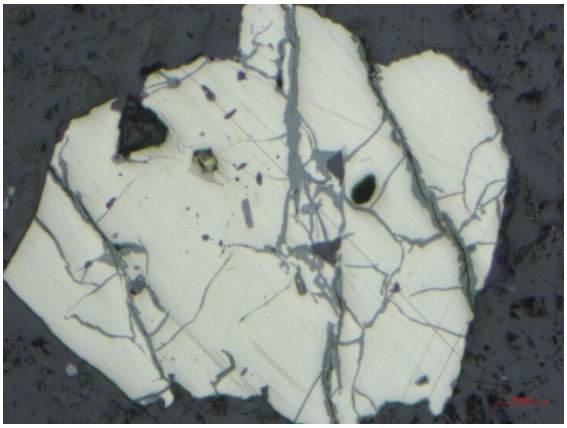

Fig. 37. Photomicrograph of ultramafic volcanic rock. Partly oxidized, pyrite crystal with small inclusions of chalcopyrite and pyrrhotite. Reflected light, field of view ~2.4 mm.

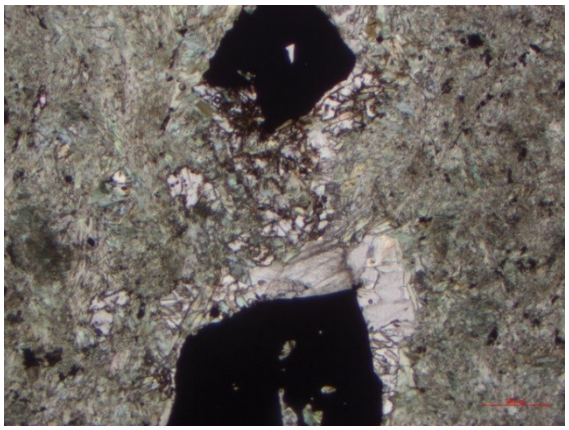

Fig. 38. Photomicrograph of ultramafic volcanic rock. Calcite veining with large pyrite crystals. The carbonate vein gets overgrown by more euhedral tremolite. Parallel polarizers, field of view ~6mm.

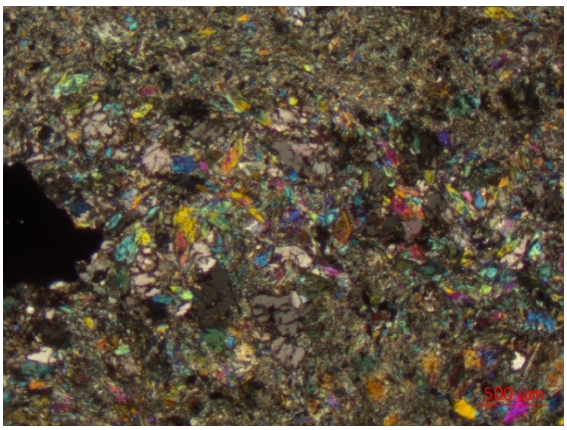

Fig. 39. Photomicrograph of ultramafic volcanic rock. Euhedral tremolite, with larger grain sizes, overprinting early stage calcite veinlets. Crossed polarizers, field of view ~6 mm.

Komatiitic basalts

Komatiitic basalts are the least common rock type of the volcanic rock unit. Similar to the komatiites, they occur as massive layers in the rock package with thicknesses of up to approx. 15 m. Moreover, they can occur as gradual interlayers in the ultramafic lavas (Fig. 32). The color of the rock is generally darker and does not have a distinct greenish tint like the komatiites (Figs. 32 and 40).

The komatiitic basalts have a lepidoblastic texture with a weak to distinct foliation, whereby no schistosity has been observed. The petrography of the komatiitic basalt is different to the komatiites, with actinolite being the dominant amphibole instead of tremolite, which explains the color difference to the ultramafic rock. Actinolite is fine grained, fibrous and subhedral and is dominating the matrix. Abundant chlorite is again forming a weak foliation in the rock. Furthermore, the komatiitic basalts contain abundant epidote, commonly along smallish veins together with chlorite and magnetite (Fig. 41), but also disseminated in the matrix (Fig. 42). Rare titanite occurs as accessory mineral.

The rock has abundant early stage quartz-plagioclase veins. These veins are often sheared along magnetite bands in the direction of the foliation (Fig. 43). Commonly, they are reopened or overprinted by later stage carbonate ± pyrite + chalcopyrite veins whose contacts are characterized by large euhedral chlorite-biotite crystals (Fig. 44). In the contact zones of large veins, euhedral and coarse-grained amphibole is formed (Fig. 45).

Fig. 40. Drill core showing least altered komatiitic basalt (dry surface). Drill core MJ-6, depth 15.7 m.

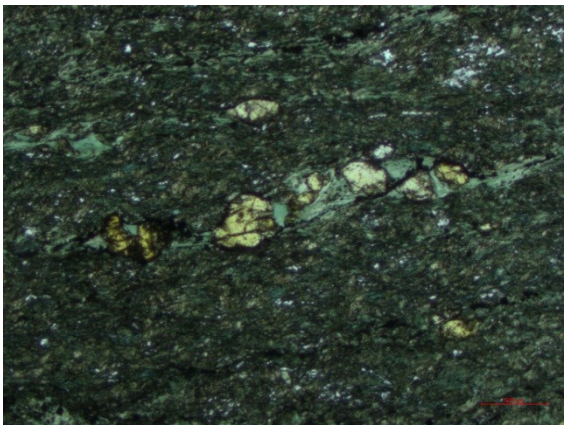

Fig. 41. Photomicrograph of komatiitic basalt. Coarse grained epidote associated with chlorite and magnetite. Parallel polarizers, field of view ~6 mm.

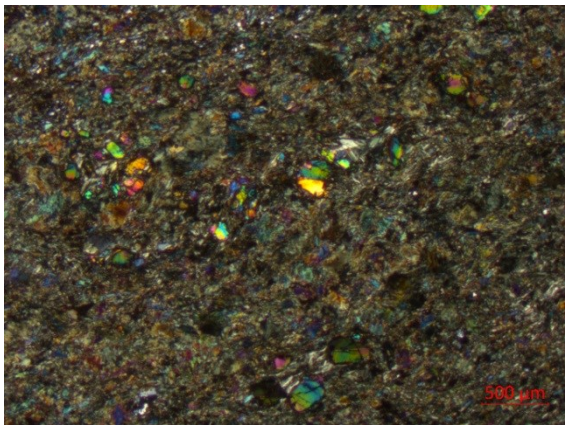

Fig. 42. Photomicrograph of komatiitic basalt. Epidote disseminated in the matrix. Crossed polarizers, field of view ~6 mm.

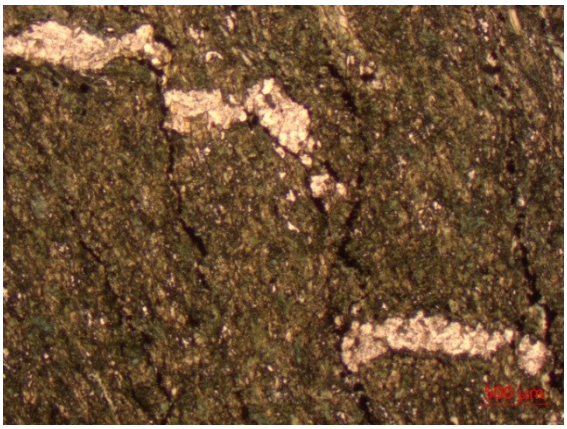

Fig. 43. Photomicrograph of komatiitic basalt. Early stage qtz-plag veins are getting displaced along thin magnetite bands that follow the foliation. Parallel polarizers, field of view ~6 mm.

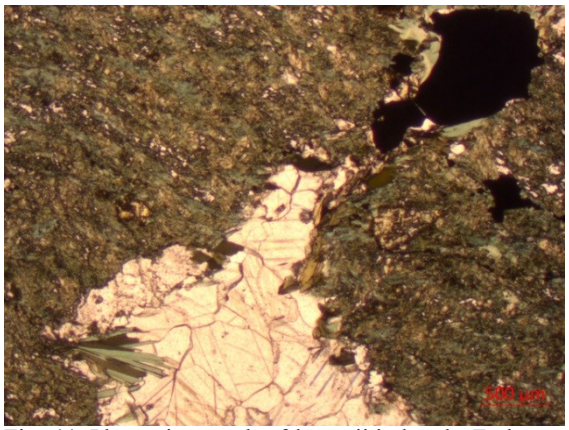

Fig. 44. Photomicrograph of komatiitic basalt. Early stage qtz-plag vein getting overprinted by coarse-grained euhedral carbonate. On the contacts of vein and matrix are euhedral biotite-chlorite crystals. Parallel polarizers, field of view ~6 mm.

Fig. 45. Photomicrograph of komatiitic basalt. Quartz-plagioclase vein with coarse grained euhedral amphibole in the contact zone. Parallel polarizers, field of view ~6 mm.

Mafic metavolcanic rocks

Unfortunately, no thin section studies of the mafic metavolcanic rocks were conducted since during the initial sampling campaign, mafic metavolcanic rocks were only found as angular boulders at the Mustajärvi property. Firefox's first drilling campaign at Mustajärvi confirmed the mafic metavolcanic rocks to be part of the volcanic rock unit at the Mustajärvi study site, comprising mafic lavas and mafic tuffs.

The mafic lavas occur as massive units with thicknesses of more than 17 m. Macroscopically, the rock inhabits a massive texture with a weak foliation (Fig. 46). In most cases, the rock is highly magnetic, which represents an effective tool to distinguish

between komatiitic basalts and mafic lavas, since the komatiitic basalts are only weakly magnetic.

The mafic tuff layers are usually thinner than the lavas and not as massive, with individual layer thicknesses ranging from 0.1 m to 5 m. The tuffs are tightly banded, consisting of a mafic matrix, which is interbedded with lenses or bands made of albite and quartz (Figs. 47 and 48). Occasionally, these bands and lenses are deformed and reoriented. In one drill core, at intersects near the general contact zone of siliciclastic metasediments and volcanics, altered mafic tuffs show an intense interbedding with graphitic cherts (Fig. 48) over an interval of approx. 7 m. The graphitic chert interval generally appears as a zone of strong deformation and shows cross-cutting veining by pyrite-rich quartz-albite ± carbonate veins, with pyrite and carbonate commonly being oxidized (Fig. 48). Graphite occurs in graphite-rich bands with thicknesses of more than 0.3 m (Fig. 48).

Fig. 46. Drill core showing massive mafic lava. Drill core 18MUS013, depth 36 m.

Fig. 47. Drill core showing a strongly banded mafic tuff layer. Perhaps a zone of strong deformation. Drill core 18MUS013, depth 131 m.

Fig. 48. Drill core showing interbedded mafic tuff and graphitic chert. The mafic tuff in the top row shows albite and quartz veins in a mafic matrix and is most likely a zone of strong deformation. The unit is strongly veined with pyrite rich quartz-albite-(carbonate) veins, that are commonly oxidized. The bottom row comprises abundant graphite that is broken up, unlike the rest of the core. Drill core 18MUS013, depth 45 m.

5.2. Alteration

5.2.1 Regional alteration

The degree of regional alteration is generally high in the Honkavaara Formation metasediments and weak to moderate in the Savukoski volcanic rocks (Lehtonen et al. 1998). It mainly consists of an overall moderate to strong albitization, mostly in the metasediments, and a weak to strong carbonate overprint in both rock units. Furthermore, abundant very early-stage quartz-albite veins, commonly with a carbonate overprint and early-stage carbonate veins occur in all host rocks.

Siliciclastic metasediments

Regional alteration in the siliciclastic metasediments consists of an overall moderate to strong albitization, a moderate carbonate overprint and a minor sericitization. Regional albitization caused the replacement of all feldspars by albite, which make up 20-60 % of the rock (see Chapter 5.1.1) and furthermore caused an enrichment of sodium in strongly albitized rocks. This resulted in a strong beige to pinkish appearance of the altered rocks (Fig. 49). Thin section studies show that the regional carbonate overprint is pronounced in these strongly albitized rocks. Carbonatization is occasionally the strongest in the most intensively albitized rocks, however, this could not be identified as a common rule. Furthermore, regional albitization includes local albite micro-veinlets reminding of stockwork veining (Fig. 51), quartz-albite veinlets and abundant massive quartz-albite ± carbonate veins. The quartz-albite veinlets and the more massive veins show distinct bleached albitization halos in the metasedimentary host rock unit (Fig. 50) that is caused by a replacement of micas by albite. Additional to the albite enrichment, quartz-albite veins commonly relate to a moderate to strong silicification in the rock. This silicification correlates with albitization and occurs both as vein halos and as a pervasive alteration in brecciated, strongly veined rocks (Fig. 53). Regional silicification is thought to be minor, mostly caused by excess Si being released by regional alteration processes with a subsequent recrystallization of the Si as quartz, whereas the most strongly silicified rocks are thought to be part of an intermediate to proximal alteration zone related to mineralizing fluids. There appear to be many veining events at Mustajärvi, including multiple quartz-albite ± carbonate vein sets, and whereas some of these veins might be attributed to mineralization, some of them were likely formed during earlier-stage regional alteration. Some of the existing veins show narrow veinlets of tourmaline in the

contact zones of vein and host rock. More rarely, tourmaline veining can also be massive and strongly brecciate the host rock, which is likely related to mineralization processes.

Regional carbonatization is indicated by disseminated carbonate crystals in the matrix, usually making up 5-10 % of the rock mass, by abundant thin calcite veinlets and by massive quartz-albite ± carbonate veins. Carbonate clearly overprints the albitized matrix and is thought to be of a later stage than the albitization. Also in the massive quartz-albite veins, carbonate is mostly seen as an overprinting feature rather than being a primary component.

A weak sericite overprint, which can be observed in all studied samples, could also be attributed to regional alteration. The fine-grained sericite mainly grows in the grain boundaries of the quartz and albite matrix, but also occasionally weakly overprints the centers of albite and carbonate crystals, indicating the sericite alteration to be later stage. Furthermore, rarely weak to moderate scapolitization can be observed in the siliciclastic metasediments, occasionally related to veins (Fig. 52) but often also as dissemination in the matrix.

Fig. 49. Drill core showing regionally strongly albitized rock. Drill core 18MUS013 at depth 86 m.

Fig. 50. Drill core showing a quartz-albite vein with a distinct albitization halo in the least altered intermediate tuffites. Drill core 18MUS014, depth 127 m.

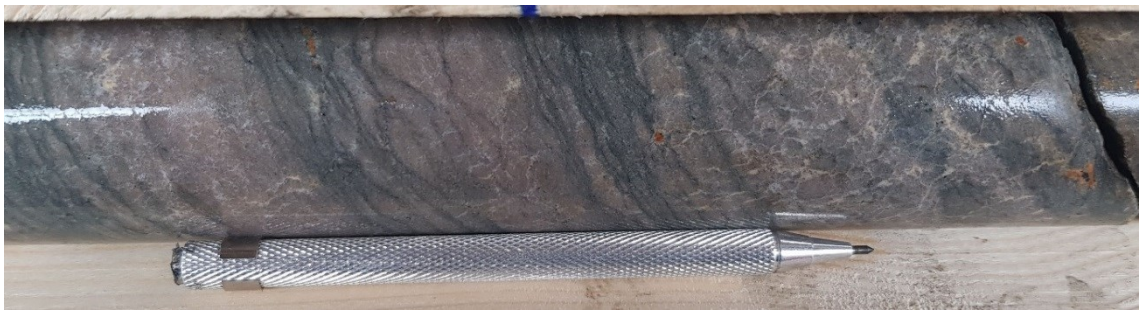

Fig. 51. Drill core showing least altered intermediate tuffite with thin albite micro veinlets in the more brittle parts of the rock. Drill core 18MUS013, depth 50 m.

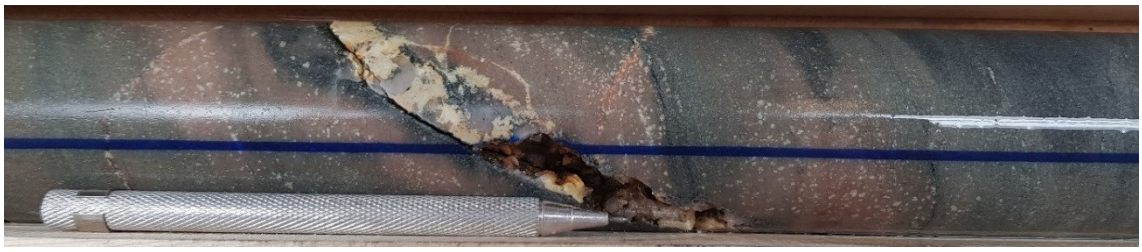

Fig. 52. Drill core showing scapolitization in weakly altered intermediate tuffite. Drill core 18MUS014, depth 143 m.

Mafic to ultramafic volcanic rocks

The metavolcanic rock unit is less affected by regional alteration compared to the siliciclastic metasediments. Alteration mostly includes the same early-stage quartz-albite veins with a carbonate overprint that occur in the metasediments. However, in the volcanic rocks, only very rarely a clear alteration halo can be seen. In most cases, these veins also have notable sulphide minerals, mainly pyrite, some chalcopyrite and minor pyrrhotite. Also abundant carbonate veins occur, mainly concordantly, in the rock.

Despite the observed weak regional alteration in the metavolcanic rock unit, the ultramafic tuffs are generally strongly altered. They show strong carbonate veining, with the matrix often being completely altered to biotite. Moreover, rare listvenites were observed in drill core as products of intense carbonate + potassic alteration in ultramafic tuffs. In most cases, listvenites occur in the contact zone between ultramafic tuffs and siliciclastic metasediments (Fig. 53). Listvenites are often referred to as “chromium marbles” in the local literature and are known to occur in several locations along the Sirkka line, e.g. at Hirvilavanmaa and Levijärvi-Loukinen (Holma & Keinänen, 2007). The listvenites at Mustajärvi mainly consist of fuchsite and carbonate, including calcite and dolomite-ankerite, and accessory minerals including chlorite, biotite, quartz, albite, rutile, pyrite and minor chalcopyrite. Despite the strong alteration intensity of the

listvenites, the rocks are considered to be have been generated by regional alteration, since the observed ultramafic tuffs near the known mineralization are not altered to this extent.

Fig. 53. Drill core showing ultramafic tuff (top row) in contact with albitized and silicified siliciclastic metasediments (bottom row). In the contact zone between the rock units occurs listvenite as a totally carbonate altered ultramafic tuff (middle row). Drill core 18MUS001, depth 63 m.

5.2.2 Alteration related to mineralization

Mineralization-related alteration halos in orogenic gold systems are commonly cryptic and less developed than in many other hydrothermal mineral deposits (Goldfarb et al., 2005). Especially in clastic metasedimentary host rocks, as at Mustajärvi, such alteration can be subtle due to a low reactiveness of the rocks (Goldfarb et al., 2005). Due to an overall strong regional alteration, the mineralization-related alteration is especially ambiguous at Mustajärvi and is mostly difficult to determine. Moreover, there appear to be different mineralization styles at Mustajärvi, with each of them having individual alteration assemblages. Figure 54 gives a unified overview of the spatial alteration sequence related to ore-forming fluids that is distinctively different from regional alteration and generally applies to most mineralization styles.

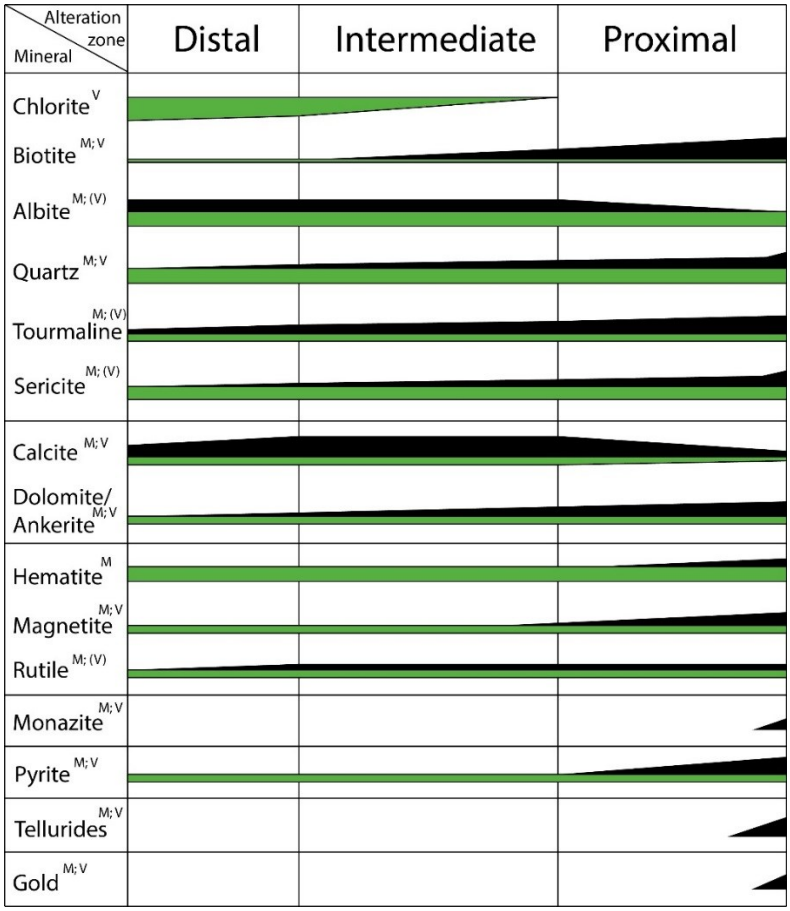

Fig. 54. Schematic overview of the paragenetic alteration sequence around the known mineralization at Mustajärvi. The letters M and V stand for metasediments and volcanic rocks, respectively, indicating in which rock unit the alteration occurs. Black represents alteration that is most likely related to mineralization; green represents regional background alteration. The data is based on drill core observations. The proximal zone ranges from 0-5 m distance to mineralization, the intermediate zone from 5-25 m and the distal zone from 25 m to 100 m.

Albitization

The degree of mineralization-related albitization is ambiguous due to the siliciclastic metasediments being locally strongly albitized through regional alteration throughout the rock package. However, it is evident that the metasediments in the proximal alteration zone are in all cases strongly albitized (Figs. 56 and 57). This is emphasized by outcrop observations and shallow-depth drill core intercepts, which show a total kaolinization in the proximal surroundings of the mineralization (kaolinization mainly replaces the feldspars in the rock, whereas quartz remains unaffected) (Figs. 98 and 101). Furthermore, quartz-albite veining appears to increase with a decreasing distance to mineralization. The veining increases in vein sizes, alteration halos and abundancy. Whereas regional albite-quartz veins are mostly parallel to the foliation, possible mineralization related quartz-albite veins often cut across the foliation (Fig. 55).

Silicification

The host rocks at Mustajärvi are regionally weakly silicified, with the degree of silicification mostly strongly correlating with the degree of albitization. Silicification occurs as alteration halos around quartz- and quartz-albite veins and is locally pervasive in strongly veined and brecciated rocks. In general, the silicification increases with a decreasing proximity to the mineralization, however the degree of it varies strongly. Some mineralization intervals were observed to exhibit no substantial amounts of silicification, not even increased amounts of quartz veins (Fig. 56), whereas other mineralization types show intense silicification in their proximal alteration zone comprising a pervasive quartz overprint in the matrix, which is often recognizable by a red-colored staining of the matrix likely due to oxidation of Fe-oxide inclusions in quartz grains (Fig. 57). These distinct alteration features do not only occur in the siliciclastic metasediments but also more rarely in the volcanic rock unit (Fig. 58).

Fig. 55. Drill core showing a cross cutting quartz-albite vein albitizing the siliciclastic host rock. Drill core MJ-5, depth 45 m.

Fig. 56. Drill core showing massive pyrite mineralization in strongly albitized intermediate tuffite. The mineralization is atypically poor in quartz and general silicification. This intersection grades 2 m at 45.1 ppm Au. Drill core 18MUS010, depth 126 m.

Fig. 57. Drill core showing tourmaline-rich pyrite mineralization in intensively silicified intermediate tuffite. The mineralization itself lacks quartz veining, but the silicification is very strong. Drill core 18MUS014, depth 90 m.

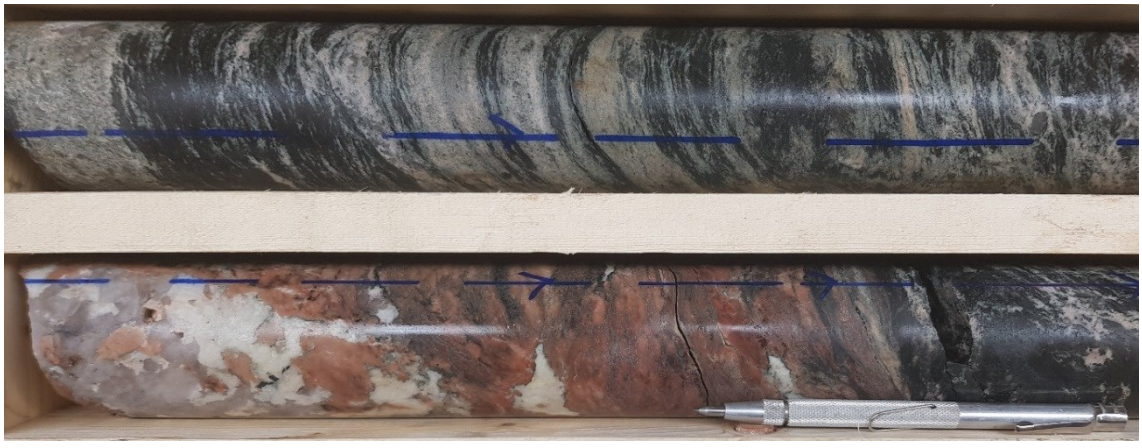

Fig. 58. Drill core showing a massive quartz-albite vein silicifying and albitizing the mafic tuff host rock. Drill core 18MUS013, depth 128 m.

Carbonatization

Regional alteration-related carbonatization most likely consists of an early-stage carbonate overprint of the matrix, including early-stage, mostly concordant quartz-albite-carbonate veins. In the distal to intermediate alteration zone, additional quartz-calcite-

(tourmaline) veins can be observed, which clearly cut across earlier, regional alteration-related veins. In the intermediate to proximal alteration zone, the dominant mineralization-related carbonate mineral changes slightly from calcite to dolomite and ankerite, whereby calcite usually remains a major constituent of the vein. Dolomite/ankerite veins are usually thicker and more dominant than the calcite veins, and the individual ankerite-dolomite crystals have larger grain sizes than calcite. Mineralization-related carbonate veins are, furthermore, thought to be less foliation-parallel and more cross-cutting than regional alteration veins (Fig. 59). In some parts, a very strong carbonatization completely overprints the host rock, giving it a conglomerate-like appearance by overprinting all matrix minerals except for quartz (Fig. 60). Commonly these total carbonatization intervals go in hand with other strong alteration features, such as intense tourmalinization (Fig. 69) or albitization. In most cases, carbonatization is associated with albitization, with the correlation weakening in close proximity to the mineralization. In most mineralization types, the degree of carbonatization is the strongest at the boundary between intermediate and proximal alteration zone at a distance of approx. 5-15 m from the mineralization. In proximity to mineralization (<5 m), carbonatization appears to seize, both in siliciclastic metasediments and metavolcanic rocks.

In the volcanic rock unit, the carbonatization is generally stronger. Intense carbonate-(quartz) stockwork veining is frequently observed in pervasively altered biotite rocks resulting in a pure biotite-carbonate-quartz rock (Fig. 61). Common calcite stockwork veining is seen to be overgrown by biotite (Fig. 62), whereas larger ankerite/dolomite veins clearly cross-cut zones of biotitization (Fig. 63). Previously described listvenites have not been observed in the proximal to intermediate alteration zone and are thus thought to be products of regional alteration related to strong faulting of the rock package. However, given the scarcity of drilling observations and the intensity of the alteration, it is possible that they are products of intermediate mineralization-related alteration.

Fig. 59. Drill core showing a massive cross cutting ankerite-dolomite vein in strongly albitized intermediate tuffite. Drill core 18MUS013, depth 102 m.

Fig. 60. Drill core showing a laminated ankerite-dolomite vein with quartz clasts which give the vein a conglomeratic appearance. A small late stage calcite vein is cutting the vein perpendicularly. Drill core MJ-9, depth 41.3 m.

Fig. 61. Grab sample of a strongly carbonatized ultramafic rock from the artisanal mining pit (sample MJ-1). The center of the sample mainly comprises stockwork calcite veining, whereas on the right part thicker ankerite/dolomite veining dominates that cross cuts the calcite veining. The matrix of the rock has been pervasively altered to biotite.

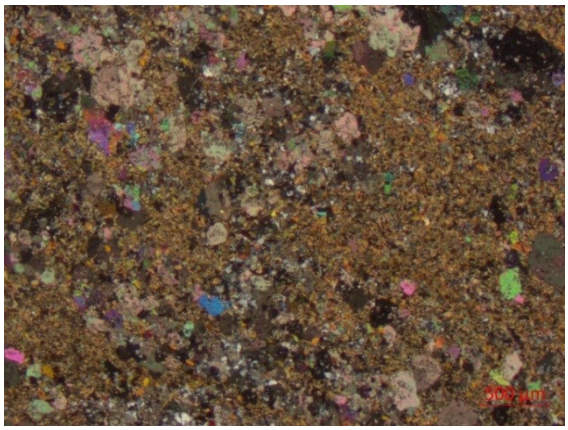

Fig. 62. Photomicrograph of carbonatization. Matrix of stockwork calcite veining and biotite. No cross cutting of the veins with biotite was observed Microscopic view of Fig. 61. Crossed polarizers, field of view ~6 mm.

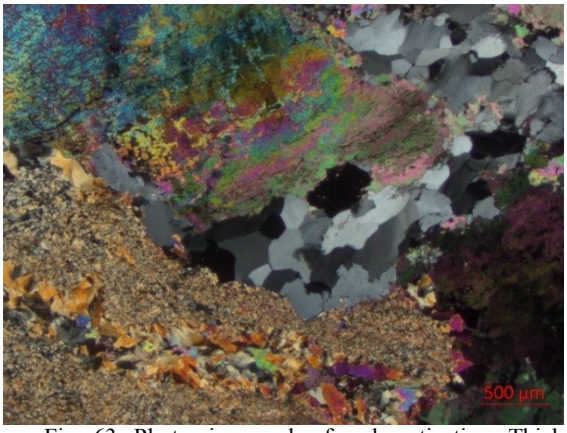

Fig. 63. Photomicrograph of carbonatization. Thick ankerite/dolomite-quartz veining is clearly cross-cutting biotite that forms the matrix. Biotite is locally observed to be recrystallized in the contact zone of biotite and vein (see bottom of the picture). Microscopic view of Fig. 61. Crossed polarizers; field of view ~6 mm.

Biotitization

Biotitization related to mineralization occurs both in the siliciclastic metasediments and in the metavolcanic rocks. In the metavolcanic rocks it mostly consists of a pervasive alteration from chlorite to biotite, typically associated with intense carbonate-(quartz) veining (Figs. 61-63). This pervasive biotitization in the metavolcanic rocks is believed

to be an intermediate to proximal alteration feature. In the metasediments, biotite enrichment occurs as biotite stringers, which have no apparent main orientation (Fig. 64), and as disseminated biotite in the matrix, which is easily distinguishable as dark spots in a bleached matrix (Fig. 65). However, in both features, biotite can be easily mistaken as tourmaline. Biotitization in siliciclastic metasediments has been observed to be restricted to the proximal alteration zone, making it a useful tool to predict nearby mineralization.

Fig. 64. Drill core showing biotitization. The top row shows relatively unaltered intermediate tuffite outside of the proximal alteration zone. The bottom row shows the onset of the proximal alteration zone with strong biotitization. The rock appears bleached and shows intense biotite stringers. Drill core 18MJ010, depth 122.4 m.

Fig. 65. Dill core showing biotitization. Both rows show gold mineralized intermediate tuffite that is strongly enriched with biotite, which occurs as biotite stringers (e.g. top row on the left) and disseminated in the host rock matrix that is distinguishable as dark spots in a bleached matrix (e.g. bottom row on the left). Drill core 18MJ010, depth 126.5 m.

Sericitization

The host rocks generally show a minor sericite overprint related to regional alteration. With increasing proximity to mineralization, in the intermediate to proximal alteration zone sericitization can increase to a strong and pervasive alteration feature (Fig. 66). In these parts, albite and carbonate minerals in the host rocks matrix are partly altered to

sericite. Sericitization often terminates in the immediate surroundings of mineralization. The strongly sericitized rocks macroscopically appear dull greyish and have a decreased hardness. In the immediate vicinity to thin barren quartz-pyrite veins, the rocks that appear macroscopically non-sericitized also show an increased sericite overprint on a microscopic scale.

Fig. 66. Drill core showing a weakly altered and veined intermediate tuffite (top row) being affected by strong sericitization (bottom row). Original albite- and carbonate-bearing veins have been mostly weathered away in the sericitized part. Drill core 18MUS013, depth 113 m.

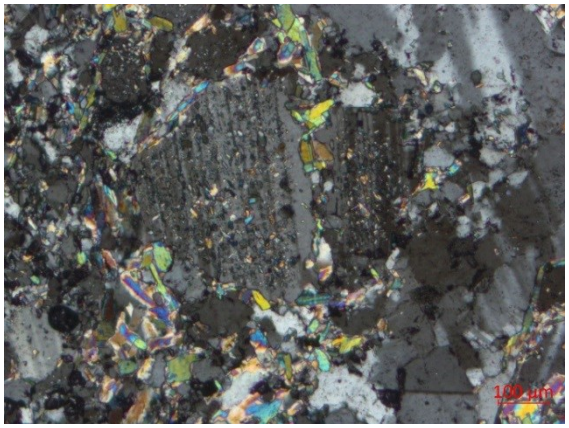

Fig. 67. Photomicrograph of sericitization. Weak to moderate sericitization with relatively coarse-grained sericite overprinting the matrix grain boundaries as well as the cores of albite crystals. Crossed polarizers, field of view ~1.2 mm.

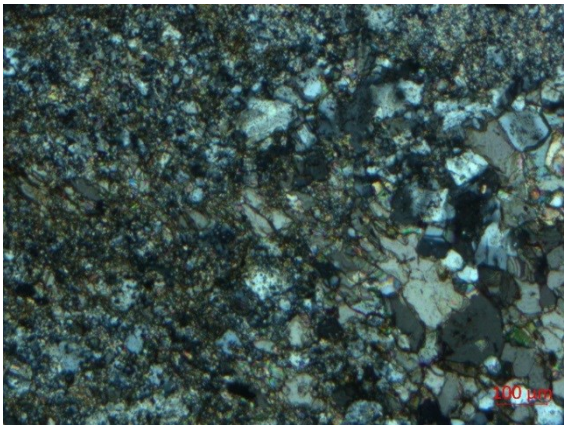

Fig. 68. Photomicrograph of sericitization. Proximal alteration zone with intense and pervasive sericitization overprinting albite and carbonate minerals in the matrix (on the left side), whereas coarser-grained, vein-related albite and carbonate is mostly not overprinted. Crossed polarizers, field of view ~6 mm.

Tourmaline enrichment

Thin tourmaline veinlets, often in the contact zone between quartz-albite veins and host rocks, occur throughout the host rock units. It is unclear whether these veins are caused by regional alteration or are a distal alteration zone feature related to mineralizing fluids. It is evident however, that tourmaline veining gets more abundant and more massive with increasing proximity to the mineralization where it can be a major constituent of the auriferous pyrite mineralization (Figs. 57 and 76). In extreme cases, tourmaline veins are observed to completely brecciate the host rocks (Fig. 69). Elevated amounts of tourmaline are in most cases observed in association with other alteration processes, such as albitization, strong carbonate veining (Fig. 70), intense sericitization, pyrite enrichment and silicification. The temporal association of tourmaline is ambiguous and unclear as it is often seen overprinting other alteration types, but multiple stages of tourmaline veining during ore formation are assumed. It is furthermore assumed that tourmaline-bearing quartz and carbonate veins are more likely to be related to mineralization than non-tourmaline-bearing ones, as indicated by tourmaline bearing veins commonly cutting across earlier non-tourmaline-bearing veins.

Fig. 69. Drill core showing a massive tourmaline vein brecciating a strongly albitized intermediate tuffite host rock (top row). In the center of the bottom row, massive tourmaline in totally altered mafic host rock (left), with a totally carbonated zone on the right. Drill core 18MUS013, depth 174 m.

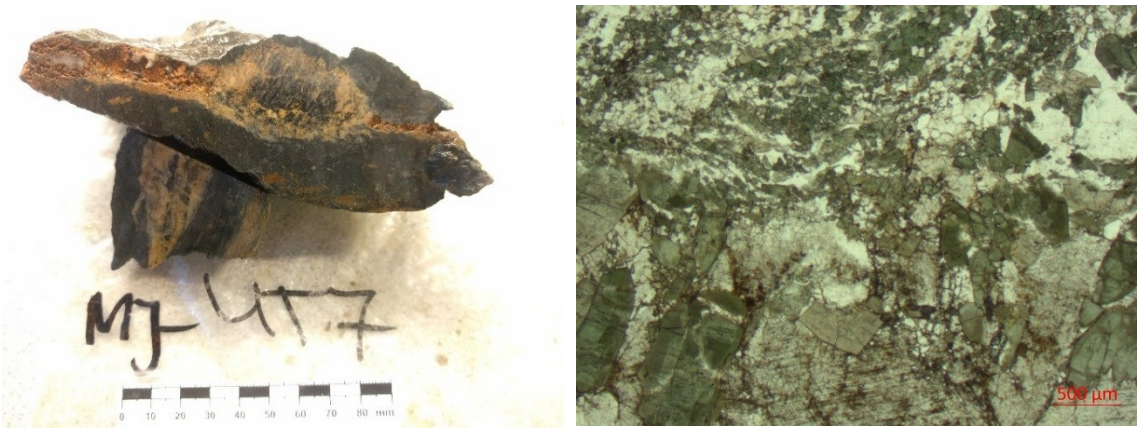

Fig. 70. Tourmaline enrichment. (Left) Grab sample of a mafic tuffite with strong carbonate-tourmaline veining, collected from a trench near the artisanal mining pit (sample MJ-UT7). (Right) Photomicrograph of tourmalinization (microscopic view of sample MJ-UT7 (Left)). Tourmaline (green) is not only present in the carbonate vein (bottom of the picture), but also occurs abundantly as finer grains in the quartz-dominated matrix of the host rock (top part). Parallel polarizers, field of view ~6 mm.

Veining

Within the intermediate to proximal alteration zone, barren quartz-pyrite ± albite-carbonate veins are typical, with pyrite amounting up to 75 % of the vein (Figs. 71 and 72). The host rocks of the veins rarely show similar alteration features as the mineralized veins, including intense silicification. Occasionally, gold is clearly anomalous in the pyrite-bearing veins with concentrations up to 0.4 ppm Au and 4 ppm Te. These anomalous Au and Te concentrations are thought to be another indicator for proximal mineralization. Coevally with quartz-pyrite veins, quartz ± carbonate ± albite ± tourmaline veins are increasingly enriched from the distal to the proximal alteration zone. Similar veins were formed during regional metamorphism, however clear cross-cutting relationships show that many quartz veins, often with abundant tourmaline, are of a later stage and most likely related to the mineralization event. Furthermore, multiple quartz veining phases during the mineralizing event with complex cross-cutting relationships are likely.

Another indicator of mineralization is the presence of magnetite-pyrite-carbonate veining that occasionally occurs in the proximal alteration zone (Fig. 73). These veins can be either barren, anomalous for gold or clearly mineralized. Also hematite-pyrite-quartz veins with anomalous gold concentrations of up to 0.3 ppm Au were observed in proximity to the mineralization (Fig. 74).

Fig. 71. Drill core showing a typical barren quartz-pyrite vein with proximal alteration zone. Drill core MJ-7, depth 30 m.

Fig. 72. Drill core showing a massive pyrite vein with only little quartz, yielding a gold value of 0.37 ppm Au. Drill core MJ-9, depth 50.9 m.

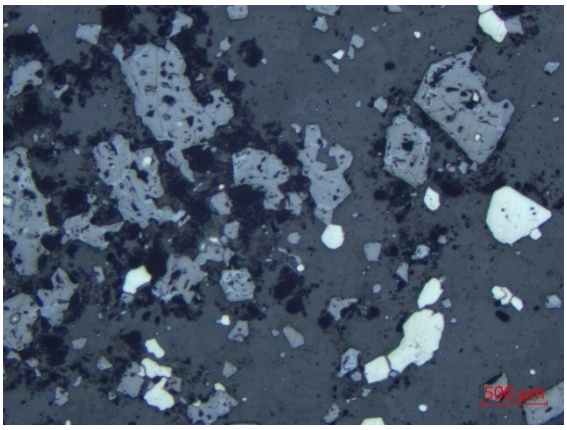

Fig. 73. Magnetite-pyrite-carbonate vein. (Left) Drill core showing a magnetite-pyrite-carbonate vein in the proximal alteration zone. This sample is not anomalous for gold, however other magnetite-pyrite veins have been reported to be clearly mineralized. Drill core MJ-4, depth 35.78 m. (Right) Photomicrograph of magnetite-pyrite-carbonate vein (microscopic view of left figure) In bright grey is pyrite, in moderate grey is magnetite, with a dark grey matrix of carbonates. Reflective light, field of view ~6 mm.

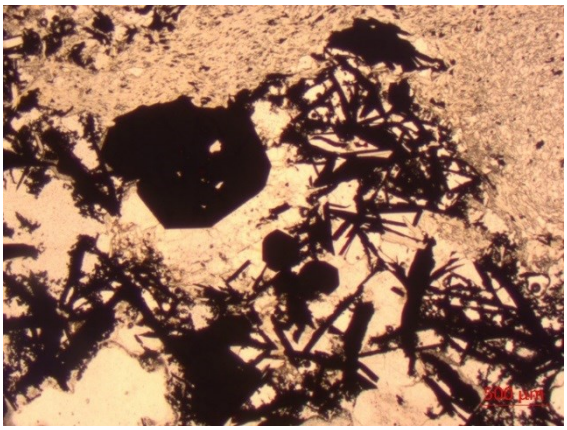

Fig. 74. Quartz-hematite-pyrite vein. (Left) Drill core sample showing a quartz-hematite-pyrite vein in the intermediate alteration zone, anomalous for gold and tellurium (0.28 ppm Au & 0.65 ppm Te). Drill core MJ-5, depth 52.86 m. (Right) Photomicrograph of quartz-hematite-pyrite vein (microscopic view of left figure). Hematite needles with euhedral pyrite and quartz in a lepidoblastic matrix of muscovite. Parallel polarizers, field of view ~6 mm.

6. MINERALIZATION

6.1. Petrography of the mineralized veins

The petrographic observations of the mineralization are mainly based on grab samples from the artisanal pit, since these samples were the basis for the thin section study. The entire historical drill core related to the gold system has been re-assayed by Outokumpu, resulting in a complete loss of the mineralized core. However, preliminary observations from the first FireFox Gold drilling campaign confirm the surface mineralization at depth and further indicate that different styles of mineralization exist.

The outcropping mineralization at Mustajärvi consists of quartz-pyrite-tourmaline veins that show typical pinch and swell features. The microprobe work of this study shows that gold within the veins occurs as Au-(Bi)-telluride micro-inclusions in pyrite and as likely remobilized free gold. Pyrite makes up 5 to 25 % of the veins (Figs. 75-78). The amount of tourmaline varies strongly and ranges from ~5 % to as much as ~35 % of the vein volume. Accessory minerals are white mica and rare monazite. In addition to Au-(Bi)-tellurides, the veins contain a wide array of telluride minerals including Ni-tellurides, Bi-tellurides and Se-Bi-tellurides.

The surface grab samples are partly heavily weathered, which has resulted in oxidation of pyrite to goethite causing a remobilization and possible enrichment of gold due to a loss of rock volume. Other supergene processes include strong kaolinization of the veins and the proximal host rock, and the formation of Mn-weathering crusts on the mineralized and barren quartz veins with MnO concentrations of up to 9.43 wt. % (see section 6.4).

During the first drilling campaign of FireFox Gold in December 2018, a high-grade mineralized zone was intersected at a vertical depth of approx. 90 m. The mineralized zone comprises a 2-m-wide interval of massive pyrite (up to 55 %) with only marginal amounts of quartz and relatively low tourmaline contents (Fig. 79). The pyrite zone is mainly oriented along the foliation of the intermediate tuffite host rock. This interval represents the highest-grade drill core intersection so far obtained at Mustajärvi with 2 m at 45.1 ppm Au. No thin section studies were performed on this new style of mineralization as it was discovered very recently. The following detailed descriptions solely concern the surface grab samples.

Quartz

Due to several recrystallization features, the primary grain sizes of quartz are difficult to determine. The present-stage quartz sizes range from 0.1 mm to 10 mm. Most quartz grains show at least one of several dynamic recrystallization features consisting of bulging recrystallization, grain boundary migrations with strongly lobate contacts (Fig. 80) and subgrain rotation (Fig. 81) including subgrain formation deformation lamellae (Fig. 82). All quartz grains display a strong undulose extinction, which varies from sweeping to patchy. Fully recrystallized quartz with 120° triple junctions was not observed. More rarely, in some parts of the veins, quartz does not show strong signs of recrystallization (Fig. 87).

Pyrite

Pyrite occurs in grain sizes ranging from 0.1 to 10 mm, with an average of ~2 mm. The shape of the grains is mostly subhedral, but also euhedral and anhedral pyrite can be observed. Most pyrite is hosted in the finer-grained, more deformed and recrystallized quartz parts and is only accessory in veins parts of larger quartz grains (Figs. 77, 83 and 84). Additionally, pyrite is generally closely associated with tourmaline. In tourmaline-enriched parts, in which tourmaline is overprinting the rock in a vein-like fashion, pyrite has significant amounts of euhedral tourmaline inclusions with almost every pyrite grain enclosing finer-grained tourmaline (Figs. 83-86). In some cases, tourmaline even makes up 75% of the entire pyrite grain (Fig. 85). The borders of strong tourmaline enrichment are quite sharp, with pyrite outside of the enrichment zone having almost no tourmaline inclusions (Fig. 86). The overprinting relationships of pyrite and tourmaline are ambiguous, and multiple events of pyrite and tourmaline formation are assumed. This is supported by the fact that tourmaline inclusions partly occur only in the center of the pyrite grain or only in the rims of pyrite, suggesting multi-stage growth of pyrite and multiple tourmaline enrichment events.

Tourmaline

Tourmaline has grain sizes between 20 μm and 250 μm with an average of 100 μm. It is mostly euhedral, but with smaller grain sizes commonly being anhedral. Similarly to pyrite, tourmaline only rarely occurs in coarse-grained, less-deformed quartz-rich parts. It usually occurs in thick vein-like bands spatially associated with pyrite. Moreover, tourmaline is observed to form fine-grained “nests” (Fig. 87) representing either a

pseudomorph after a different unidentified mineral or fine-grained, recrystallized tourmaline after itself.

Accessory minerals

White mica is a common accessory mineral in the mineralized veins. It occurs as subhedral inclusions in pyrite and more rarely as subhedral disseminated grains in the quartz matrix. In most cases, it is spatially associated with pyrite and tourmaline. It reaches grain sizes of 0.2 mm with an average of 0.1 mm. Some white mica grains, especially with larger sizes, are euhedral and appear to overprint the quartz matrix (Fig. 88). These grains are possibly a product of supergene processes.

Monazite is another accessory gangue mineral in the mineralized veins. It was only found in one sample (grab sample MJ-41). The monazite grains occur in a cluster with grain sizes of 0.1 to 0.5 mm (Fig. 89). The observed monazite clusters are spatially associated with tourmaline and oxidized pyrite. Monazite could potentially be used for further studies to date the mineralization event.

Telluride minerals

The mineralized quartz-pyrite-tourmaline veins encompass a wide range of telluride minerals, of which calaverite (Au-telluride) and montbrayite (Au-Bi-telluride) are gold bearing. Other non-auriferous tellurides are abundant melonite (Ni-telluride), kawazulite (Se-Bi-telluride) and tellurobismuthite (Bi-telluride). Based on the only limited microprobe study (69 measurements), the following non-statistical order of abundance was observed, starting with the most abundant mineral: montbrayite, melonite, calaverite, kawazulite, tellurobismuthite. The telluride mineral classifications are solely based on their chemical composition measured with quantitative microprobe analysis (Tables 5 and 6).

All telluride minerals occur as micro-inclusions in pyrite, with grain sizes of 1 µm to 10 µm. They are usually emplaced in strings or clusters in the pyrite grains (Figs. 90 and 91), with the exception of melonite, which occurs more commonly as a single grain disseminated in pyrite and also shows on average larger grain sizes than the other telluride minerals (Fig. 92). No spatial relationship, neither between the telluride minerals themselves nor between the tellurides and their location in the host pyrite grain, was observed.

Gold

For a detailed description of native gold in the mineralized veins and for further descriptions of the auriferous tellurides see Chapter 6.2.

Fig. 75. Grab sample of a relatively unoxidized quartz-tourmaline-pyrite vein grading 10.95 ppm Au (sample MJ-35). Sample width is approx. 15 cm.

Fig. 76. Grab sample of a tourmaline rich, oxidized quartz-tourmaline-pyrite vein grading 9.91 ppm Au (sample MJ-47). Sample width is approx. 15 cm.

Fig. 77. Grab sample of a tourmaline poor, quartz rich, strongly oxidized quartz-tourmaline-pyrite vein grading 63.8 ppm Au (sample MJ-27). Sample width is approx. 15 cm.

Fig. 78. Grab sample of a relatively tourmaline poor, moderately oxidized quartz-tourmaline-pyrite vein grading 14.75 ppm Au (sample MJ-34). Sample width is approx. 15 cm.

Fig. 79. Drill core showing a two-meter-thick drill intercept of high-grade pyrite mineralization (2 m at 45.1 ppm Au). The mineralization comprises only marginal amounts of tourmaline and quartz. Tourmaline occurs as small bands in pyrite. Drill core MJ010, depth 126 m.

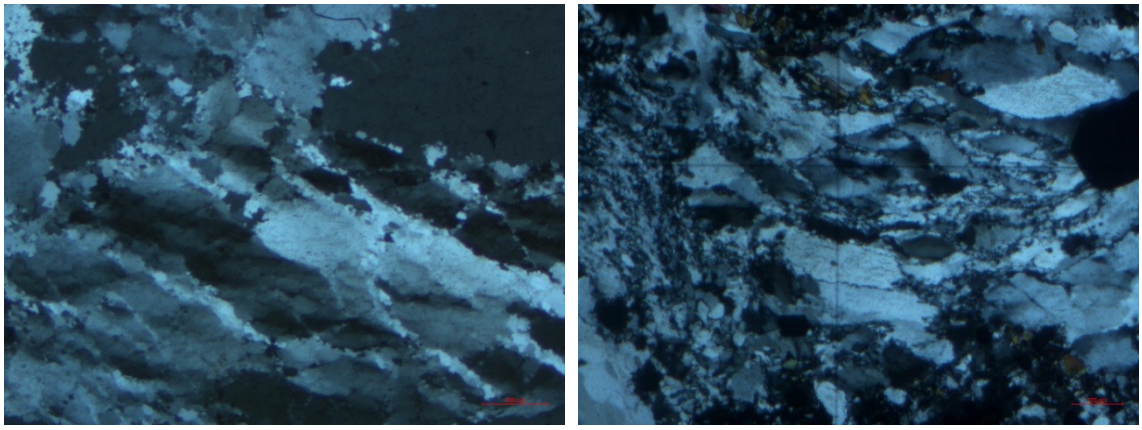

Fig. 80. Photomicrographs of dynamic recrystallization of quartz (Left) Dynamic recrystallization of quartz, consisting of bulging recrystallization with grain boundary migration with lobate contacts. In the center of the photograph, subgrain formation can be observed. The undulose extinction is in a transition between sweeping and patchy. Crossed polarizers; field of view ~6 mm. (Right) Dynamic recrystallization of quartz, consisting of grain boundary migration, bulging, and likely subgrain rotation in parts. Crossed polarizers; field of view ~2.4 mm.

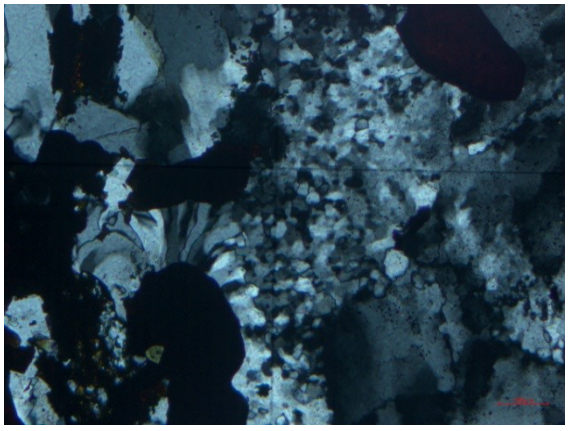

Fig. 81. Photomicrograph of dynamic recrystallization of quartz due to subgrain rotation. The undulose

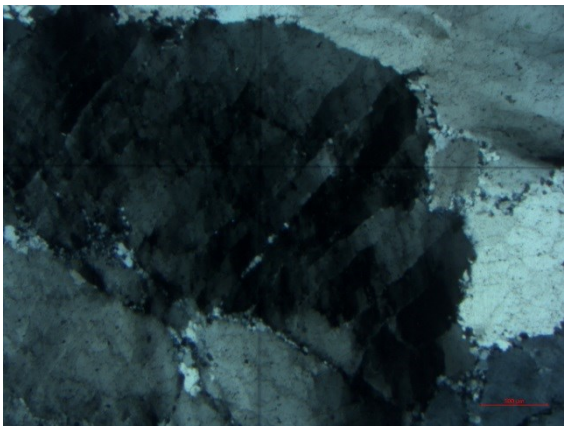

Fig. 82. Photomicrograph of deformation lamellae with elongated subgrains. The contacts of the quartz

extinction is mostly patchy. Crossed polarizers; field of view ~1.2 mm.

grain are lobate due to grain boundary migration. Crossed polarizers; field of view ~6 mm.

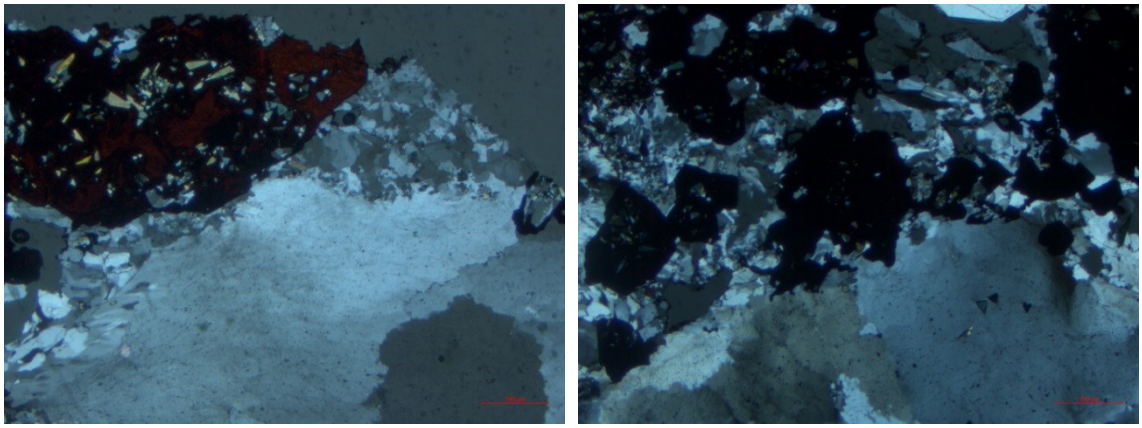

Fig. 83. Photomicrographs of pyrite and tourmaline in parts of finer-grained and more deformed and recrystallized quartz. Crossed polarizers; field of view ~6 mm.

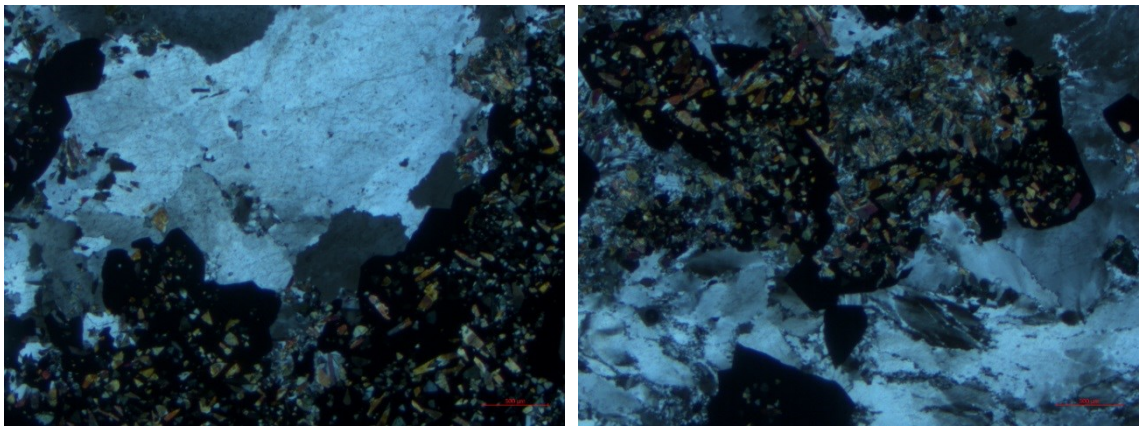

Fig. 84. Photomicrographs of pyrite and tourmaline being spatially closely associated. Only little tourmaline can be seen in the quartz-rich parts. Crossed polarizers; field of view ~6 mm.

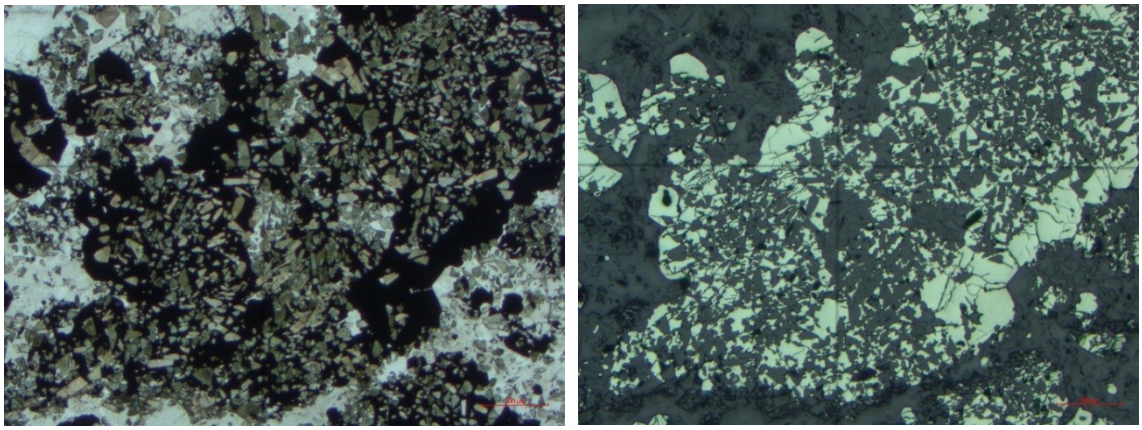

Fig. 85. Photomicrographs of tourmaline association with pyrite. (Left) Linear polarizers; field of view ~6 mm. (Right) Reflected light; field of view ~6 mm. Strong tourmaline (green-yellow in left figure; and grey inclusions in bright pyrite in right figure) enrichment in-pyrite rich parts of the mineralized vein.

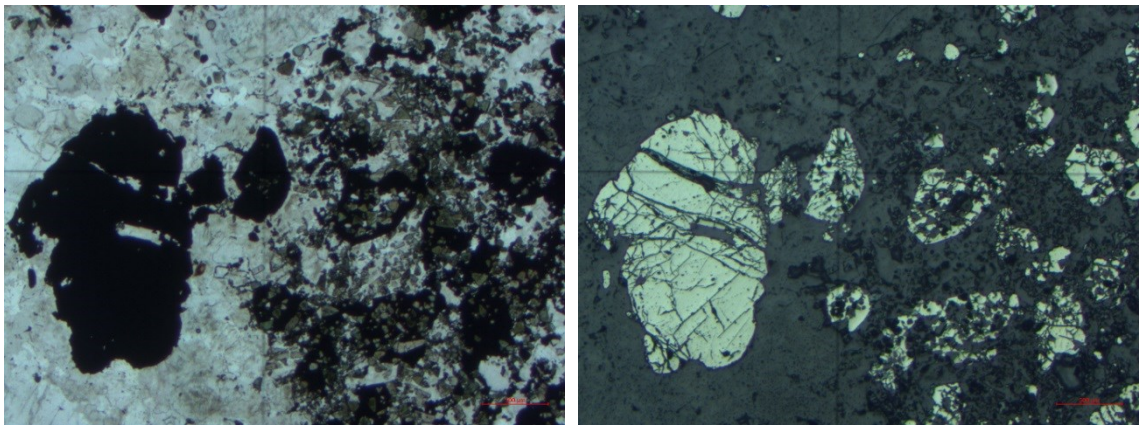

Fig. 86. Photomicrographs of tourmaline association with pyrite. On the right of the photographs, strongly tourmaline enriched part with pyrite of smaller grain sizes. On the left of the photograph, almost no tourmaline and the pyrite grain is larger, possibly indicating multiple stages of pyrite and tourmaline formation. (Left) Linear polarizers; field of view ~6 mm. (Right) Reflected light field of view ~6 mm.

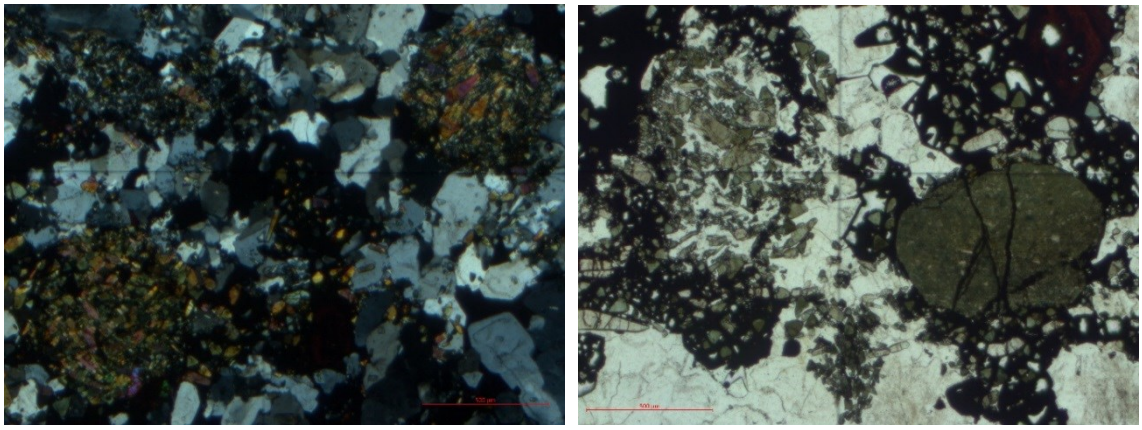

Fig. 87. Photomicrographs of pseudomorph clusters of tourmaline in a relatively undeformed quartz matrix. (Left) Crossed polarizers; field of view ~6 mm. (Right) Linear polarizers; field of view ~6 mm.

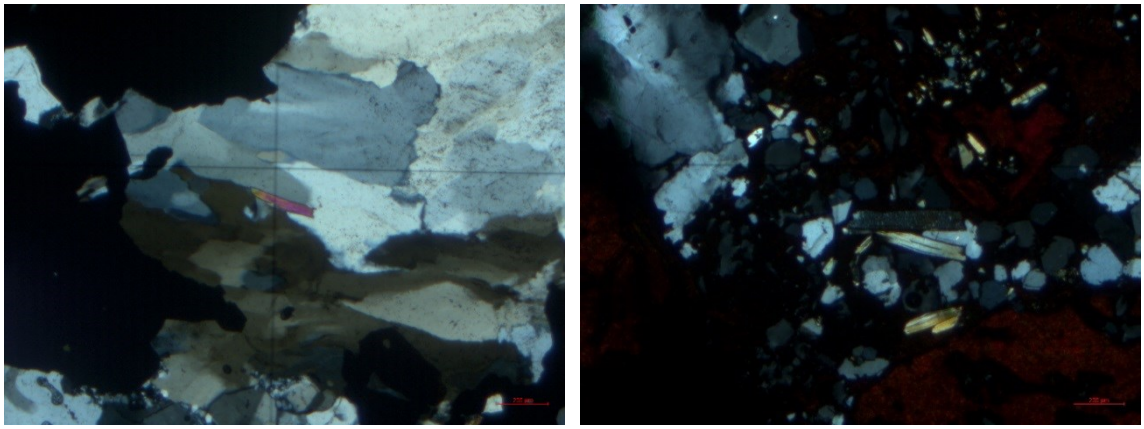

Fig. 88. Photomicrographs of accessory white mica. (Left) White mica in the quartz matrix. Quartz shows subgrain formation with a patchy undulose extinction. Crossed polarizers; field of view ~2.4 mm. (Right) Large euhedral white mica crystals, possibly related to supergene processes. Crossed polarizers; field of view ~2.4 mm.

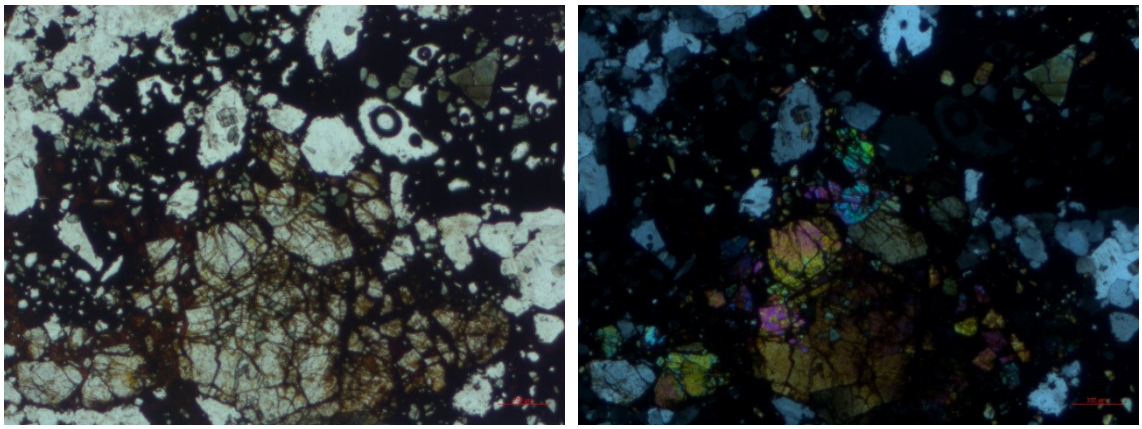

Fig. 89. Photomicrographs of monazite grain cluster, together with oxidized pyrite and tourmaline. (Left) Linear polarizers; field of view ~2.4 mm. (Right) Crossed polarizers; field of view ~2.4 mm.

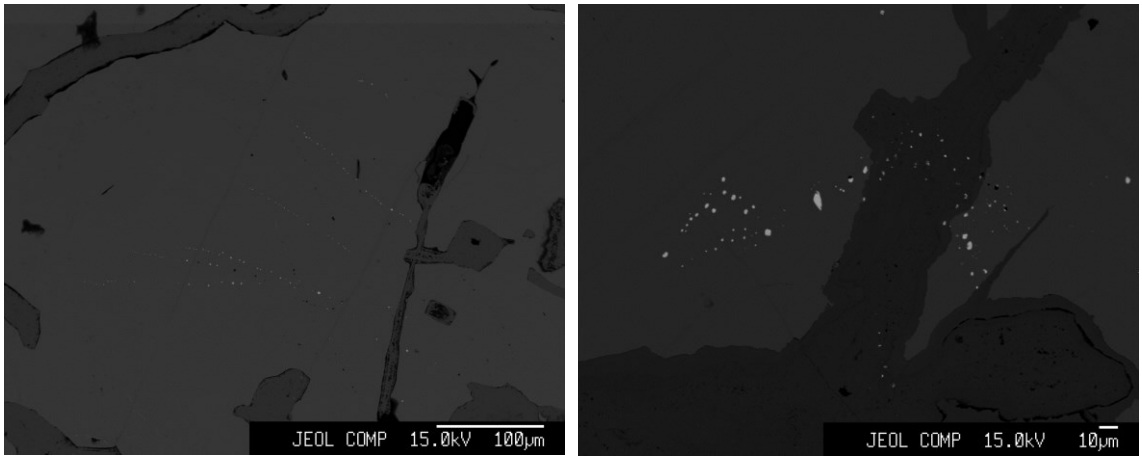

Fig. 90. Back-scattered electron images of telluride micro-inclusions in pyrite. (Left) Set of parallel strings of 1-5 µm large montbrayite (bright grey) micro-inclusions in unoxidized pyrite (medium grey). (Right) Cluster of montbrayite micro-inclusions in unoxidized pyrite and in oxidized pyrite (dark grey) in the center of the picture.

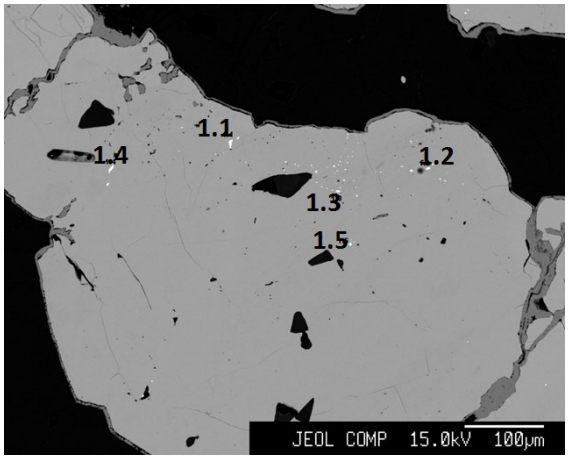

Fig. 91. Back-scattered electron image of telluride micro-inclusions in unoxidized pyrite. The telluride minerals are melonite (1.1), montbrayite (1.2 and 1.3), kawazulite (1.4), and calaverite (1.5).

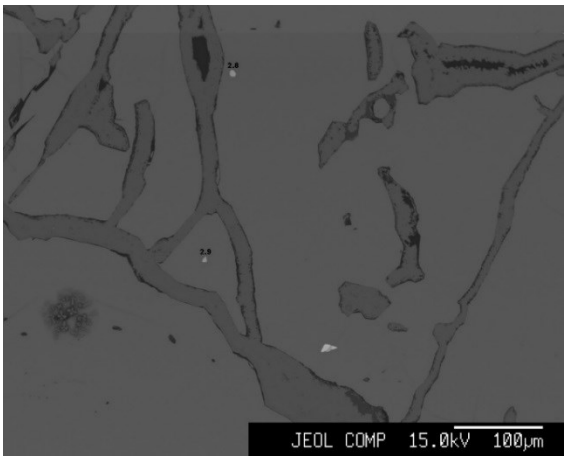

Fig. 92. Back-scattered electron image of single disseminated melonite micro-inclusions in the matrix of unoxidized pyrite, which is getting oxidized along cracks.

6.2 Gold mineralogy and distribution

All collected grab samples of auriferous quartz-pyrite-tourmaline veins have been affected by supergene processes to various degrees, hence it was impossible to study representative unweathered mineralization. The observations can thus vary from gold mineralization at depth.

As shortly described in the previous section, gold in the auriferous quartz-pyrite-tourmaline veins occurs as Au-(Bi)-telluride micro-inclusions in pyrite and as native gold mainly in the cracks of oxidized pyrite grains.

Gold in tellurides

In unoxidized mineralized veins, gold is hosted by 1 to 10 µm sized micro-inclusions of calaverite and montbrayite in pyrite (Table 5). Calaverite and montbrayite mostly occur in a set of parallel strings or in clusters in pyrite grains and have not been observed to be evenly disseminated over the entire grain. With the oxidation of pyrite, most telluride crystals are destroyed, resulting in the formation of native Au in the oxidized pyrite grains (Fig. 93). Also, the formation of Se-Au-Ag solid solutions in cracks of oxidized pyrite has been observed once (Fig. 93), though this appears to be rare.

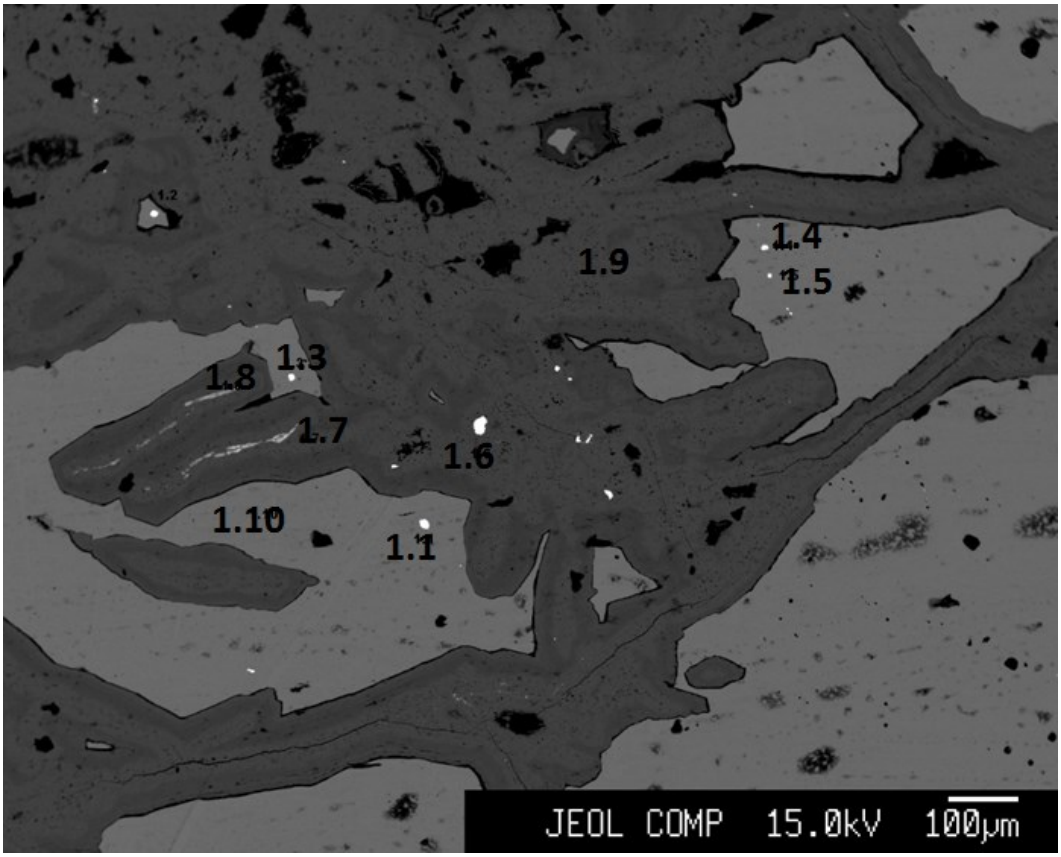

Fig. 93. Back-scattered electron image of telluride inclusions in pyrite and native gold in oxidized pyrite. Pyrite (grey: 1:10) being oxidized to goethite (dark grey: 1.9). In the matrix of goethite are disseminated grains of native Au (white-bright, e.g.: 1.6) and rare solid solutions of Se-Au-Ag in cracks of goethite (1.7 and 1.8). Inside the unoxidized pyrite grain are tellurobismuthite (1.1), calaverite (1.3 and 1.4) and montbrayite (1.5).

Native gold

Native gold was found in every grab sample of the auriferous quartz-pyrite-tourmaline veins. Most gold grains appear remobilized and occur along cracks of heavily oxidized pyrite (Fig. 94). However, individual smaller gold grains can also occur more disseminated in the matrix of goethite, mostly in proximity to unoxidized pyrite. These were likely formed by destruction of auriferous tellurides during oxidation and are not strongly remobilized (Figs. 93 and 95). Observed grain sizes of the native gold range between 5 µm up to 200 µm, though gold flakes up to 0.5 cm in size have also been extracted during artisanal mining (H. Siitonen, pers. comm., 2018). Generally, the more intensely the sample is oxidized, the coarser grained and more remobilized the native gold appears. In all cases, the remobilized gold is very pure and does not have significant Ag contents (Table 5).

Native gold is spatially strictly related to goethite and was not found in unoxidized pyrite, further indicating that the observed native gold is remobilized. However, given the scarcity of studied samples and the supergene overprint, non-remobilized native gold being part of the unweathered gold mineralization remains a possible scenario.

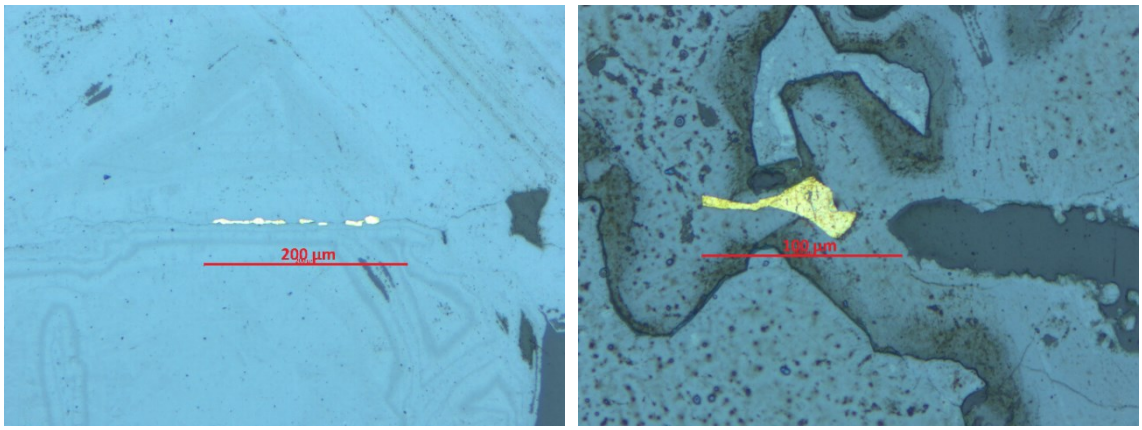

Fig. 94. Photomicrographs of remobilized native gold grains in cracks of oxidized pyrite. (Left) Multiple remobilized gold grains elongated over 200 µm along a crack in oxidized pyrite. Reflected light. (Right) Single, approx. 100 µm large remobilized gold grain in a crack of oxidized pyrite. Reflected light.

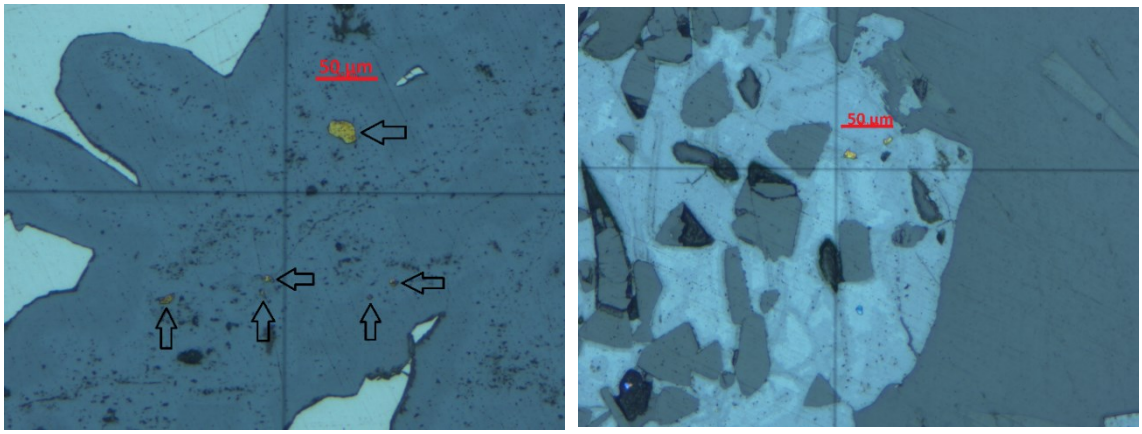

Fig. 95. Photomicrographs of native gold in oxidized pyrite. (Left) Cluster of disseminated gold grains in goethite, in proximity to unoxidized pyrite. Position and shape indicate little remobilization. Reflected light. (Right) Two disseminated gold grains in oxidized pyrite, likely not strongly remobilized. Reflected light.

6.3 Geochemistry of the mineralized veins

The geochemical description of the mineralized veins is based on non-weathered drill core samples provided by FireFox Gold Corp (Table 7). The samples consist of drill core intercepts exceeding gold concentrations of 0.1 ppm. These non-weathered samples were not available during the mineralogical study described in the previous section (6.1 and 6.2), which is based on weathered supergene samples. Supergene samples, consisting of channel samples along the main known outcropping gold-mineralized vein, grab samples from pyrite-rich boulders in the artisanal mining pit and weathered drill core intercepts exceeding 0.1 ppm Au, are shown in Table 8 for a comparison to evaluate supergene processes. The surface sampling was selective; hence the supergene samples show naturally higher average gold values making the evaluation of potential supergene gold enrichment, and the enrichment of other pathfinder elements difficult.

The geochemistry of the mineralized veins shows strong enrichments of elements that are commonly elevated in orogenic gold deposits. At Mustajärvi, these elements include: Au, B, Bi, C (CO_2), Te, and Se. Other pathfinder elements that are commonly enriched in orogenic gold deposits, such as Ag, As, Sb, and W (e.g. McCuaig and Kerrich, 1998; Goldfarb et al., 2005), are clearly elevated at Mustajärvi and correlate with gold but are not enriched to the same extent as the former elements. The Au/Ag ratio at Mustajärvi is 21.4, being notably higher than the average Au/Ag ratios of orogenic gold deposits typically ranging between 5 to 10 (Goldfarb et al., 2005). Compatible with the low As values, no arsenopyrite is known from Mustajärvi and only once arsenic pyrite was observed in a thin section sample. Elements that are not commonly recognized to be elevated in orogenic gold deposits but are clearly enriched at Mustajärvi are Co and Ni, and moderately elevated Mo.

Tellurium is significantly enriched with an average value of ~73 ppm and maximum values of more than 819 ppm in the unweathered mineralized veins (Table 7). The high Te concentration is related to the abundance of several telluride minerals in pyrite in the mineralized veins, as can be seen by the correlation factor of ~0.70 between Te and S (Table 7). The telluride minerals montbrayite and calaverite are the major known gold hosts at Mustajärvi, hence the correlation factor between Te and Au is high with ~0.77. With the detected concentrations, tellurium constitutes a potentially economic by-product, comparable to the Au-Te Kankberg mine in Sweden where ore with an average Te grade of 186 g/t is mined (Bergman, 2011). In the supergene mineralized rocks, Te

reaches an average value of ~132 ppm (Table 8). The selective sampling of the supergene rocks makes it difficult to evaluate the possible supergene enrichment of Te.

Cobalt concentrations in the non-weathered mineralization reach an average value of 0.044 wt%, with maximum values up to 0.286 wt%. In the supergene mineralized rocks, Co concentrations average at 0.057 wt% with a maximum concentration of 0.267 wt%. The Co concentrations in the unweathered and weathered samples are very similar, making a supergene enrichment unlikely. Microprobe analyses yield Co concentrations of 0.12-0.76 wt%, with an average value of 0.41 wt%, in the matrix of unoxidized pyrite, showing that Co is bound in the lattice of pyrite (Table 6). The correlation factor between Co and S of 0.94 supports this claim (Table 7). During oxidation, cobalt remains in the lattice of pyrite, as indicated by average Co concentrations of 0.39 wt% in microprobe analyses of goethite, furthermore suggesting that Co is not subject of supergene enrichment. Primary cobalt minerals were not observed during thin section studies. The relatively low As concentration is in line with the fact that no common primary cobalt-arsenic minerals, such as cobaltite or skutterudite have been detected. If the metallurgy permits, Co could be an economic by-product in potential mining operations.

Nickel is relatively enriched in the mineralized veins at Mustajärvi. In the non-weathered environment, Ni has an average value of 115 ppm and a maximum of 689 ppm. Microprobe analysis shows that nickel occurs as the Ni telluride melonite in pyrite, and in the lattice of pyrite with average concentrations of 0.06%. Therefore, Ni is closely related to the amount of pyrite in the veins, as shown by the correlation factor of 0.77 between Ni and S. In weathered, supergene samples, the average Ni concentration is at a level of 200 ppm. Given the selective supergene sampling, no clear enrichment processes can be interpreted. In the supergene environment, Ni is hosted by goethite, which has an average Ni concentration of 0.09 wt%. The relatively high Ni concentration in the mineralized veins could partly be explained by the Ni-rich ultramafic host rocks.

The bismuth concentrations in the non-weathered mineralized veins are significantly enriched with an average of 42.2 ppm and a maximum value of 728 ppm. Microprobe studies show that the Bi enrichment at Mustajärvi is related to micro-inclusions of the Bi-tellurides tellurobismuthite and kawazulite, and the Au-Bi telluride montbrayite in non-oxidized pyrite (Tables 5 and 6), as indicated by correlation factors of 0.72 between Bi and S, and 0.75 between Bi and Au. However, the correlation between Bi and Te, with a

factor of 0.59, is surprisingly low. As pyrite becomes oxidized during weathering, Bi-tellurides will be destroyed. Bismuth is not enriched in the resulting goethite grains and no supergene Bi-bearing phases were observed in the supergene oxidized pyrite assemblages. The supergene mineralized rocks have an average Bi concentration of only 16.7 ppm, suggesting depletion in Bi during weathering processes.

Selenium concentrations of non-weathered mineralized rocks closely resemble those of Bi, with an average of 48.6 ppm Se and a maximum of 621 ppm Se. Similarly to Bi, selenium appears to become depleted during weathering, with an average supergene Se concentration of only ~17 ppm. The microprobe study shows that in non-oxidized mineralized rocks, Se occurs both as kawazulite micro inclusions in pyrite and in the lattice of pyrite, as indicated by correlation factors of 0.71 between Se and Te, and 0.92 between Se and S. In the lattice of pyrite, Se constitutes 0.05 wt% of the mineral, and with average pyrite volumes of ~10 % (indicated by an average S concentration of 5 %) in the mineralized veins, this amounts to ~50 ppm Se in the rock, suggesting that the lattice of pyrite is the main carrier of Se. In oxidized pyrite, Se was observed to form Se-Au-Ag solid solutions which yielded up to 67.8 wt% Se. During stronger weathering, these phases are possibly destroyed, explaining the depletion of Se in supergene mineralized rocks.

With an average non-weathered concentration of 5.3 ppm and a maximum of 104 ppm, molybdenum is moderately elevated at Mustajärvi. The average supergene concentration of 7.9 ppm Mo, does not suggest a clear enrichment or depletion of the element during weathering, given the selective supergene sampling. The source of elevated molybdenum is yet to be identified. No Mo-bearing minerals, such as easily identifiable molybdenite, have been observed during mapping, thin section studies or core logging. Molybdenum was not among of the elements of the microprobe analysis. Correlation factors of Mo with Au, Bi, Co, Se and Te are relatively high with values ranging between 0.50-0.65.

Gold is significantly enriched in the non-weathered mineralized veins with an average value of ~6.5 ppm Au and a maximum grade of 73.7 ppm, based on 35 drill core samples exceeding 0.1 ppm in Au. Supergene gold values with an average of 12.6 ppm Au and a maximum of 140.5 ppm are higher. The average supergene gold concentration is partly higher due to a selective sampling of the supergene samples along, and not across, the main known mineralized gold vein. The maximum supergene gold concentration derives

from highly oxidized samples and is possibly a product of supergene enrichment, caused by a general loss of rock volume and major components during intense oxidation. In non-weathered mineralized rock, the gold concentration is largely dependent on the amount of pyrite in the vein, as shown by the high correlation factor of 0.79 between Au and S. This is furthermore indicated by recent drill core intervals of FireFox Gold Corp, which intersected a 2-m-wide zone of non-oxidized massive pyrite mineralization that yielded 45.1 ppm Au. The microprobe study shows that in non-oxidized mineralized rock, gold occurs in montbrayite and calaverite hosted by pyrite, which is indicated by the strong correlation of Au with Bi (0.75) and Te (0.77). Montbrayite shows varying chemical compositions, with gold concentrations ranging between 8.8 and 46.2 wt%, with an average of 35.0 wt%, whereas Au and Bi appear to substitute for each other, with a negative correlation between them in the mineral. In weathered environments, gold also occurs as native, remobilized gold, formed by destruction of the gold-telluride micro-inclusions during the oxidation of pyrite. An expected decreased correlation factor of Au with Bi and Te cannot be observed, however, the correlation between Au and S (0.53) is clearly decreased in the supergene environment. The observed native gold grains are relatively low in silver, with an average Ag concentration of 2.75 wt%, which emphasizes the generally low enrichment of Ag at Mustajärvi, though low silver contents in free gold can also be caused by possible loss of Ag from the grains during weathering.

Although boron was not part of the geochemical analysis, its high concentrations can be inferred from the high abundance of tourmaline in the mineralized veins and proximal wall rock. Similarly, the enrichment of CO_2 can be seen by intense carbonate veining related to mineralization.

The non-weathered S concentrations, with an average of ~5 wt%, indicate average pyrite amounts of approx. 10 %, as pyrite is the only sulphide mineral in the gold-mineralized veins. The maximum S value of 27.4 wt% represents the intersected 2-m-thick, massive pyrite zone with up to 55 % pyrite. These high values skew the averages slightly. Nevertheless, petrographic observations are consistent with an average pyrite amount of approx. 10 % in the gold-mineralized veins.

Antimony is only slightly elevated in the non-weathered environment with an average concentration as low as 60 ppb and a maximum of 180 ppb. Microprobe analysis showed that Sb occurs in all telluride micro-inclusions with concentrations ranging between 0.2

and 0.5 wt% (Tables 5 and 6). In the supergene environment, antimony is clearly enriched with an average concentration of 290 ppb and a maximum of 1.1 ppm.

Table 5. Chemical compositions of the Au-bearing minerals at Mustajärvi. For calaverite, the stochiometric pure mineral composition is given as comparison. In the case of montbrayite and native Au, different compositions were observed which are separately listed. The number of analyses is given by [n].

Mineral	Montbrayite						Calaverite		native Au	
Formula	$(Au,Ag,Sb,Bi,Pb)_{23}(Te,Sb,Bi,Pb)_{38}$						$AuTe_2$		Au (Ag)	
[wt%]	Avg. meas. comp [n=5]	Meas. comp.	Avg. meas. comp [n=2]	Meas. comp.	Meas. comp.	Meas. comp.	Official comp.	Avg. meas. comp. [n=4]	Avg. meas. comp. [n=5]	Meas. comp.
Ag		0.13						0.20	1.86	7.27
As										
Au	44.21	43.24	35.81	24.05	15.92	8.78	43.56	42.73	98.32	93.63
Bi	5.77	1.78	13.80	24.80	36.86	39.47				
Co										
Cu			0.13	0.10						
Fe	2.55	3.31	3.18	3.46	2.56	5.00				
Ni	0.27		0.36	0.77		0.28				
Pb										
S	0.41	0.72	0.83	0.80	0.21	4.93				
Sb	0.29	0.34	0.27	0.33	0.37	0.28		0.34		
Se						0.17				
Te	45.28	54.06	46.42	45.77	51.20	43.86	56.44	56.15		
Sum	98.78	103.57	100.81	100.07	107.13	102.77	100.00	99.42	100.18	100.90

Table 6. Chemical compositions of non-auriferous telluride minerals, the observed Ag-Au-Se-goethite solid solution, pyrite, and goethite. Stochiometric pure mineral compositions are given as comparison. For the Ag-Au-Se-goethite solid solution, different compositions were measured, which are listed separately. The number of analyses is given by [n].

Mineral Formula	Melonite $NiTe_2$		Telluro-bismuthite Bi_2Te_3		Kawazulite $Bi_2Te_{1.8}Se_{0.9}S_{0.3}$		Ag-Au-Se-goethite solid solution		Pyrite FeS2		Goethite FeO(OH)	
[wt%]	Offic. comp.	Avg. meas comp [n=6]	Offic. comp.	Avg. meas comp [n=2]	Offic. comp	Avg. meas comp [n=9]	Meas. comp	Meas. comp	Offic. comp.	Avg. meas comp [n=7]	Offic. comp.	Avg. meas comp [n=4]
Ag							26.14	15.67				
As										0.03		0.04
Au							10.70	7.21				
Bi			52.20	52.44	57.39	54.95						
Co							0.23	0.33		0.41		0.39
Cu												
Fe						3.11	31.52	38.42	46.55	46.09	62.85	51.94
Ni	18.70	17.97								0.06		0.09
Pb												
S					1.32	2.96			53.45	52.68		0.03
Sb		0.48		0.22		0.21						
Se				0.15	9.76	5.51	8.16	5.48		0.05		0.01
Te	81.30	80.35	47.80	44.91	31.54	32.15				0.01		0.03
Sum	100.0	98.79	100.00	97.71	100.0	98.88	76.75	67.11	100.00	99.33	62.85	52.53

Table 7. Left: Selected element concentrations of unweathered gold-mineralized drill intercepts exceeding 0.1 ppm Au (data from FireFox Gold). Right: Correlation of selected elements, based on the same samples as left column.

Geochemistry of unweathered gold mineralization					Correlation of selected elements for unweathered gold mineralization					
Nr. of samples: 35					Nr. of samples: 35					
Element	Min.	Max.	Avg.	Std. deviation	Ag	Au	Bi	Co	Se	Te
Ag_ppm	0.50	2.40	0.62	0.44	**1.00**	0.45	0.40	0.45	0.42	0.38
Al_wt%	0.04	2.50	0.60	0.66	0.10	-0.04	0.12	0.09	0.16	0.13
As_ppm	2.50	19.00	5.29	4.35	0.49	0.54	0.59	0.59	0.61	0.37
Au_ppm	0.11	73.72	6.46	15.41	0.45	**1.00**	0.75	0.82	0.74	0.77
Ba_ppm	3.00	581.00	46.06	118.32	-0.15	0.00	-0.07	0.08	0.05	-0.16
Bi_ppm	0.03	728.00	42.19	133.68	0.40	0.75	**1.00**	0.78	0.76	0.59
Ca_wt%	0.01	12.90	1.91	2.75	-0.24	-0.62	-0.58	-0.66	-0.49	-0.44
Co_ppm	1.20	2860.00	440.55	759.30	0.45	0.82	0.78	**1.00**	0.95	0.70
Cr_ppm	7.40	1030.00	110.27	234.42	-0.14	-0.11	0.01	0.02	-0.06	-0.26
Cu_ppm	1.10	39.10	6.77	8.84	0.42	0.60	0.53	0.68	0.79	0.57
Fe_wt%	0.68	28.40	6.14	7.67	0.48	0.76	0.80	0.83	0.86	0.69
K_wt%	0.01	2.31	0.28	0.59	0.10	0.00	0.04	0.09	0.12	0.06
Mg_wt%	0.01	2.95	0.99	0.90	-0.11	-0.35	-0.14	-0.21	-0.06	-0.26
Mn_ppm	35.00	2550.00	548.00	651.34	-0.25	-0.59	-0.57	-0.62	-0.46	-0.47
Mo_ppm	0.50	104.00	5.28	18.14	0.30	0.54	0.65	0.56	0.59	0.50
Na_wt%	0.02	0.08	0.05	0.02	-0.04	-0.10	0.00	-0.19	-0.28	-0.08
Ni_ppm	8.20	689.00	114.81	158.75	0.44	0.72	0.78	0.86	0.86	0.68
P_ppm	73.00	2060.00	402.54	337.14	-0.29	-0.35	-0.35	-0.40	-0.31	-0.24
Pb_ppm	2.50	87.90	10.24	15.62	0.22	0.58	0.60	0.62	0.62	0.46
S_wt%	0.00	27.40	5.06	8.13	0.48	0.79	0.72	0.94	0.92	0.70
Sb_ppm	0.02	0.18	0.06	0.05	0.42	0.51	0.66	0.46	0.52	0.27
Se_ppm	0.12	621.00	48.61	121.94	0.42	0.74	0.76	0.95	**1.00**	0.71
Sr_ppm	1.50	46.70	11.16	10.24	-0.27	-0.51	-0.41	-0.54	-0.35	-0.41
Te_ppm	0.32	819.00	73.16	170.42	0.38	0.77	0.59	0.70	0.71	**1.00**
Th_ppm	5.00	21.00	6.06	3.30	-0.11	-0.03	0.13	-0.04	-0.07	-0.14
Ti_ppm	4.00	2540.00	288.23	679.36	-0.03	-0.13	-0.16	-0.07	-0.09	-0.16
V_ppm	1.10	292.00	33.68	64.10	-0.06	-0.08	-0.06	-0.02	-0.05	0.01
Zn_ppm	0.50	135.00	12.24	24.94	-0.01	0.23	0.37	0.28	0.27	0.28

Table 8. Left: Selected element concentrations of supergene mineralized samples at Mustajärvi comprising weathered drill core intersects exceeding 0.1 ppm Au, weathered bedrock channel samples and weathered grab samples from the artisanal mining pit (both also exceeding 0.1 ppm Au). The sampling was selective. Right: Correlation of selected elements, based on the same samples as left column.

Geochemistry of weathered gold mineralization					Correlation of selected elements for weathered gold mineralization					
Nr. of samples: 53					Nr. of samples: 53					
Element	Min.	Max.	Avg.	Std. deviation	Ag	Au	Bi	Co	Se	Te
Ag_ppm	0.02	4.20	0.78	0.87	**1.00**	0.64	0.50	0.39	0.45	0.30
Al_wt%	0.08	55.80	3.93	7.65	-0.32	-0.08	-0.13	0.00	-0.36	0.12
As_ppm	1.30	62.30	14.14	14.36	0.47	0.69	0.43	0.68	0.39	0.73
Au_ppm	0.05	140.50	12.57	23.89	0.64	**1.00**	0.73	0.77	0.68	0.79
Ba_ppm	10.00	1560.00	219.55	356.27	-0.40	-0.21	-0.45	0.04	-0.42	0.14
Bi_ppm	0.01	193.50	16.71	33.51	0.50	0.73	**1.00**	0.54	0.72	0.49
Ca_wt%	0.02	0.46	0.19	0.12	-0.19	-0.27	-0.26	-0.25	-0.52	-0.07
Co_ppm	22.20	2670.00	569.44	508.31	0.39	0.77	0.54	**1.00**	0.75	0.81
Cr_ppm	21.90	1100.00	192.87	216.47	-0.15	0.23	-0.03	0.40	0.03	0.53
Cu_ppm	1.10	47.70	14.69	13.33	0.12	0.35	0.16	0.57	0.20	0.54
Fe_wt%	1.60	194.00	30.45	38.82	0.50	0.26	0.17	0.28	0.44	0.12
K_wt%	0.01	8.71	1.01	1.56	-0.20	-0.49	-0.72	-0.41	-0.59	-0.39
Mg_wt%	0.02	2.28	0.49	0.45	-0.09	-0.20	-0.17	-0.15	-0.36	-0.10
Mn_ppm	49.00	73000	3704	12302	-0.43	-0.08	-0.22	0.29	-0.11	0.33
Mo_ppm	0.40	31.70	7.92	8.36	0.31	0.73	0.47	0.81	0.49	0.80
Na_wt%	0.03	4.41	0.91	1.03	-0.15	-0.15	-0.30	-0.17	-0.46	0.06
Ni_ppm	14.00	642.00	199.78	139.71	0.32	0.63	0.29	0.86	0.53	0.82
P_ppm	0.01	2560.00	596.81	524.33	0.10	0.22	0.01	0.32	-0.03	0.47
Pb_ppm	2.40	281.00	41.85	45.75	0.27	0.36	0.26	0.30	0.33	0.41
S_wt%	0.00	39.10	1.68	5.68	0.39	0.53	0.42	0.45	0.72	0.28
Sb_ppm	0.00	1.13	0.29	0.23	0.14	0.49	0.30	0.70	0.41	0.70
Se_ppm	0.24	89.00	16.96	23.09	0.45	0.68	0.72	0.75	**1.00**	0.51
Sr_ppm	2.50	603.00	44.85	98.12	-0.37	0.01	-0.08	0.33	-0.04	0.29
Te_ppm	0.55	750.00	131.69	193.44	0.30	0.79	0.49	0.81	0.51	**1.00**
Th_ppm	0.16	16.30	5.18	3.51	-0.09	-0.12	-0.17	0.13	-0.15	0.20
Ti_ppm	5.00	2030.00	491.19	537.90	-0.27	-0.18	-0.30	-0.05	-0.32	-0.02
V_ppm	0.06	365.00	98.54	82.94	-0.04	0.13	0.05	0.37	0.12	0.33
Zn_ppm	5.00	121.00	52.60	31.56	0.04	0.09	0.03	0.29	0.05	0.34

Figure 96 compares the Te/Au ratio at Mustajärvi with the ratio of other orogenic Au and intrusion-related Au deposits. The data shows that the Te/Au ratio of 11.3 at Mustajärvi is greater than that of the mantle and continental crust and significantly above the average ratio of orogenic and intrusion-related gold deposits, but still within the range of these gold systems. However, it is not yet clear what implications tellurium-rich gold deposits have. The relationship between tellurium-rich gold deposits and their size, gold grade, formation age, host lithologies, sulphide volumes, etc. are still unclear and subject of future research (Goldfarb et al., 2017).

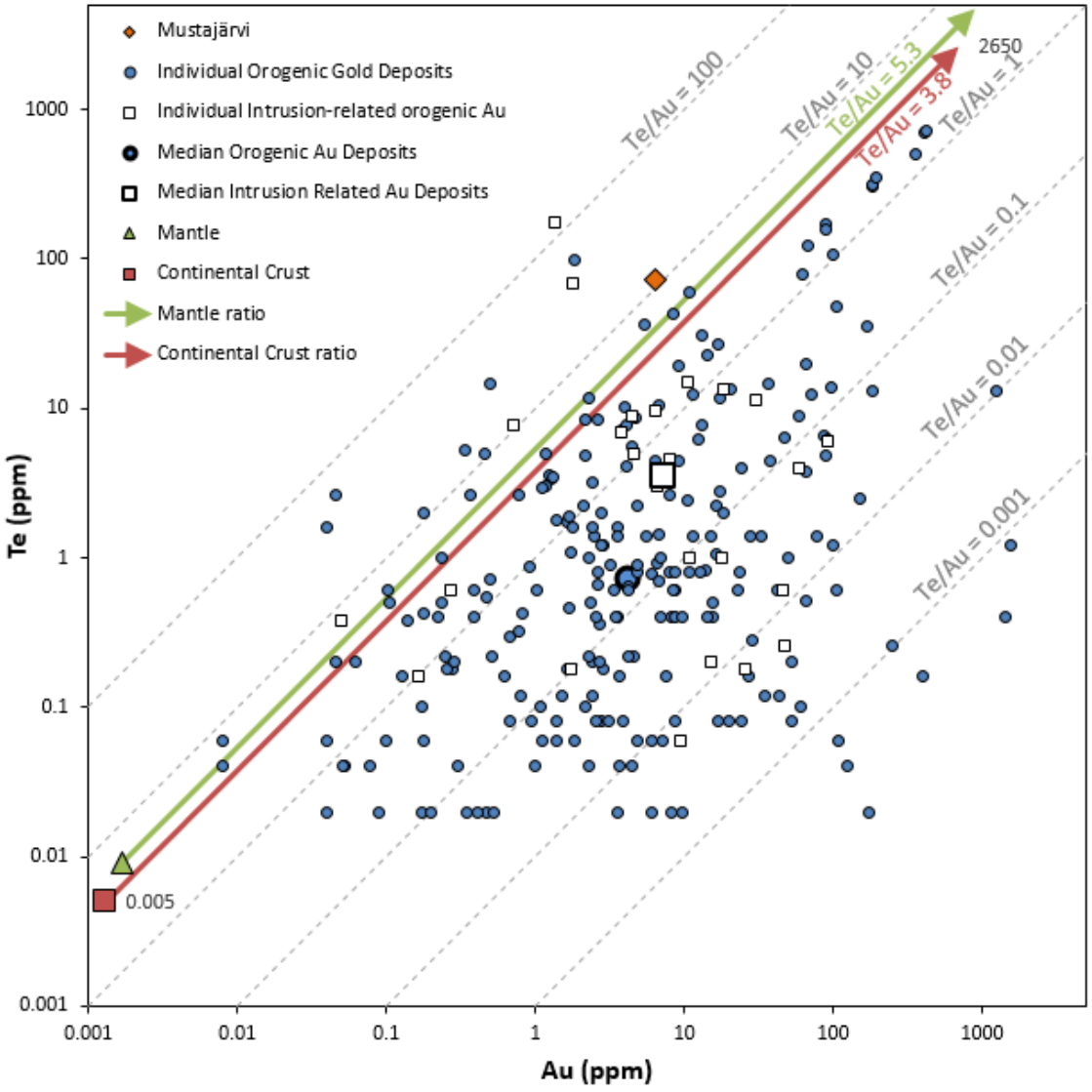

Fig. 96. Diagram showing Te and Au concentrations of multiple orogenic and intrusion-related Au deposits including their median and the Mustajärvi gold deposit. The data from Mustajärvi is based on non-weathered mineralized drill core intercepts exceeding 0.1 ppm in Au (amount of samples: 35) (Table 7). Also shown are average Te/Au ratios of the mantle and continental crust. (Modified after Spence-Jones & Jenkin et al., 2018).

6.4 Supergene processes

The outcropping mineralized rocks at Mustajärvi are subject to intense weathering processes. The outcropping veins and the proximal host rock are affected by strong clay alteration of feldspar (Fig. 98) resulting in the formation of pink and white-beige clay minerals, likely kaolinite. This is emphasized by the enrichment of Al in the weathered mineralized rocks with average values of 3.9 wt%; and a maximum of 55.8 wt% Al, as opposed to average Al concentrations of 0.6 wt% in the non-weathered gold-bearing veins. Furthermore, gossan-like, dark-blue-greyish Mn-weathering crusts form in the intensively clay-altered zones of the artisanal mining pit. The weathering crust has only been observed to form on quartz-rich mineralized- and non-mineralized veins (Fig. 100). The Mn concentrations reach up to 7.3 wt% in these samples (Table 8). No Mn-weathering crusts have been described or observed in any parts of the drill core, likely because the process is restricted to the surface. The intense clay alteration zone reaches from the surface to a depth of at least 25 m, based on Outokumpu and FireFox Gold drill holes that intercepted heavily kaolinized mineralization up to a vertical depth of 26 m (Drill core MJ-4 and 18MUS002; Fig. 101). This strong weathering caused heavy core losses of up to 50 %, in the mineralized zone. However, not all parts of the mineralization show signs of intense clay alteration to the same level of depth. The Outokumpu drill holes also intercepted non-kaolinized mineralized veins at vertical depths of 15.8 m (Drill core MJ-1). Overall, the intensive clay alteration is interpreted to be generally 5-25 m deep (Fig. 97).

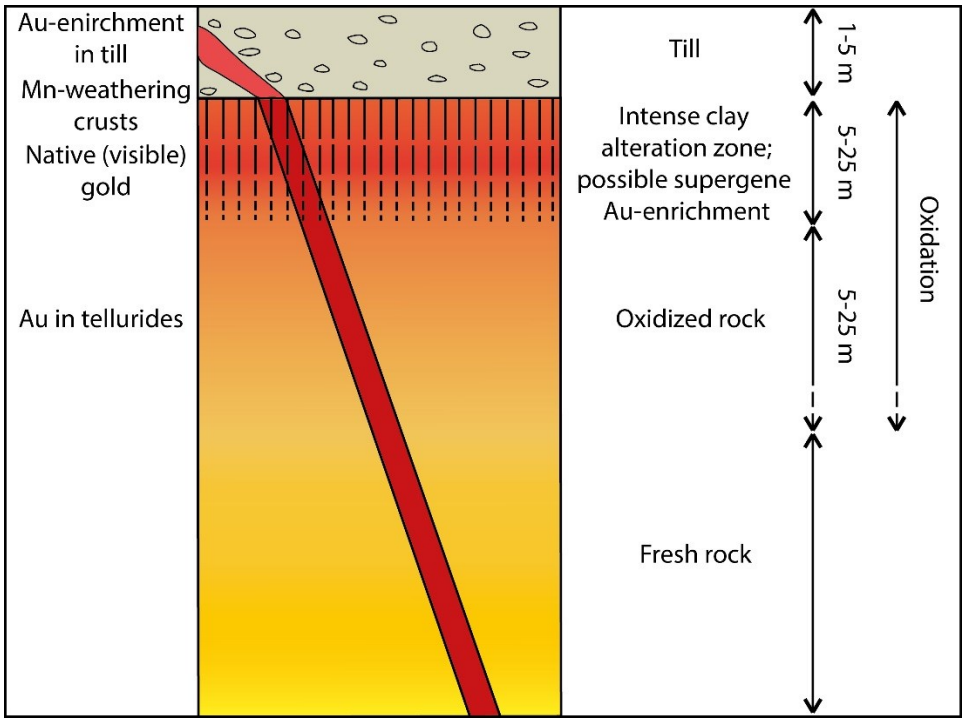

Fig. 97. Sketch profile through the soil and rock package at Mustajärvi (sketch after Craw and Kerr, 2017).

Other supergene processes within this zone are the heavy oxidation of pyrite to goethite and the weathering of carbonates. The majority of grab samples of mineralized veins at Mustajärvi are heavily oxidized (Fig. 99), however also few relatively unoxidized samples were found. The oxidation and weathering of the mineralized rocks possibly causes a supergene enrichment of gold in the clay-altered zone due to a loss of rock volume. Heavily weathered samples yielded gold concentrations of up to 140.5 ppm (Fig. 98) and visible gold has been observed. The remobilization of gold due to oxidation has been described in greater detail in section 6.2. Partial oxidation of the mineralization is thought to continue deeper than the clay altered zone, generally down to depths of ~50 m. The intensity of both clay alteration and oxidation are strongly structurally controlled. The first drill cores by FireFox Gold Corp show that short intervals of strong kaolinization and partial oxidation of pyrite can be observed until depths of 120 m in a zone of heavily broken rock that likely represents a fault zone.

Fig. 98. Weathering of the gold-mineralized veins in the artisanal pit. (Left) View of the main outcropping mineralized vein towards ENE. The vein is heavily oxidized and kaolinized and thus was easily recoverable during artisanal mining. (Top right) Same vein as in left figure, view from the top. This section of the oxidized and kaolinized vein graded 140.5 ppm Au. The brown oxidized pyrites and the beige clay minerals are easy to identify. Visible gold is present. (Bottom right) Strong kaolinization in the western part of the pit, looking south. Beige and pink clay minerals and brown Fe-oxides are easily distinguishable. This western section of the pit has gold concentrations of up to ~7 ppm Au.

Fig. 99. Grab sample of a heavily oxidized quartz-tourmaline-pyrite vein grading 79.8 ppm Au (sample Mus-3). Only a large quartz clast and some relictic pyrite are recognizable. Sample width is approx. 15 cm.

Fig. 100. Grab sample of a Mn weathering crust (blueish-grey) (sample MJ-25). The Mn crust is located on the outer, vuggy parts of a quartz-pyrite vein. The center of the sample is oxidized pyrite (brown). The sample is grading 13.1 ppm Au. Sample width is approx. 15 cm.

Fig. 101. Drill core showing strongly kaolinized and oxidized mineralized zone. Intense kaolinization causes strong core loss. At 34.35 m is a 0.3-m-wide quartz-pyrite vein that grades 11.6 ppm Au. Drill core 18MUS105, depth 30-37 m.

7. STRUCTURAL CONTROL

The mineralized veins at Mustajärvi appear to be mainly structurally controlled by the contact between Sodankylä Group siliciclastic metasediments and Savukoski Group volcanics, outlined by ground magnetic studies and IP resistivity studies (see Chapter 4.3). The main outcropping vein is oriented nearly parallel to the main lithological contact and to the orientation of the host rock, with an average strike and dip of ~70/55 SSE (Fig. 102). This is emphasized by BoT Au anomalies and drill core intercepts, which furthermore indicate that the main mineralizing trend consists of several parallel aligned veins offset from the main lithological contact (Fig. 10). The contact itself is interpreted to be a fault zone (Mustajärvi fault), as indicated by several geophysical features comprising demagnetization in ground magnetic surveys (Fig. 11A), a low apparent resistivity (Fig. 11B) and a high chargeability (Fig. 11C). As the Mustajärvi fault is associated with the contact between the host rocks, it is striking roughly NE with a dip of ~45° to the SE (Fig. 10). This orientation coincides with the nearby terminating Porkonen shear zone (Fig. 108). In the southwest of the study area, the Mustajärvi fault is interpreted to be connected to the first-order transcrustal Venejoki thrust system (Fig. 108), which can be traced to reach the mantle at a depth of 42 km (Patison et al., 2006; Niiranen et al., 2014).

One subcropping auriferous vein, which is exposed in the western part of the artisanal pit, is oriented perpendicular to the main mineralizing trend and strikes near parallel to the main joint direction with an average strike of 150-160° (Figs. 103 and 107). This vein trend was proven to continue at depth by FireFox Golds drilling, where vertical veins, partly auriferous, with a strike of 155° occur. Veins of this second trend appear to have lower grades of Au. This vein trend 2 could represent minor transfer faults within the rock package, partly auriferous due to possible remobilization of mineralization.

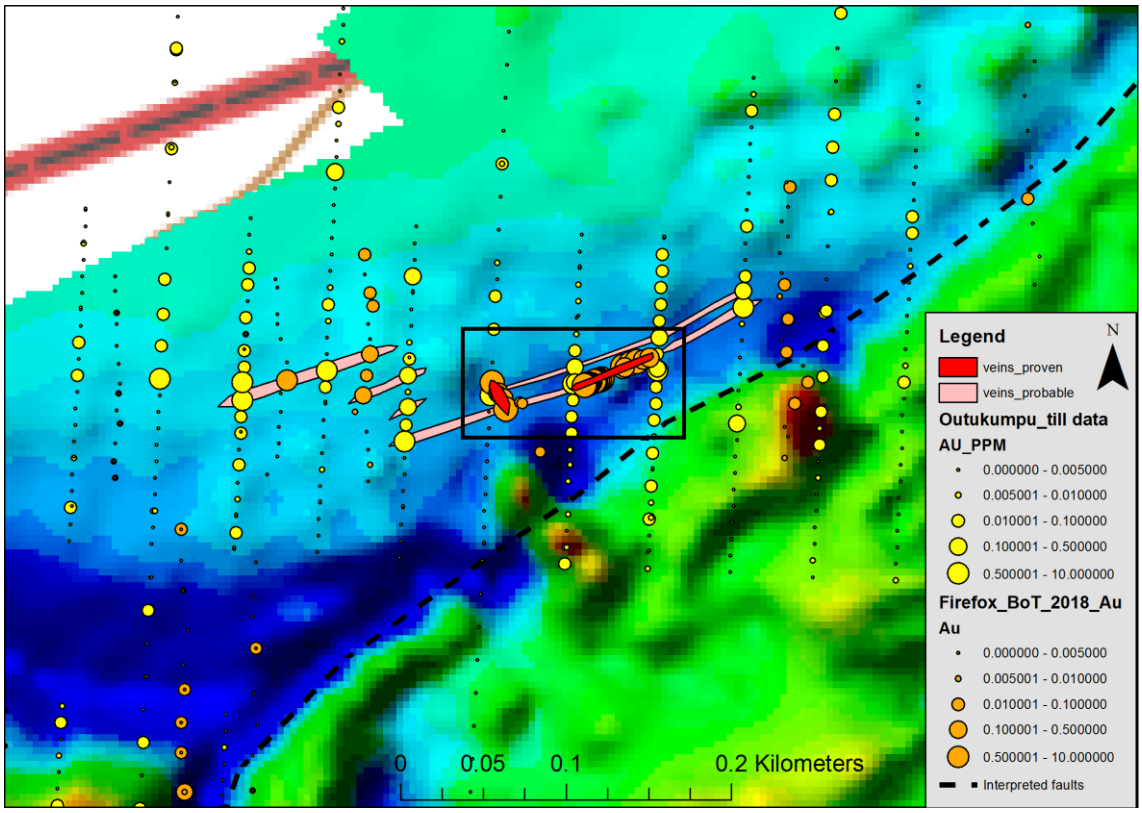

Fig. 102. Probable and proven veins at Mustajärvi, based on outcrop observations, BoT Au anomalies and drill core intercepts. The outcropping mineralization is marked with a black rectangle and is shown in detail in Fig. 103. A ground magnetic map is shown in the background.

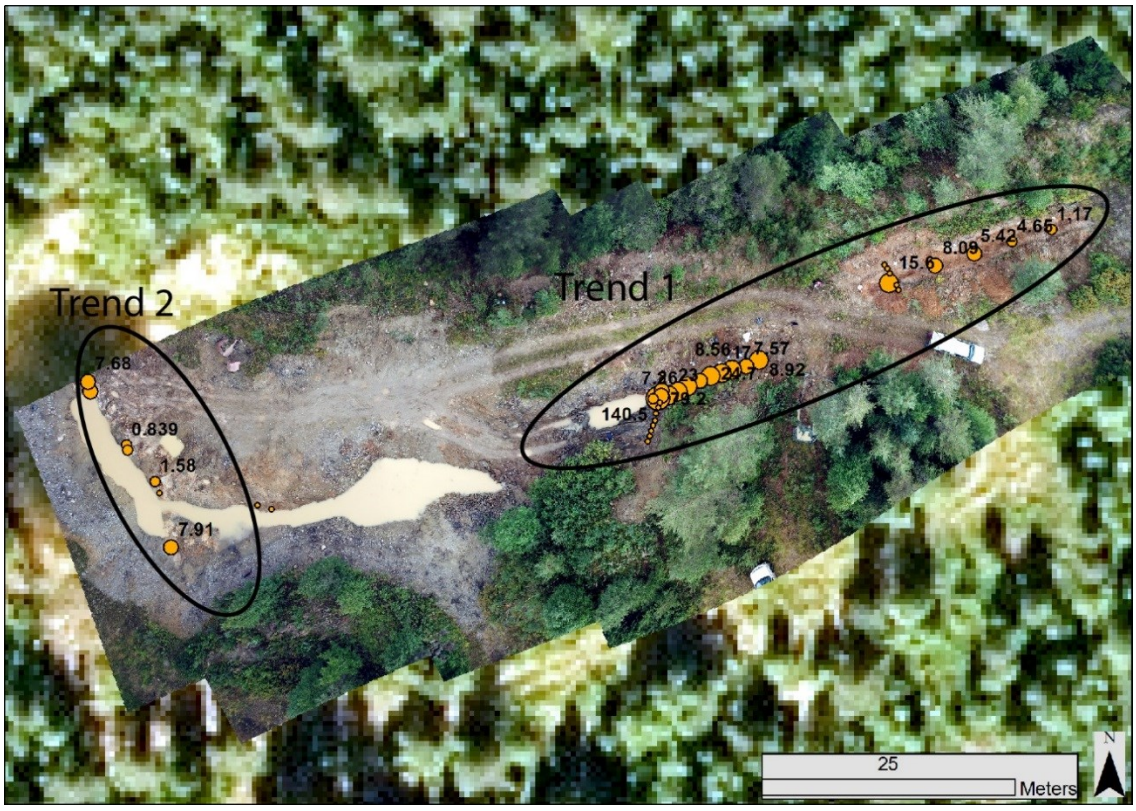

Fig. 103. Two gold mineralization trends in the artisanal mining pit, indicated by FireFox Gold channel sampling. For a detailed view of the western part of trend 1, see Fig. 104.

Fig. 104. Close up view of Fig, 103 (western part of trend 1) showing FireFox Gold channel samples with Au concentrations. The thickness and the gold grades of the outcropping main mineralized vein increase towards the left of the aerial photograph, indicating a pinch and swell structure of the mineralized veins.

The outcropping mineralization was mapped in detail to gain a more reliable understanding of the structural controls at Mustajärvi (Fig. 105). The host rocks have an average dip of 160/55. The measured joint directions in the outcrop are mainly vertical to the bedding of the host rocks, with a general trend of ~230/80-060/80 (Fig. 107). The outcropping main mineralized vein follows the orientation of the host rocks, whereby it shows a strong pinch and swell nature, which is supported by drill core observations. In the majority of the outcrop, the mineralized vein has a thickness of around 0.3 m, whereby it swells up to a minimum of 1 m in the central part of the outcrop, which was the main target of the artisanal mining (Figs. 105 and 106). In this central part, not only the thickness but also the gold grade increases drastically.

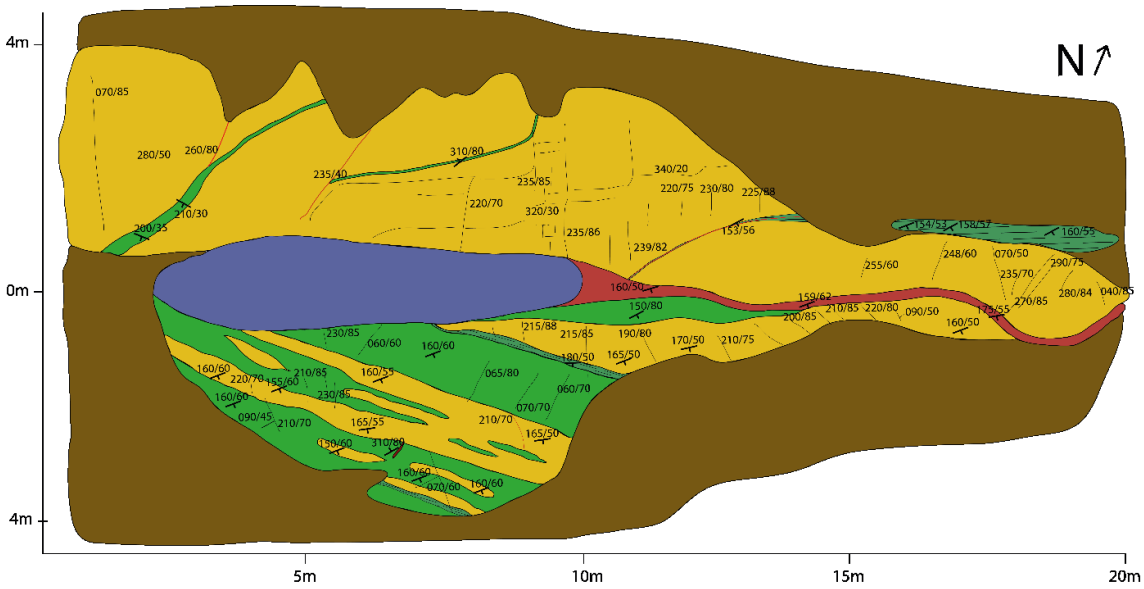

Fig. 105. Three-dimensional geological map of the artisanal mining pit. In green are shown metavolcanic rocks, in yellow siliciclastic metasediments; in red the mineralized vein; in blue water; and in brown soil cover. Numbers with a dip symbol show dip direction and dip values and those without a dip symbol show joint directions.

Fig. 106. Outcropping main mineralized vein in the artisanal mining pit. The vein is recognizable by its brown weathering colors. View towards ENE; field of view represents approx. the geological map of Fig. 105 (~8 m width).

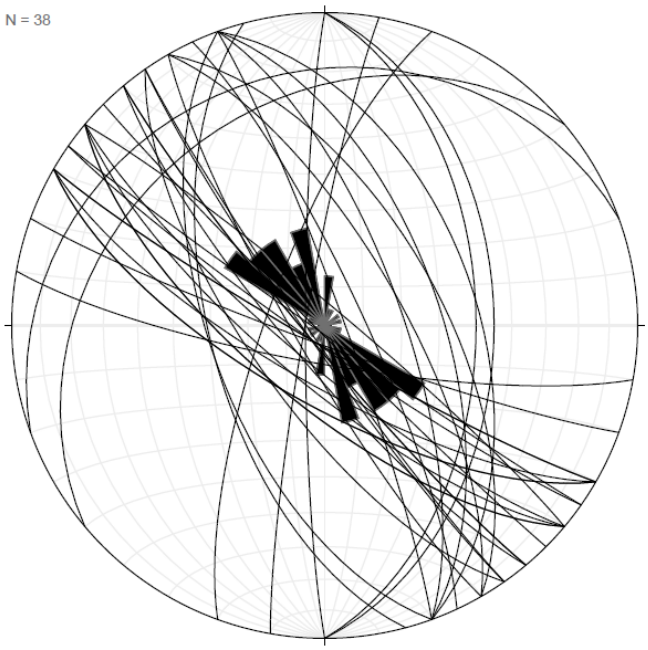

Fig. 107. Rose diagram of the measured joint directions in the artisanal mining pit outcrop.

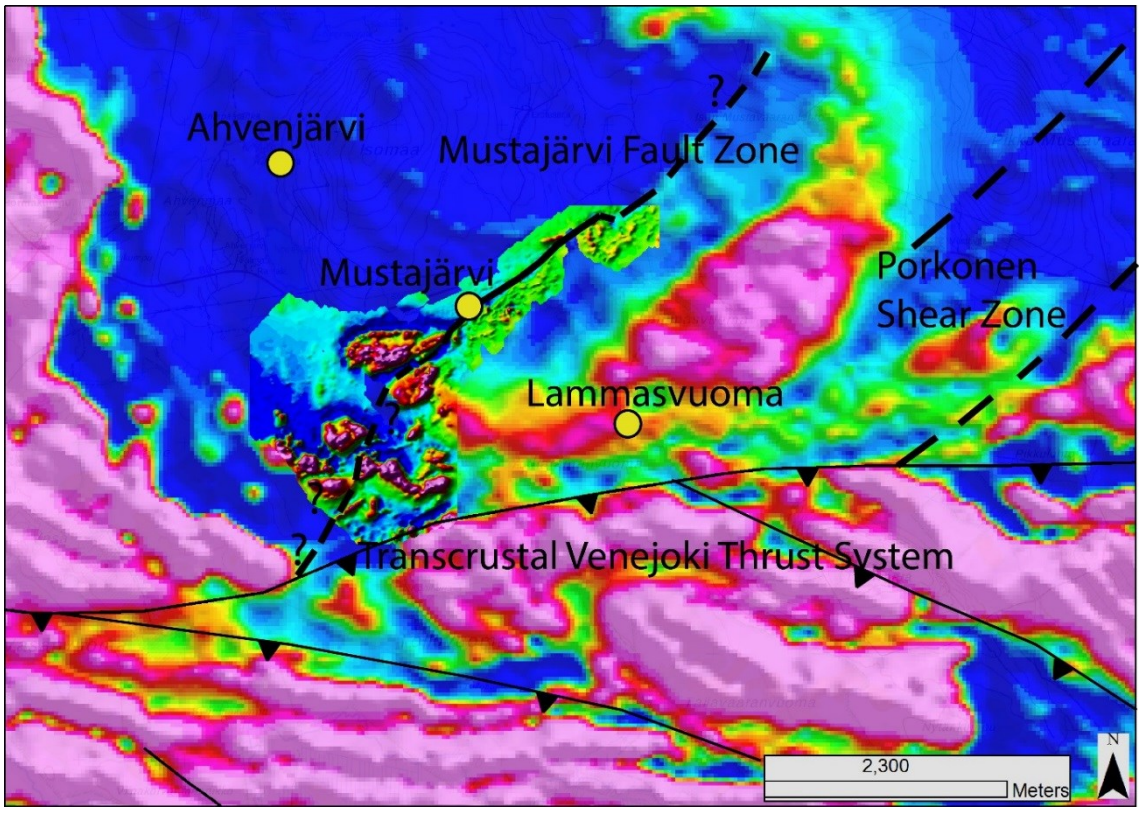

Fig. 108. Regional structural overview of Mustajärvi including the first order Venejoki thrust system and the second order Mustajärvi fault zone. Aeromagnetic- and more detailed ground magnetic geophysical data are shown in the background. Other structures than the Mustajärvi fault zone are after Niiranen (2015).

8. DISCUSSION

Geological setting

The siliciclastic metasedimentary rocks are believed to belong to the Sodankylä Group. However, it is uncertain to which formation they belong, as they share characteristics that are typical for both the Virttiövaara Formation and the Honkavaara Formation. Virttiövaara Formation rocks mainly consist of sericite quartzites, orthoquartzites and sericite schists, with fuchsite typically staining the rocks green, and cross bedding, graded bedding, herring bone structures and mud cracks (Lehtonen et al., 1998). Honkavaara Formation rocks comprise quartzites, siltstones, carbonate rocks and basic and acid volcanic rocks, which are typically strongly albitized (Eilu, 1994; Lehtonen et al., 1998). The siliciclastic metasediments at Mustajärvi consist of banded arkose quartzites and intermediate tuffites and mafic tuffites, which could be described as siltstones. Furthermore, they commonly show cross bedding and graded bedding features and rarely have a rare green coloring due to sericite-fuchsite, however, they are also generally intensively albitized. Hence, they are combining typical characteristics of both formations. Also on published geological maps, the Mustajärvi metasediments are assigned to different formations, with Lehtonen et al. (1998) assigning them to the Virttiövaara Formation and the most recent geological map (GTK:n Bedrock of Finland -DigiKp, 2016) provided by the Geological Survey of Finland (GTK) showing the rocks as part of the Honkavaara Formation.

The volcanic rocks most likely belong to the Savukoski Group. However, it is unclear to which formation they belong as the volcanic unit at Mustajärvi comprises both ultramafic metavolcanic rocks, which are typical for the upper Savukoski Group (Sattasvaara Formation), and rare graphitic schists, which are characteristic for lower Savukoski Group rocks (Matarakoski Formation) (Lehtonen et al., 1998). Lehtonen et al. (1998) regard the Mustajärvi volcanic rocks as Matarakoski Formation, whereas the most recent GTK geological map, (GTK:n Bedrock of Finland -DigiKp, 2016), assigns them to the Pittarova Formation. Hence, all map authors place the Mustajärvi metavolcanic rocks relatively low in the Savukoski Group, despite the fact that the metavolcanic rocks comprise distinct ultramafic volcanic rocks.

The contact between the siliciclastic metasediments and the metavolcanic rocks at Mustajärvi appears to be gradual with an increasing amount of volcanic interlayers in the

metasediments in proximity to the contact. Regarding the paleoenvironment, as described by Lehtonen et al. (1998), the metasediments might represent Sodankylä Group sedimentation of mainly siliciclastic material in environments, that transition from being influenced by tidal waves, over shallow water conditions, to subaqueous conditions, representing a continuous deepening of the rift basin setting. At advanced stages of the rift basin deepening, lower Savukoski Group graphitic schists started to form, which mark a key horizon in the CLGB. Those graphitic schists can rarely be seen at Mustajärvi but are a distinct feature at the contact of the metasediments and metavolcanic rocks. A reactivation of magmatic activity, likely plume related, caused the deepened basin to quickly fill with mafic and ultramafic volcanic rocks represented by the upper Savukoski Group; rocks that make up the major part of the volcanic unit at Mustajärvi. Thus, the geological evolution of the CLGB during the Sodankylä Group and Savukoski Group, as described by Lehtonen et al. (1998), fits into what can be seen in the rock package at Mustajärvi, with a strongly albitized metasedimentary unit showing bedding features in the stratigraphic bottom; rare graphitic cherts at the contact of the metasediments and volcanics; and massive mafic and ultramafic metavolcanic rocks at the stratigraphic top.

Alteration

The relationship between regional alteration and mineralization-related alteration is ambiguous. Regional alteration is interpreted to comprise moderate to strong albitization in the siliciclastic metasediments, and moderate carbonatization both in the metavolcanic unit and in the metasediments, which is consistent with many other deposits in the CLGB, e.g., Saattopora (Eilu et al., 2007). Pre-mineralization albitized metasediments are typical for the Honkavaara Formation in the Sodankylä Group (Lehtonen et al., 1998). Eilu (1994) interprets this albitization to be partly related to diagenetic processes, driven by a high heat flow regime of the rift zone, and involving sea water interaction. Eilu (1994) finds another cause for albitization and partial carbonatization in the onset of the magmatic activity that caused the formation and emplacement of the Savukoski Group volcanic rocks onto the metasediments at Mustajärvi, creating breccia zones and large hydrothermal cells in the system, triggering alteration. An additional regional alteration event could be found in association with the early Svecofennian orogeny, with the formation of intense fracture zones within the CLGB, which maintain fluid flow, likely enhanced by associated synorogenic silicic plutonism (Eilu, 1994).

Auriferous veins at Mustajärvi generally occur in the most intensively albitized parts of the metasediments. However, it is not entirely evident, whether the strongly albitized rocks that host mineralization were albitized by mineralizing fluids during the mineralization event or whether the auriferous veins preferably intruded into the most albitized rocks and thereby the most competent rocks, as is described by common models for vein formations in orogenic gold systems (e.g., Goldfarb et al., 2005). The author thinks that the latter scenario is more tenable, since equally intense albitized metasediments can be observed in the rock package without related gold-bearing veins.

The observed mineralization-related alteration features are mostly consistent with commonly described alteration processes typical for orogenic gold deposits (Goldfarb et al., 2005). Yet, the mineralization-related alteration is generally quite subtle and only occasionally, alteration features can clearly be assigned to it. This is concordant with general descriptions of orogenic gold-related alteration in clastic metasedimentary rocks, which are typically less reactive (Goldfarb et al., 2005). Furthermore, some alteration features occur only selectively and are not ubiquitous; perhaps a sign for different mineralization styles. For example, an intense biotitization can be seen in the proximal alteration zone of the high-grade massive pyrite mineralization in the metasediments, whereas generally, biotite enrichment is commonly only poorly developed in other mineralized intervals in the metasediments. The formation of biotite as an alteration product, at Mustajärvi co-present with sericite, is typically described to be an indicator for uppermost greenschist facies conditions (Eilu et al., 1999; Goldfarb et al., 2005). Other alteration features, such as tourmaline enrichment, can be seen in the proximity of almost every mineralized vein at Mustajärvi.

Mineralogy of the gold-mineralized veins

The gold mineralization at Mustajärvi is typical for orogenic gold deposits, consisting of quartz-tourmaline-pyrite veins with thicknesses commonly ranging between 0.15 m and 1.0 m. The veins mainly consist of quartz, varying amounts of tourmaline (5-35 vol.%), and average pyrite amounts of 10 vol.%. Pyrite is the only sulphide mineral in the gold-bearing veins, indicating vein formation conditions with T <400 °C and P <2.5 kbar in a hydrothermal environment that was not strongly reduced (Goldfarb et al., 2005). Orogenic gold deposits typically have average sulphide mineral amounts of 2-5 % (Goldfarb et al., 2005), which is lower than the average pyrite amount at Mustajärvi. However, this is not something extraordinary and can be seen in many orogenic gold

deposits around the world (R. Goldfarb, pers. comm., 2019). At Mustajärvi, it is evident that the gold concentration of the veins is broadly linked to the pyrite amounts, with higher gold grades in pyrite-rich veins, emphasized by gold occurring as telluride micro-inclusions in pyrite. Gold-bearing tellurides in orogenic gold deposits are not uncommon, e.g., in the giant Golden Mile deposit, Western Australia (>60 Moz mined gold) approx. 20 % of the gold is hosted by tellurides (Shackleton et al., 2003). However, it is uncommon for orogenic gold systems to have all gold hosted by tellurides. The formation of gold-bearing tellurides can be caused by a variety of mechanisms in orogenic gold deposits, including phase separation, wallrock interaction, cooling, and possibly condensation and fluid mixing (Shackleton et al., 2003). Due to a lack of data, it is not possible to determine what triggered gold-telluride formation over native Au formation at Mustajärvi. Furthermore, given the only limited amount of microprobe analysis, and the fact that all studied samples were, to some extent, affected by weathering processes, it is possible that the here presented gold mineralogy is not representative for unweathered gold mineralization at depth. Hence, it remains possible that native Au is part of the deeper, non-weathered gold-mineralized system.

At a vertical depth of 90 m, a 2-m-wide zone of massive pyrite mineralization with an average pyrite amount of ~50 vol.%, and small amounts of quartz and tourmaline has been observed. This massive pyrite mineralization yielded the highest gold grades so far observed at Mustajärvi, with 2 m at 45.1 ppm Au. It is not yet possible to say whether this zone is a different, more massive, higher-grade mineralization style that is characteristic for greater depths at Mustajärvi or whether it is just a unique structural or lithological feature, e.g., a local dilutional jog or a local replacement zone. This massive high-grade zone has not yet been followed up by further drilling and it was not part of the thin section study or microprobe analysis.

As part of future research, accessory monazite within the gold-mineralized veins could be utilized to date the vein formation event.

Geochemistry of the gold-mineralized veins

The geochemistry of the mineralized veins at Mustajärvi is typical for orogenic gold deposits with strongly enriched elements comprising Au, B, Bi, C (CO_2), Te, and Se. Other pathfinder elements that are commonly enriched in orogenic gold deposits, such as

Ag, As, Sb, and W are only elevated, but do positively correlate with gold. Atypical for orogenic gold deposits are strongly enriched concentrations of Ni and Co.

The enrichment of Ni, which is mainly hosted in the lattice of pyrite but also occurs as Ni-telluride micro inclusions in pyrite could be explained by the abundance of ultramafic rocks in the rock package. At Mustajärvi, these ultramafic lavas and tuffs were found to have Ni concentrations up to 1000 ppm, with averages of roughly 500 ppm Ni. The correlation of enriched Ni in gold mineralization and ultramafic host rocks has been observed in many gold occurrences along the Sirkka line (e.g., Korkalo, 2006). Similarly to Ni, the source of strongly enriched Co in the mineralized veins could be found in the ultramafic host rocks, as Co concentrations up to 110 ppm were detected in ultramafic lavas. The entire metavolcanic rock unit has an average Co concentration of ~50 ppm, whereas the metasediments only have ~5 ppm Co on average. An enriched Co concentration has been detected in many gold occurrences along the Sirkka line (Korkalo, 2006; Eilu et al. 2007), and it has been generally attributed to be sourced from ultramafic host rocks, however, this still remains debated.

Structural control

The assumed structural setting at Mustajärvi is in accordance with common structural models of orogenic gold deposits (e.g., Goldfarb et al., 2005), which involve a first-order structure that collects and channelizes fluids and metals, and a second-order fault that traps and precipitates the metals. In the case of Mustajärvi, these structures are likely represented by the transcrustal first-order Venejoki thrust fault system, which lies approx. 2 km south of Mustajärvi, and by the second-order Mustajärvi shear zone. Common structural models can include minor third-order splays off the second order fault; at Mustajärvi, possibly being represented by the auriferous veins, whose distribution pattern could be explained by a set of minor listric faults originating from the Mustajärvi shear zone or by a system of several smaller shear zones related to the larger Mustajärvi shear. These third-order splays would also explain the strong alteration that repeatedly occurs in the host rock package without correlating mineralization.

The first-order structure that Mustajärvi is associated with could, however, also be represented by the Porkonen shear zone, which has the same orientation as the Mustajärvi shear zone and terminates approx. 2 km east of Mustajärvi. The Porkonen shear zone is a first-order major structure that cuts through a large segment of the CLGB. The potential

association of the Mustajärvi mineralization with the Porkonen shear zone is supported by the nearby Ahvenjärvi and Lammasvuoma gold occurrences, of which the former is located ca. 2 km to the NW of Mustajärvi and the latter 2 km to the SE (Fig. 108). The gold-mineralized veins at Ahvenjärvi (also called Isomaa) and Lammasvuoma have the same structural orientation as those at Mustajärvi, striking roughly 45-70° with a ~45° dip to the SE (Huhtelin, 1991; Patison, 2007). The same strike direction and the proximity of the first-order Porkonen shear zone and the Mustajärvi, Ahvenjärvi and Lammasvuoma gold occurrences suggests a potential structural connection between the features.

9. CONCLUSIONS

The Mustajärvi mineralization represents a typical orogenic gold occurrence. It has a strong structural control, being hosted by the second-order Mustajärvi shear zone, which is interpreted to be a splay off the first-order transcrustal Venejoki thrust complex, situated approx. 2 km south of the occurrence. The Mustajärvi shear zone likely formed due to the competency contrast between the Sodankylä Group siliciclastic metasedimentary rocks and Savukoski Group metavolcanic host rocks. The auriferous veins are interpreted to be related to minor third-order structures associated with the second-order Mustajärvi shear zone.

Gold within the veins occurs as Au-telluride (calaverite) and Au-Bi-telluride (montbrayite) micro-inclusions in pyrite. Other telluride minerals include the Ni-telluride melonite, the Bi-telluride tellurobismuthite, and the Bi-Se-telluride kawazulite. As pyrite got oxidized during weathering, the telluride micro-inclusions were destroyed and gold was remobilized and deposited as free gold, mainly in the cracks of goethite. The geochemistry of the mineralized veins is typical for orogenic gold deposits, with strongly enriched elements comprising Au, B, Bi, C (CO_2), Te and Se; and with Ag, As, Sb and W being elevated and correlating positively with gold. Atypical for orogenic gold deposits are the enrichments of Ni and Co, which, however, can also be seen in many gold occurrences along the nearby Sirkka thrust system.

It appears that two different mineralization styles exist at Mustajärvi. The outcropping and near-surface mineralized veins are approx. 0.15 m to 1 m wide and consist mainly of quartz, tourmaline and pyrite. The second, higher-grade mineralization style was proven at a vertical depth of 90 m, comprising a 2-m-wide zone of massive pyrite mineralization (50 % pyrite) with only little amounts of quartz and relatively low tourmaline contents. This second style of mineralization has yet to be followed up by further drilling and indicates the openness of the gold mineralization in all directions, with great potential for a more extensive gold-mineralized system especially at depth.

10. ACKNOWLEDGMENTS

I would like to thank Firefox Gold and Magnus Minerals for providing an inspiring and constructive work place together with a great team including Aleksis, Alf, Carl, Jarkko, Juho, Mikko, Petri and Stefan. Great acknowledgments furthermore go to Pasi Eilu, who helped me with the initial drill core re-logging and guided me with his expertise all through my thesis work. Also, Tero Niiranen and Richard Goldfarb are greatly thanked for their continuous support, which helped to fundamentally improve the quality of this work. Juhani Ojala and the GTK are thanked for providing funding for the preparation of thin sections from the drill core and for geochemical analyses of the drill core samples. Also the University of Oulu, including Eero Hanski and Holger Paulick, are greatly acknowledged for funding the microprobe work and parts of the thin section studies.

At this point I would also like to thank my beloved Satu for her continuous moral support; and my friends Axel, Alex, Ellie, Matthew, Mauricio, Meseret, Nico, Richard, Semyon, and Thomas for a great, froggy time at the University of Oulu.

11. REFERENCES

Anttonen, R., 1993: Kittilän, Jerusaleminjängän; Mustajärven ja Torsavaaran Kairaukset v. 1991-92. Outokumpu Oy, Report 030/2734/RSA/93, 82 p. (in Finnish)

Craw, D. & Kerr, G., 2017: Geochemistry and mineralogy of contrasting supergene gold alteration zones, southern New Zealand. Applied Geochemistry 85, 19-34.

Eilu, P., 1994: Hydrothermal alteration in volcano-sedimentary rocks in the Central Lapland greenstone belt, Finland. Geological Survey of Finland, Bulletin 374, 145 p.

Eilu, P., Mathison, C., Groves, D. & Allardyce, W., 1999: Atlas of Alteration Assemblages, Styles, and Zoning in Orogenic Lode-Gold Deposits in a Variety of Host Rock and Metamorphic Settings. Geology and Geophysics Departments (Centre for Strategic Mineral Deposits) & UWA Extension, The University of Western Australia, Publication 30, 50 p.

Eilu, P. & Nykänen, V., 2011: Active and ongoing gold exploration and mining in Northern Finland. Excursion guide in the 25th International Applied Geochemistry Symposium 2011, 22-26 August 2011, Rovaniemi, Finland. Finnish Association of Mining and Metallurgical Engineers, Serie B92-7, 48 p.

Eilu, P. & Niiranen, T., 2013: Gold deposits in northern Finland. Geological Survey of Sweden, Excursion Guidebook FIN1, 56 p.

Goldfarb, R., Baker, T., Dubé, B., Groves, D., Hart C. & Gosselin, P., 2005: Distribution, character, and genesis of gold deposits in metamorphic terranes. Economic Geology, 100th Anniversary Volume, p. 407–450.

Goldfarb, R., Berger, B., George, M. & Seal, R., 2017: Tellurium. In: Schulz, K., DeYoung, J., Seal, R., Bradley, D. (eds.) Critical Mineral Resources of the United States—Economic and Environmental Geology and Prospects for Future Supply: U.S. Geological Survey, Professional Paper 1802, p. R1– R27.

Hanski, E., Huhma, H., Rastas, P., Kamenetsky, V.S., 2001: The Palaeoproterozoic komatiite-picrite association of Finnish Lapland. Journal of Petrology 42, 855–876.

Hanski, E. & Huhma, H., 2005: Central Lapland greenstone belt. In: Lehtinen, M., Nurmi, P.A. & Rämö, O.T. (eds.) Precambrian Geology of Finland – Key to the Evolution of the Fennoscandian Shield, Elsevier B.V., Amsterdam, p. 139–194.

Hanski, E., Huhma, H., Vuollo, J., 2010: SIMS zircon ages and Nd isotope systematics of the 2.2 Ga mafic intrusions in northern and eastern Finland. Bulletin of the Geological Society of Finland 82, 31–62

Holma, M. & Keinänen, V., 2007: The Levijärvi-Loukinen gold occurrence: An example of orogenic gold mineralisation with atypical metal association. Geological Survey of Finland, Special Paper 44, 165-186.

Hölttä, P., Väisänen, M., Väänänen, J. & Manninen, T., 2007: Paleoproterozoic metamorphism and deformation in Central Finnish Lapland. Geological Survey of Finland, Special Paper 44, 109-120.

Hugg, R., 1996: Kaivoslain 19§:n mukainen tutkimustyöselostus Mustajärvi nimisestä valtausalueesta kaiv. rek. nro 4798/1 Lapin läänissä Kittilän kunnassa. Outokumpu Oy, Report 080/2734 05/REH/96, 10 p. (in Finnish)

Huhtelin, T., 1991. Lammasvuoman Au-mineralisaation tutkimukset 1989-1991. Lapin Malmi, Report 001/2734/TH/91, 36 p. (in Finnish)

Koistinen, T., Stephens, M.B., Bogatchev, V., Nordgulen, Ø., Wennerström, M. & Korhonen, J. (comp.), 2001: Geological map of the Fennoscandian Shield, scale 1:2 000 000. Geological Survey of Finland, Espoo.

Korkalo, T., 2006: Gold and copper deposits in Central Lapland, northern Finland, with special reference to their exploration and exploitation. Acta Universitatis Ouluensis, A Scientiae Rerum Naturalium 461, 122 p.

Kortelainen, V., 1983: Sirkka-konglomeraatin ja Levitunturin kvartsiitin sedimentologia Kittilässä. Unpublished Master's Thesis, Departure of Geology, University of Helsinki, 101 p. (in Finnish)

Kyläkoski, M., Hanski, E. & Huhma, H., 2012: The Petäjäskoski Formation, a new lithostratigraphic unit in the Paleoproterozoic Peräpohja Belt, northern Finland. Bulletin of the Geological Society of Finland 84, 85–120.

Lahtinen, R., 2012: Main geological features of Fennoscandia. Geological Survey of Finland, Special Paper 53, 13–18.

Lehtonen, M., Airo, M-L., Eilu, P., Hanski, E., Kortelainen, V., Lanne, E., Manninen, T., Rastas, P., Räsänen, J. & Virransalo, P. 1998: Kittilän vihreäkivialueen geologia. Lapin vulkaniittiprojektin raportti. Summary: The stratigraphy, petrology and geochemistry of the Kittilä greenstone area, northern Finland. A Report of the Lapland Volcanite Project.

Geological Survey of Finland, Report of Investigation 140, 144 p. (Finnish with English summary)

McCuaig, T. & Kerrich, R., 1998: P-T-t-deformation-fluid characteristics of lode gold deposits: Evidence from alteration systematics. Ore Geology Reviews 12, 381–454.

Molnar, F., O'Brien, H., Lahaye, Y., Kurhila, M., Middleton, A. & Johanson, B., 2017: Multi-stage hydrothermal processes and diverse metal associations in orogenic gold deposits of the Central Lapland greenstone belt, Finland. Proceedings of the 14th SGA Biennial Meeting, 2017, Québec City, Canada, Volume 1, p. 63-66.

Mutanen, T. & Huhma, H., 2001: U-Pb geochronology of the Koitelainen, Akanvaara and Keivitsa layered intrusions and related rocks. In: Vaasjoki, M. (ed.): Radiometric Age Determinations from Finnish Lapland and Their Bearing on the Timing of Precambrian Volcano-Sedimentary Sequences. Geological Survey of Finland, Special Paper 33, 229-246.

Niiranen, T., 2015: A 3D structural model of the central and eastern part of the Kittilä terrane. Geological Survey of Finland, Report 90/2015, 17 p.

Niiranen T., Lahti I., Nykänen, V. & Karinen T., 2014: Central Lapland Greenstone Belt 3D modeling project final report. Geological Survey of Finland, Report of Investigation 209, 78 p.

Niiranen, T., Lahti, I. & Nykänen, V., 2015: The orogenic gold potential of the Central Lapland greenstone belt, northern Fennoscandian Shield. In: Maier, W.D., Lahtinen, R., O'Brien, H. (eds.) Mineral Deposits of Finland, Elsevier, Amsterdam, p. 733-752.

Nikula, R., 1985: Sodankylän Virttiö-ja Värttiövaaran metasedimenttien paleosedimentaatioympäristöt. Master's Thesis, University of Oulu, 109 p.

Patison, N. J., 2007: Structural controls on gold mineralisation in the Central Lapland Greenstone Belt. Geological Survey of Finland, Special Paper 44, 105-122.

Perttunen, V. & Vaasjoki, M., 2001: U-Pb geochronology of the Peräpohja schist belt, northwestern Finland. In: Vaasjoki, M. (ed.) Radiometric Age Determinations from Finnish Lapland and Their Bearing on the Timing of Precambrian Volcano-Sedimentary Sequences. Geological Survey of Finland, Special Paper 33, 45–84.

Rastas, P., Huhma, H., Hanski, E., Lehtonen, M.I., Härkönen, I., Kortelainen, V., Mänttäri, I. & Paakkola, J., 2001: U–Pb isotopic studies on the Kittilä greenstone area, Central Lapland, Finland. In: Vaasjoki, M. (ed.) Radiometric Age Determinations from Finnish

Lapland and Their Bearing on the Timing of Precambrian Volcano-Sedimentary Sequences. Geological Survey of Finland, Special Paper 33, 95–141.

Shackleton, M., Paul, J. & S., Bateman, R., 2003: Telluride Mineralogy of the Golden Mile Deposit, Kalgoorlie, Western Australia. Canadian Mineralogist 41, 1503-1524.

Sorjonen-Ward, P., Nironen, M. & Luukkonen, E., 1997: Greenstone associations in Finland. In: de Wit, M.J., Ashwal, L.D. (eds.) Greenstone Belts. Clarendon Press, Oxford, p. 677– 698.

Spence-Jones, C., Jenkin, G., Boyce, A., Hill, N., Sangster, C., 2018: Tellurium, magmatic fluids and orogenic gold: An early magmatic fluid pulse at Cononish gold deposit, Scotland. Ore Geology Reviews 102, 894-905.

Väänänen, J. & Lehtonen, M. I., 2001: U-Pb isotopic age determinations from the Kolari–Muonio area, western Finnish Lapland. In: Vaasjoki, M. (ed.) Radiometric Age Determinations from Finnish Lapland and Their Bearing on the Timing of Precambrian Volcano-Sedimentary Sequences. Geological Survey of Finland, Special Paper 33, 85–93.

Väisänen, M., 2002: Structural features in the central Lapland greenstone belt, northern Finland. Geological Survey of Finland. Archive Report K 21.42/2002/3. 20 p.

Ward, P., Härkönen, I. & Pankka, H.S., 1989: Structural studies in the Lapland greenstone belt, northern Finland and their application to gold mineralization. Geological Survey of Finland, Special Paper 10, 71–78.

Wyche, N.L., Eilu, P., Koppström, K., Kortelainen, V., Niiranen, T. & Välimaa, J., 2015: The Suurikuusikko Gold Deposit (Kittilä Mine), Northern Finland. In: Maier, W.D., Lahtinen, R. & O'Brien, H., (eds) Mineral Deposits of Finland. Elsevier, Amsterdam, p. 411-433.

Internet sources:

Agnico Eagle: https://www.agnicoeagle.com/English/operations-and-development-projects/reserves-and-resources/default.aspx (Last accessed 30.01.2019)

Bergman, 2011: http://fem.lappi.fi/c/document_library/get_file?folderId=506958&name=DLFE-10167.pdf (Last accessed 30.01.2019)

DigiKP200, Bedrock of Finland. 2016. Digital map database. Espoo: Geological Survey of Finland, Version 2.1.: https://gtkdata.gtk.fi/Kalliopera/index.html (last accessed 18.03.2019)

Appendices

1.1 EPMA results for telluride minerals

Sample ID	Analysis No.	Se	S	Co	Au	As	Fe	Ni	Bi	Ag	Sb	Te	Cu	Pb	Total	Mineral
MJ-19	21	0	0.719	0.081	43.24	0	3.312	0	1.782	0.125	0.34	54.056	0.079	0	103.734	Montbrayite
MJ-19	16	0	0.138	0.064	46.152	0	2.027	0.205	5.532	0.045	0.264	46.993	0	0	101.42	Montbrayite
MJ-27	35	0	0.824	0.09	40.752	0	3.346	0.722	4.582	0	0.309	45.49	0.022	0	96.137	Montbrayite
MJ-27	36	0	0.54	0.028	43.433	0	2.61	0.107	5.58	0.013	0.291	43.783	0	0	96.385	Montbrayite
MJ-27	51	0	0.295	0.013	44.871	0	2.271	0.268	5.27	0.033	0.338	45.893	0	0	99.252	Montbrayite
MJ-41	58	0	0.251	0.108	45.858	0	2.491	0.036	7.899	0	0.258	44.238	0	0	101.139	Montbrayite
MJ-27	45	0	1.285	0	36.08	0	3.559	0.223	11.652	0.053	0.22	44.899	0.189	0	98.16	Montbrayite
MJ-41	64	0	0.377	0.08	35.542	0	2.792	0.5	15.951	0.05	0.328	47.944	0.079	0	103.643	Montbrayite
MJ-27	46	0	0.795	0.072	24.052	0	3.456	0.771	24.797	0.064	0.327	45.769	0.101	0	100.204	Montbrayite
MJ-41	66	0	0.212	0.022	15.924	0	2.562	0	36.86	0.029	0.365	51.204	0	0	107.178	Montbrayite
MJ-19	18	0.166	4.933	0.049	8.781	0	5.004	0.283	39.471	0	0.281	43.855	0	0	102.823	Montbrayite
MJ-41	55	0	0.058	0	42.772	0	1.441	0.008	0.026	0.289	0.341	57.503	0	0	102.438	Calaverite
MJ-41	56	0	0.098	0.008	43.55	0	1.416	0.07	0.021	0.051	0.382	56.57	0	0	102.166	Calaverite
MJ-41	57	0	0.094	0	43.173	0	1.713	0.04	0	0.347	0.288	57.025	0.048	0	102.728	Calaverite
MJ-41	65	0	0.111	0.063	41.421	0	1.563	0.084	0	0.093	0.358	53.517	0.007	0	97.217	Calaverite
MJ-27	40	5.802	5.632	0.057	0	0	5.613	0.016	52.085	0.015	0.217	31.105	0	0	100.542	Kawazulite
MJ-27	39	5.998	2.031	0.045	0	0	1.445	0	56.028	0.008	0.174	32.429	0	0	98.158	Kawazulite
MJ-27	37	6.046	1.948	0	0	0	2.761	0.007	54.237	0.016	0.291	31.958	0	0	97.264	Kawazulite
MJ-27	39	5.998	2.031	0.045	0	0	1.445	0	56.028	0.008	0.174	32.429	0	0	98.158	Kawazulite
MJ-27	40	5.802	5.632	0.057	0	0	5.613	0.016	52.085	0.015	0.217	31.105	0	0	100.542	Kawazulite
MJ-27	42	6.015	2.118	0.103	0	0	2.934	0	56.635	0.01	0.181	32.203	0.031	0	100.23	Kawazulite
MJ-27	43	5.26	5.686	0.062	0	0	5.12	0.015	53.257	0.043	0.178	30.942	0.025	0	100.588	Kawazulite
MJ-27	44	6.065	1.731	0.038	0	0	2.231	0	55.175	0.078	0.241	32.64	0.022	0	98.221	Kawazulite
MJ-27	49	6.215	1.759	0.022	0	0	2.946	0.008	55.181	0	0.232	32.303	0	0	98.666	Kawazulite
MJ-27	50	2.21	3.516	0	0	0	1.72	0.035	57.141	0.019	0.165	33.375	0	0	98.181	Kawazulite
MJ-27	52	5.951	2.18	0.035	0	0	3.23	0.041	54.845	0	0.204	32.363	0	0	98.849	Kawazulite
MJ-19	6	0.056	0.573	0.019	0	0	2.47	0.01	52.517	0.028	0.224	45.108	0	0	101.005	Tellurobismuthite
MJ-41	54	0.234	0.168	0.027	0	0	1.268	0	52.364	0.016	0.214	44.709	0.009	0	99.009	Tellurobismuthite
MJ-19	5	0	1.216	0.038	0	0	3.589	17.544	0.056	0	0.444	79.361	0.03	0.034	102.312	Melonite
MJ-19	15	0	0.152	0.043	0	0	1.181	18.35	0.019	0	0.515	81.872	0	0	102.132	Melonite
MJ-19	22	0	0.689	0.019	0	0	2.038	18.744	0.011	0.002	0.447	82.732	0	0	104.682	Melonite
MJ-19	23	0	0.438	0	0	0	2.116	18.382	0.051	0	0.514	80.944	0.048	0	102.493	Melonite
MJ-27	34	0	0.453	0.065	0	0	2.668	18.03	0.032	0	0.499	81.115	0	0	102.862	Melonite
MJ-27	47	0	0.419	0.055	0	0	2.26	16.741	0.004	0	0.449	76.073	0.021	0	96.022	Melonite

1.2 EPMA results for pyrite, native Au, goethite, and Ag-Au-Se-goethite solid solution

Sample ID	Analysis No.	Se	S	Co	Au	As	Fe	Ni	Bi	Ag	Sb	Te	Cu	Pb	Total	Mineral
MJ-19	7	0.058	52.63	0.295	0	0	46.464	0.081	0	0.015	0.014	0	0.02	0	99.577	Pyrite
MJ-19	20	0.003	52.452	0.254	0	0.054	46.004	0.063	0	0.012	0	0.016	0	0	98.858	Pyrite
MJ-9	32	0.015	52.684	0.415	0.008	0.019	45.353	0.089	0	0	0.009	0	0	0	98.592	Pyrite
MJ-4	33	0.024	52.503	0.76	0.033	0.061	46.097	0.093	0	0	0.014	0	0	0	99.585	Pyrite
MJ-27	41	0.061	52.438	0.539	0	0	46.588	0.038	0	0	0	0	0.004	0	99.668	Pyrite
MJ-41	63	0.078	53.374	0.501	0.02	0	46.21	0.084	0	0.018	0.003	0.025	0	0	100.313	Pyrite
MJ-47	67	0.081	52.713	0.122	0.005	0.058	45.88	0	0	0	0.039	0	0.013	0	98.911	Pyrite
MJ-19	24	0	0.282	0.034	98.314	0.054	2.409	0	0	0.283	0	0	0.002	0	101.378	Native Au
MJ-27	48	0.058	0.186	0.022	98.151	0.037	1.749	0	0	1.188	0.006	0	0.024	0	101.421	Native Au
MJ-19	8	0	0.047	0	99.595	0.018	1.141	0	0	1.224	0.024	0.007	0.097	0	102.153	Native Au
MJ-41	59	0	0.093	0.044	97.917	0.032	0.339	0	0	2.559	0.009	0.045	0	0	101.038	Native Au
MJ-19	10	0	0.009	0.015	97.638	0.003	0.952	0.007	0	4.054	0	0	0	0	102.678	Native Au
MJ-19	9	0.02	0	0.033	93.63	0	1.548	0.024	0	7.266	0	0.005	0	0	102.526	Native Au
MJ-41	60	8.158	0.034	0.232	10.699	0.002	31.521	0.038	0	26.144	0	0.095	0	0	76.923	Ag-Au-Se-goethite
MJ-41	61	5.481	0.013	0.334	7.212	0.034	38.415	0.039	0.012	15.669	0	0.071	0	0	67.28	solid solution
MJ-19	12	0.029	0.05	0.384	0.018	0.063	52.123	0	0	0	0	0	0	0	52.667	Goethite
MJ-19	13	0.017	0.046	0.479	0	0.012	51.513	0.26	0	0	0	0.008	0	0.001	52.336	Goethite
MJ-19	14	0	0.01	0.327	0	0	51.593	0.108	0.014	0	0	0.025	0	0	52.077	Goethite
MJ-41	62	0	0.019	0.361	0.002	0.088	52.54	0	0.077	0.004	0	0.073	0	0	53.164	Goethite

1.3 EPMA results for standards, and unassigned and void measurements

Sample ID	Analysis No.	Se	S	Co	Au	As	Fe	Ni	Bi	Ag	Sb	Te	Cu	Pb	Total	Mineral
std FeS2	1	0.013	52.231	0.006	0.049	0.052	46.727	0.029	0	0	0	0	0	0	99.128	Stdandard: Pyrite
std FeS2	2	0.027	52.893	0.018	0	0	46.517	0	0	0	0	0	0	0	99.455	Stdandard: Pyrite
std FeS2	3	0.004	52.688	0	0.039	0	47.084	0.056	0	0.007	0	0.028	0	0	99.906	Stdandard: Pyrite
MJ-19	31	0	1.912	0.046	0	0	2.723	0.055	0	0.011	0.211	34.285	0.052	37.244	76.539	unassigned-Pb phase
MJ-19	4	0.258	1.499	0.044	0	0	2.488	1.968	48.593	0.033	0.325	47.312	0	0	102.52	unassigned/void
MJ-19	17	0	0.373	0.013	43.092	0	2.69	0.047	1.035	0.06	0.442	56.727	0	0	104.479	unassigned/void
MJ-19	18	0.166	4.933	0.049	8.781	0	5.004	0.283	39.471	0	0.281	43.855	0	0	102.823	unassigned/void
MJ-19	19	0	11.4	0.107	36.489	0	9.029	0.018	0	0.067	0.274	49.711	0	0	107.095	unassigned/void
MJ-19	11	0	0	0.447	0.035	0.087	52.247	0.07	0.129	0	0.012	0.189	0.059	0	53.275	unassigned/void
MJ-19	26	0.033	54.545	0.163	0.002	0.076	50.24	0.157	0	0.013	0	0.03	0.015	0	105.274	unassigned/void
MJ-19	27	1.654	33.445	0.139	0	0	29.222	0.081	29.135	0.02	0.078	18.579	0	0	112.353	unassigned/void
MJ-19	28	0	45.935	0.179	8.135	0	41.481	0.363	0.057	0	0.09	13.735	0	0	109.975	unassigned/void
MJ-19	29	3.456	2.334	0.034	0	0	3.768	0.032	54.488	0.028	0.216	30.622	0	0	94.978	unassigned/void
MJ-19	30	67.808	0.092	0.072	0	0	12.23	0.001	0.038	0	0	1.25	0	0	81.491	unassigned/void
MJ-27	38	0	0.714	0.021	40.757	0	3.175	1.599	0.785	0	0.271	49.993	0	0	97.315	unassigned/void
MJ-27	53	0.007	0.07	0.007	100.964	0	3.437	0.041	0	0.424	0	0	0.06	0	105.01	unassigned/void
MJ-19	25	0	0.211	0	0	0	1.015	24.596	0	0	0.748	148.675	0	0.008	175.253	void

2.1 Geochemical analysis of collected grab samples (mainly from the artisanal mining pit)

SAMPLE	Description	Ag_ppm	Al_pct	As_ppm	Au_ppm	Ba_ppm	Be_ppm	Bi_ppm	Ca_pct	Cd_ppm	Ce_ppm	Co_ppm	Cr_ppm	Cs_ppm	Cu_ppm	Fe_pct	Ga_ppm	Ge_ppm	Hf_ppm	In_ppm	K_pct	La_ppm
MJ-1	Biotite altered metakomatiite with intense qtz-carb-sulfide veining	<0.01	2.28	2.7	<0.005	60	2.57	0.06	7.87	<0.02	17.3	18	1350	20.3	32.8	7.47	9.19	0.13	0.6	0.035	2.45	8.7
MJ-3	Intensively oxidised quartz-pyrite-tourmaline vein	2.78	0.38	21.9	55.8	20	0.54	44.6	0.07	0.18	177	1450	193	0.09	41.6	33.8	4.26	0.56	0.3	<0.005	0.02	88.2
MJ-4	Oxidised quartz-pyrite-tourmaline vein	0.96	1.34	11.4	8.67	50	0.4	44.2	0.08	0.58	18.1	629	78	0.05	4.2	17.8	6.97	0.19	0.6	0.007	0.02	8.4
MJ-10	Strongly albitized and carbonatised arkose quartzite	<0.01	6.76	7.8	0.058	30	0.59	0.29	4.09	0.03	44.3	144	36	0.06	2.1	4.64	16.35	0.15	5.7	0.011	0.18	21
MJ-10.1	Siliciclastic Metasediment	0.01	7.38	4.5	0.052	30	0.7	0.26	3.22	0.03	10.85	44	8	<0.05	3.3	2.87	20.2	0.07	6.4	0.01	0.17	4.4
MJ-12	Siliciclastic Metasediment; quartz-plagioclase & carbonate veins	<0.01	5.35	3.3	0.012	30	0.4	0.06	4.9	0.03	17.55	68.5	23	0.08	1.6	5.55	12.7	0.08	2.7	0.019	0.14	8.1
MJ-19	Oxidised quartz-pyrite-tourmaline vein; quartz rich, tourmaline poor	0.68	0.08	4.7	13.45	10	0.11	14.4	0.02	0.04	4.36	513	222	<0.05	2.4	10	0.63	0.15	<0.1	0.006	0.01	2.3
MJ-20	Quartz vein	0.12	0.09	1.4	1.905	10	0.05	14.25	0.02	0.04	2.68	48.7	41	0.05	1.1	1.6	0.5	<0.05	0.1	<0.005	0.01	1.2
MJ-22	Least altered albitized arkose quartzite	0.01	6.1	0.5	0.022	200	0.87	1.77	0.23	<0.02	2.45	1.7	84	0.08	0.5	0.75	15.2	<0.05	4.5	0.006	0.59	1.2
MJ-23	Quartz vein	0.01	0.07	1	0.016	20	0.1	0.2	0.02	<0.02	3.11	13.1	43	0.07	1.2	0.69	0.34	0.05	<0.1	<0.005	0.01	1.3
MJ-24	Intensively carbonated and brecciated intermediate tuffite	0.01	4.5	22.2	0.016	190	0.86	0.05	6.74	0.14	5.07	24.8	79	0.08	95.4	4.94	9.54	0.1	1.4	0.029	1.2	2.2
MJ-25	Mn weathering crust on quartz vein	0.37	0.26	7.4	13.1	1370	1.25	0.5	0.08	1.16	8.38	1290	227	0.06	22.1	16.05	3.09	0.14	0.1	0.006	0.34	5
MJ-26	Carbonate-magnetite-pyrite vein	<0.01	0.03	0.9	0.018	10	<0.05	0.03	11.5	0.04	7.84	49	1	<0.05	1.1	27.5	3.93	0.32	<0.1	0.016	0.01	3.6
MJ-27	Oxidised quartz-pyrite-tourmaline vein; quartz rich, tourmaline poor	2.42	0.66	12.4	63.8	30	0.37	193.5	0.11	0.07	32	1180	115	0.05	8.2	28.8	4.42	0.42	0.3	0.005	0.02	16
MJ-28	Listvenite	<0.01	4.17	22.2	0.051	160	0.76	0.2	3.83	0.03	3.95	22.3	1330	0.25	34.3	9.26	10.75	0.13	0.8	0.065	1.43	1.9
MJ-29	Albitised intermediate tuffite with magnetite veining	<0.01	3.28	0.4	0.015	2240	1.06	0.06	0.06	<0.02	44.5	9.8	67	0.23	3.9	10.9	10.9	0.17	2.1	0.041	1.75	22.9
MJ-30	Intensively altered ultramafic tuff; carbonated	<0.01	2.35	5.9	0.028	520	0.37	0.18	4.11	0.17	1.77	69.1	1120	0.34	3.2	6.2	7.5	0.07	0.5	0.032	1.16	0.6
MJ-31	Listvenite	0.01	2.89	1	<0.005	410	0.82	0.04	10.15	0.02	3.92	7.5	1630	0.24	1.7	4.47	9.5	0.09	0.5	0.113	1.62	1.5
MJ-32	Least altered mafic lava	0.03	6.84	3.2	0.01	230	0.58	0.07	5.85	0.1	16.3	52	86	0.07	85.7	7.93	17.35	0.11	2.5	0.085	0.29	6.7
MJ-33	Quartz vein	0.01	0.08	1	0.313	30	0.09	0.75	0.04	<0.02	1.64	11.8	52	0.06	1.7	0.73	0.34	<0.05	<0.1	<0.005	0.01	0.8
MJ-34	Oxidised quartz-tourmaline-pyrite vein	1.2	1.21	10.4	14.75	70	0.31	64.2	0.07	0.38	17.85	562	74	0.08	4.3	19.2	5.74	0.25	0.6	0.006	0.05	8.6
MJ-35	Rel. unoxidised quartz-pyrite-tourmaline vein	0.85	0.88	7.3	10.95	20	0.31	32.1	0.03	0.13	4.75	869	61	<0.05	4.4	16.05	4.5	0.33	0.3	<0.005	0.01	2.1
MJ-36	Deformed intermediate tuffite	0.02	6.29	0.6	0.112	280	1.17	0.22	0.31	0.03	24.4	97	99	0.3	2.9	1.32	15.25	0.08	5.4	0.009	1.01	12.3
MJ-37	Least altered banded arkose quartzite	0.01	7.84	0.4	0.014	1260	1.94	0.1	0.15	<0.02	2.14	3.3	162	0.3	0.4	1.53	33.6	0.08	4	0.03	2.46	1.3
MJ-38	Strongly altered ultramafic tuff	<0.01	5.77	<0.2	0.007	390	1.38	0.08	2.11	<0.02	12.55	48.8	1400	3.3	0.2	7.12	20.2	0.18	1.6	0.027	4.13	6.2
MJ-39	Oxidised quartz-pyrite-tourmaline vein	0.41	1.42	5.5	5.25	10	0.32	22	0.06	0.04	3.61	564	65	<0.05	3.3	11.45	7.16	0.27	0.8	0.007	0.01	1.6
MJ-40	Mn weathering crust on quartz vein	0.18	0.23	4.1	3.9	1560	0.94	0.47	0.08	1.99	14.15	793	137	<0.05	5.1	7.9	3.62	0.11	0.1	<0.005	0.43	6.9
MJ-41	Oxidised quartz-pyrite-tourmaline vein	0.9	1.09	8.2	12	30	0.3	36.9	0.06	0.29	13.65	636	89	<0.05	4.9	16.5	6.03	0.23	0.4	0.006	0.02	6.2
MJ-42	Intensively oxidised quartz-pyrite-tourmaline vein	1.18	0.47	17.5	34.7	20	0.47	40.6	0.05	0.19	272	1060	221	0.07	41.3	31.6	5.34	0.61	0.3	0.006	0.02	134.5
MJ-44	Least altered komatiite-chlorite shist	<0.01	4.21	1.1	0.044	90	0.94	0.12	4.55	0.05	3.68	65.6	1640	0.22	22.9	7.9	12.55	0.11	0.7	0.074	0.22	1.8
MJ-46	Strongly altered ultramafic tuff	<0.01	5.84	0.9	0.018	270	1.87	0.06	3.69	<0.02	7.2	37.8	1390	3.4	0.9	7.6	20.5	0.13	1.5	0.03	3.76	3.2
MJ-47	Oxidised quartz-tourmaline-pyrite vein; tourmaline rich	0.72	1.99	7.8	9.91	20	0.46	28.7	0.08	0.18	15.5	702	104	<0.05	30.7	15.3	9.97	0.27	0.8	0.01	0.03	7.4
MJ-UT1	Mafic tuffite?!	0.01	7.54	4	0.033	130	0.85	0.1	0.79	<0.02	8.4	36.1	196	0.12	196	7.17	19.05	0.12	0.9	0.057	0.34	3.4
MJ-UT3	Least altered mafic lava	0.03	6.68	2.1	0.011	80	0.47	0.03	5.54	0.16	15.5	54.6	37	0.33	90.1	10.85	18.3	0.13	1.7	0.089	0.11	6.8
MJ-UT5	Least altered komatiite	<0.01	3.17	1.7	<0.005	150	0.47	0.09	6.97	0.03	6.81	112.5	1660	0.17	36.4	7.74	10.7	0.11	0.8	0.062	0.17	2.7
MJ-UT7	Intensively veined, carbonated albitized mafic tuffite	0.01	7.28	0.8	0.005	470	2.47	0.05	1.33	<0.02	25	13.1	121	1.24	1.3	3.54	27	0.1	4.7	0.019	2.59	10
MJ-UT7.2	Intensively veined, carbonated albitized mafic tuffite	<0.01	6.71	0.5	<0.005	390	2.47	0.04	1.84	<0.02	19.45	12.4	103	1.23	0.9	3.56	23.7	0.1	4.2	0.02	2.27	7.4

SAMPLE	Li_ppm	Mg_pct	Mn_pct	Mo_ppm	Na_pct	Nb_ppm	Ni_ppm	P_pct	Pb_ppm	Rb_ppm	Re_ppm	S_pct	Sb_ppm	Sc_ppm	Se_ppm	Sn_ppm	Sr_ppm	Ta_ppm	Te_ppm	Th_ppm	Ti_pct	Tl_ppm	U_ppm	V_ppm	W_ppm	Y_ppm	Zn_ppm	Zr_ppm
MJ-1	44.7	7.55	0.328	0.28	0.02	0.2	445	0.022	1.2	470	<0.002	0.1	0.11	17.6	1	1.8	32.3	<0.05	0.21	0.11	0.212	2.06	0.2	128	0.8	6.4	8	12.9
MJ-3	1.9	0.1	0.0257	17.8	0.04	0.1	329	0.256	43.8	1.7	<0.002	0.16	0.27	10.3	37	0.2	9.4	<0.05	440	6.06	0.008	<0.02	60	62	4.7	17.7	54	10.1
MJ-4	3.3	0.37	0.0397	11.75	0.14	0.3	173.5	0.108	50.6	1.1	<0.002	0.43	0.28	11	30	0.4	31.7	<0.05	44.2	1.49	0.031	<0.02	30	111	2.4	10.7	17	20.3
MJ-10	0.7	1.56	0.101	0.79	5.52	9.1	50	0.138	1.2	5.3	<0.002	0.98	0.72	13.4	2	1.9	43.8	0.62	0.89	3.97	0.685	<0.02	1.6	105	3.6	16.8	11	209
MJ-10.1	1.6	1.03	0.0903	0.92	6.12	16.2	28.6	0.139	1.5	2.8	<0.002	0.38	0.69	8.9	1	1.6	46	1.07	0.3	3.23	1.125	0.02	1.8	139	6.6	13.8	8	234
MJ-12	0.8	1.92	0.127	0.41	4.27	2.2	42.6	0.094	1.2	4.3	<0.002	0.45	0.3	21.5	1	0.9	39.9	0.17	0.24	1.26	0.269	<0.02	0.6	99	1	10.3	9	96.4
MJ-19	0.5	0.02	0.0073	3.7	0.03	<0.1	154	0.038	10.9	0.4	<0.002	1.4	0.11	1.8	30	<0.2	2.5	<0.05	70.7	0.27	<0.005	<0.02	7.8	17	0.8	2.5	12	1.3
MJ-20	1	0.02	0.0073	2.38	0.04	0.1	14	0.007	6	0.4	<0.002	0.02	0.11	1	3	<0.2	3.7	<0.05	32.1	0.22	<0.005	<0.02	1.7	7	0.3	1.2	5	3.4
MJ-22	1.4	0.14	0.004	0.97	4.78	2.6	7.6	0.063	2.6	13.8	<0.002	<0.01	0.16	3.7	<1	1.1	38.6	0.22	0.39	7.37	0.108	0.03	1.2	32	6.1	6.3	2	150
MJ-23	0.5	0.01	0.0181	2.65	0.04	0.1	6.9	0.004	1.7	0.9	<0.002	0.01	0.12	1.4	1	<0.2	2.8	<0.05	0.7	0.1	<0.005	<0.02	2.4	5	2.9	0.9	<2	0.9
MJ-24	4.3	3.05	0.182	0.76	1.89	2	39.2	0.042	0.6	19.7	<0.002	0.03	0.34	33.8	1	0.6	52.6	0.15	0.1	0.83	0.279	<0.02	0.4	114	0.6	7.4	91	45.6
MJ-25	2	0.05	5.26	29.1	0.05	0.1	292	0.057	5.3	3.2	<0.002	0.04	0.17	4.4	14	0.2	438	<0.05	369	0.41	0.005	0.09	18.3	31	0.8	4.8	23	5.3
MJ-26	0.5	5.22	0.53	0.45	0.01	<0.1	157.5	0.001	5.9	0.3	<0.002	0.47	0.12	11	1	<0.2	202	<0.05	0.21	0.77	<0.005	<0.02	1.2	97	0.1	14.7	10	0.5
MJ-27	1.4	0.2	0.0381	7.32	0.08	0.1	249	0.075	27.6	0.7	<0.002	0.89	0.22	7.2	81	0.3	16.3	<0.05	201	4.19	0.015	<0.02	17.9	76	3.7	9.5	39	12.1
MJ-28	2.9	4.93	0.279	0.31	1.31	0.2	273	0.018	1.1	41.6	<0.002	0.08	0.58	29.2	<1	0.8	30	<0.05	0.1	0.16	0.164	0.05	0.3	184	2	4.2	3	26.5
MJ-29	2.8	0.49	0.0122	1.2	0.07	4.3	23.1	0.026	0.7	52.4	<0.002	0.03	0.24	3.9	<1	1.5	17.5	0.1	0.05	5.2	0.081	0.07	1.5	37	4.3	4.1	3	70
MJ-30	10.5	10.3	0.161	0.32	0.04	0.1	951	0.011	2	46.1	<0.002	0.15	1.45	18.7	1	0.2	150.5	<0.05	0.24	0.03	0.134	0.3	0.1	126	<0.1	2.4	85	12.2
MJ-31	3.8	5.9	0.239	0.8	0.05	0.1	301	0.011	0.6	67.2	<0.002	0.01	0.65	21.7	<1	0.3	85	<0.05	0.05	0.1	0.073	0.08	0.2	151	0.1	6.1	5	11.6
MJ-32	8.3	3.81	0.144	1.25	2.03	6.5	69.6	0.059	0.9	6.5	0.002	0.2	0.16	47	1	1	107.5	0.43	0.13	0.57	0.865	0.12	0.5	311	<0.1	26.6	128	81.2
MJ-33	0.4	0.02	0.0348	3.55	0.04	0.2	7.1	0.002	1.1	0.6	<0.002	0.02	0.11	1.2	1	<0.2	3.7	<0.05	1.53	0.16	<0.005	<0.02	2.1	3	1.1	0.9	<2	0.7
MJ-34	2.7	0.3	0.0673	8.75	0.12	0.3	154.5	0.092	23.3	1.7	<0.002	2.06	0.24	9.9	45	0.3	25.2	<0.05	56	1.45	0.025	<0.02	26.9	92	2	9.3	19	18.9
MJ-35	2.8	0.25	0.0099	4.11	0.1	0.2	174.5	0.026	17.9	0.3	0.006	9.53	0.21	7.9	89	0.3	20.9	<0.05	41	0.65	0.017	<0.02	7.1	59	0.7	13.9	11	8.4
MJ-36	3.7	0.57	0.0414	0.69	4.28	3.5	56.1	0.061	<0.5	29.2	<0.002	0.01	0.18	5.8	<1	1.5	74	0.34	0.71	7.53	0.148	0.06	1.5	49	2	7.3	8	182
MJ-37	2.8	0.34	0.0043	0.48	3.43	4.4	11.7	0.039	0.8	83.7	<0.002	0.01	0.25	12.4	<1	1.8	52	0.39	0.57	7.87	0.217	0.15	1.9	112	4.3	5.9	4	133.5
MJ-38	18.2	6.53	0.0719	0.38	0.03	2.8	455	0.029	1.1	233	<0.002	0.01	0.14	25	1	1.1	14.3	0.18	0.2	0.84	0.45	0.5	1.6	217	0.6	5	9	52.7
MJ-39	2.3	0.42	0.0076	4.91	0.16	0.3	129.5	0.016	18.2	0.5	0.003	6.27	0.15	12.4	71	0.5	37.3	<0.05	28.9	0.76	0.033	<0.02	5.8	97	0.7	6.4	8	26.3
MJ-40	1.9	0.06	7.3	31.7	0.05	0.1	176.5	0.054	6.5	2.1	<0.002	0.04	0.19	2.2	5	0.2	603	<0.05	99	0.54	<0.005	0.13	16.7	53	0.7	8.4	28	2.9
MJ-41	3	0.3	0.0334	7.75	0.12	0.2	170.5	0.094	36.6	0.6	<0.002	1.86	0.23	9.9	49	0.4	24.7	<0.05	45.6	1.08	0.022	<0.02	21.5	87	1.5	7.9	21	13.7
MJ-42	1.9	0.1	0.0305	25.2	0.04	0.1	292	0.319	47.2	1	<0.002	0.03	0.25	10.2	29	0.2	11.7	<0.05	439	9.21	0.008	<0.02	68.2	62	4.4	15.7	63	13
MJ-44	13.8	12.15	0.142	0.34	0.29	0.8	1070	0.013	<0.5	16.9	0.002	0.01	0.19	32.4	1	0.5	21.5	0.05	0.54	0.1	0.114	0.04	0.5	180	<0.1	10.8	61	23.5
MJ-46	21.5	6.73	0.0659	0.25	0.03	2	526	0.028	0.8	229	0.003	0.01	0.24	27.3	1	2.9	16.3	0.14	18.5	0.78	0.427	0.45	7.2	223	0.5	5.3	11	53.4
MJ-47	2.4	0.57	0.0244	7.35	0.22	0.5	181.5	0.053	20.1	1	0.004	4.49	0.26	17.1	67	0.7	47.3	<0.05	29.6	1.06	0.045	<0.02	16.1	151	1.9	11.4	15	30.9
MJ-UT1	16.3	4	0.044	0.92	2.06	3.5	98.4	0.031	0.6	3.7	0.003	0.17	0.15	45.7	1	0.4	183	0.24	0.41	0.32	0.646	0.04	0.3	277	0.1	4.4	24	32.7
MJ-UT3	5.1	3.32	0.178	0.56	2.4	4.7	43.1	0.058	1.3	2.5	0.005	0.09	0.41	45.7	1	1.2	144	0.3	0.21	0.45	0.885	0.03	0.2	350	<0.1	32.7	118	56.5
MJ-UT5	11.8	11.05	0.116	0.18	0.25	0.7	962	0.017	<0.5	6.3	0.003	0.58	0.3	25.4	1	0.6	46.7	0.05	0.07	0.11	0.231	0.04	0.6	172	<0.1	14.4	63	28.6
MJ-UT7	14.7	3.85	0.0639	0.5	2.75	3.4	114.5	0.024	1.1	78.5	0.003	0.01	0.32	16.6	1	2.1	97	0.35	0.15	7.39	0.252	0.23	1	161	0.4	7.5	6	168
MJ-UT7.2	14.5	3.94	0.0516	0.35	2.66	6.7	88.8	0.022	1	108.5	0.002	0.01	0.28	14.6	1	2	86.8	0.37	0.07	7.96	0.242	0.2	4.5	116	0.5	7	6	149

2.2 Geochemical analysis of historic Outokumpu drill core (the sample format MJ-X-YYYY gives information about the core ID (X) and depth of the sample (YY.YY = e.g. 12.34 m down dip)).

SAMPLE	Description	Ag_ppm	Al_pct	As_ppm	Au_ppm	Ba_ppm	Be_ppm	Bi_ppm	Ca_pct	Cd_ppm	Ce_ppm	Co_ppm	Cr_ppm	Cs_ppm	Cu_ppm	Fe_pct	Ga_ppm	Ge_ppm	Hf_ppm	In_ppm	K_pct	La_ppm
MJ-3-4225	Quartz-tourmaline-pyrite vein in arkose quartzite host rock	0.01	6.64	0.7	0.079	20	0.74	0.44	0.72	1.14	3.25	74.7	142	0.14	11	2.42	15.2	0.06	2.3	<0.005	0.18	1.6
MJ-3-4273	Quartz-pyrite vein in arkose quartzite host rock	<0.01	4.04	1.3	0.073	20	0.49	0.14	0.26	0.04	1.16	137.5	69	0.06	5.5	4.42	8.62	0.13	1.4	0.005	0.08	0.6
MJ-3-5002	Albitized, carbonated intermediate tuffite	<0.01	6.01	<0.2	0.005	130	0.98	0.06	2.43	<0.02	5.05	1.2	92	0.47	0.7	1.24	17.9	0.07	3.6	0.009	0.83	2.4
MJ-3-5570	Altered intermediate tuffite	<0.01	5.38	0.5	<0.005	20	0.73	0.1	3.18	<0.02	13.9	4.8	19	0.82	2.8	1.18	11.5	0.06	0.7	0.005	0.39	8
MJ-4-3578	Magnetite-pyrite-carbonate vein	0.01	3.24	2.5	0.018	1660	2.29	0.22	9.26	<0.02	51.8	64.9	246	0.42	3.7	21.5	8.38	0.18	1	0.404	1.54	23
MJ-4-3876	Least altered mafic tuffite; albitised	0.01	6.87	0.5	<0.005	690	1.83	0.03	0.59	<0.02	3.85	9	111	0.97	6.1	3.32	24.6	0.09	5	0.02	2.87	1.4
MJ-4-4098	Mafic tuffite, carbonated, albitised, hematite rich	<0.01	6.16	0.3	<0.005	490	1.53	0.03	3.49	<0.02	7.48	16.1	103	1.1	1	5.11	20	0.11	4.3	0.019	2.89	3
MJ-4-4204	Brecciated, albitized and carbonated quartzite/intermediate tuffite	0.01	6.57	0.6	0.005	250	1	0.03	3.87	<0.02	5.46	2.3	91	0.24	2.3	1.71	15.7	0.06	4.7	0.009	1.2	3
MJ-5-0885	Intensively carbonated and albitized arkose quartzite	<0.01	6.58	0.5	<0.005	30	0.99	0.03	4.69	<0.02	13.7	2.2	69	<0.05	2.8	1.65	17.5	<0.05	4.5	0.007	0.09	11.2
MJ-5-1305	Intermediate tuffite	0.01	6.42	0.5	<0.005	310	2.07	0.04	4.34	<0.02	17	6.4	82	0.68	1.8	2.33	18.45	0.07	4	0.011	1.01	7.2
MJ-5-4690	Quartz vein with carbonate-(tourmaline) overprint	0.04	0.94	0.5	0.029	70	0.16	0.2	3.05	<0.02	10.35	6.1	27	0.23	2.8	0.84	2.38	<0.05	0.5	<0.005	0.43	7.2
MJ-5-4880	Strongly albitized, carbonated veined arkose quartzite	0.01	6.7	<0.2	0.041	70	1.43	0.15	2.22	0.03	12.5	4.1	121	0.33	4.1	1.19	16.3	0.05	5.2	<0.005	0.36	9.1
MJ-5-4970	Albitized intermediate tuffite with quartz-pyrite vein	0.01	6.35	0.4	0.025	120	1.41	0.13	2.34	<0.02	4.7	5.2	109	0.4	1.1	1.93	13.05	0.05	5	<0.005	0.51	2.4
MJ-5-5286	Intermediate tuffite with qtz-pyrite-hematite veining	<0.01	7.06	1	0.283	780	2.2	1.05	0.63	<0.02	5.52	76.6	107	0.46	1.7	4.91	23.3	0.09	4.6	0.037	3.05	2.6
MJ-6-1573	Least altered komatiitic basalt	0.03	5.49	1.1	0.012	90	0.37	0.27	6.63	<0.02	7.39	60	835	0.21	236	8.12	14.45	0.06	0.5	0.069	0.46	2.5
MJ-6-2532	chloritized, pyritized mafic volcanic with quartz-plagioclase veining	0.03	6.58	80.3	0.02	740	2.73	4.35	0.44	<0.02	3.96	228	104	0.26	97.1	7.82	14.25	0.08	1.2	0.06	1.81	1.6
MJ-6-3218	Intensively albitized, and carbonate arkose quartzite	0.01	6.49	0.6	<0.005	20	0.83	0.04	2.07	<0.02	1.78	1.5	12	<0.05	2.4	0.84	15.15	<0.05	3.5	<0.005	0.06	0.6
MJ-6-3374	Least altered intermediate tuffite	<0.01	6.75	0.3	<0.005	410	1.86	0.06	0.55	<0.02	3.42	2.5	160	0.75	1.9	1.81	19.3	<0.05	4.2	0.007	1.45	1.6
MJ-6-4632	Least altered intermediate tuffite	<0.01	7.95	0.2	<0.005	1210	2.88	0.02	0.62	<0.02	26.7	5.3	115	0.49	1.3	2.63	23.5	0.1	3.6	0.042	4.03	12.5
MJ-6-4785	Intensively albitized, and carbonate arkose quartzite	<0.01	5.55	0.3	<0.005	40	0.79	0.03	2.35	<0.02	7.23	1.6	51	0.05	1.4	1.03	12.4	<0.05	2	<0.005	0.22	3.4
MJ-6-5676	Least altered intermediate tuffite	<0.01	6.39	0.2	<0.005	390	1.5	0.02	0.67	<0.02	3.55	4.5	91	0.46	1	1.56	18.1	0.06	1.9	0.012	1.58	1.5
MJ-6-6468	Albitized and carbonated intermediate tuffite (partly bleached)	<0.01	5.89	0.3	<0.005	80	0.91	0.02	1.62	<0.02	3.14	2.4	80	0.14	1.6	1.11	12.4	<0.05	2	<0.005	0.34	1.4
MJ-7-2947	Arkose uartzite with quartz-pyrite- (tourmaline) vein	<0.01	5.99	1.3	0.207	90	0.93	0.33	0.51	<0.02	28.2	225	115	0.17	4.2	3.86	12.45	0.19	3.5	<0.005	0.35	15.6
MJ-7-3018	Silicified arkose quartzite with quartz- (tourmaline) veining	0.01	5.91	0.4	<0.005	100	1.26	0.03	0.59	<0.02	8.53	1.5	72	0.21	1.9	0.77	16.9	<0.05	2.3	<0.005	0.4	5.2
MJ-9-2683	Brecciated intermediate tuffite, veined	<0.01	6.66	0.4	0.031	210	1.39	0.04	0.52	<0.02	2.56	2.1	100	0.7	2.2	1.85	19.1	<0.05	4.4	0.007	0.76	1.4
MJ-9-3495	Brecciated, carbonated mafic tuffite; veined	<0.01	5.61	<0.2	<0.005	450	1.2	0.03	4.12	<0.02	11.3	11.6	87	1.52	1	3.34	16.15	0.07	4.2	0.012	1.81	6.4
MJ-9-4130	Completely altered carbonate rock; relictic quartz clasts	0.03	2.1	<0.2	0.006	250	0.62	0.13	13.05	<0.02	67.3	8.8	111	0.3	2	3.24	8.19	0.11	0.7	0.014	0.33	35.5
MJ-9-5087	Quartz-pyrite veining in altered arkose quartzite	0.09	4.51	3.3	0.371	60	0.62	2.2	0.2	0.02	27.7	467	116	0.3	9.2	7.69	12.3	0.13	1.7	<0.005	0.34	13.2
MJ-9-6093	Least altered arkose quartzite/intermediate tuffite	0.01	6.21	0.2	<0.005	830	1.31	0.05	0.39	0.02	9.59	1.6	162	0.2	2.1	0.83	18.8	0.05	3	0.021	1.39	5.1
MJ-9-6450	heavily altered komatiitic basalt	0.01	5.04	0.3	<0.005	180	1.78	0.04	5.8	<0.02	7.48	24.7	978	0.95	1.1	5.91	21.9	0.08	1.5	0.012	1.49	3.8

SAMPLE	Li_ppm	Mg_pct	Mn_pct	Mo_ppm	Na_pct	Nb_ppm	Ni_ppm	P_pct	Pb_ppm	Rb_ppm	Re_ppm	S_pct	Sb_ppm	Sc_ppm	Se_ppm	Sn_ppm	Sr_ppm	Ta_ppm	Te_ppm	Th_ppm	Ti_pct	Tl_ppm	U_ppm	V_ppm	W_ppm	Y_ppm	Zn_ppm	Zr_ppm
MJ-3-4225	1.3	0.36	0.0223	1	5.37	1.8	34.6	0.024	6.9	4.8	<0.002	1.7	0.15	2.7	6	0.7	48.5	0.12	0.57	0.85	0.041	0.03	1.1	32	3.9	4.1	28	84.5
MJ-3-4273	0.7	0.09	0.0074	1.47	3.23	0.5	63.3	0.016	4.7	1.8	<0.002	4.41	0.11	0.5	6	0.4	28.9	<0.05	0.91	0.65	0.015	0.02	1	18	2	4.6	9	47.2
MJ-3-5002	2.8	1.39	0.0955	0.35	4.16	2.8	8.3	0.032	0.9	23.2	<0.002	0.01	0.1	7.6	<1	0.8	28.2	0.19	0.12	3.87	0.11	0.05	1.4	60	1.7	4.8	<2	128.5
MJ-3-5570	6.9	1.98	0.143	0.58	3.35	1.7	11.2	0.022	0.7	15.7	<0.002	0.01	0.07	2.4	<1	0.3	28.1	0.06	<0.05	0.71	0.03	0.05	2	12	1	7.2	<2	25.3
MJ-4-3578	2.9	4.55	0.605	0.64	0.25	0.8	108	0.013	1.5	51.2	<0.002	0.9	0.15	16.4	3	1.3	44.1	<0.05	0.18	1.07	0.144	0.07	2.3	85	7.8	14.8	13	32.5
MJ-4-3876	7.5	1.72	0.0268	0.8	2.07	9.3	55.3	0.056	1.3	116.5	<0.002	0.02	0.11	10.9	1	1.9	39.2	0.56	0.09	9.82	0.27	0.22	1.9	85	2.2	5.8	12	170.5
MJ-4-4098	9.1	3.98	0.0701	0.44	1.37	5.3	96.2	0.056	1.3	127	<0.002	<0.01	0.09	11	<1	1.3	51.1	0.5	<0.05	10.6	0.303	0.23	3.4	84	1.3	7.2	10	150
MJ-4-4204	3.5	0.69	0.0467	0.58	3.93	3.6	18.3	0.057	1.3	36	<0.002	<0.01	0.23	5.4	1	1.2	75.1	0.33	<0.05	8.65	0.176	0.07	1.7	48	1.4	7.8	5	162
MJ-5-0885	0.5	1.96	0.0825	0.4	5.56	2.2	24.4	0.056	2.1	1.4	<0.002	<0.01	0.3	10.8	<1	0.4	87.4	0.2	<0.05	3.64	0.099	<0.02	3.6	37	1.6	10	6	159
MJ-5-1305	13	3.64	0.106	0.66	3.66	3.6	102.5	0.053	1.1	47.6	<0.002	<0.01	0.53	9.8	<1	1	96.9	0.24	<0.05	4.43	0.183	0.1	4.3	61	0.6	13.7	9	137.5
MJ-5-4690	3.1	0.57	0.102	1.11	0.36	0.3	9.8	0.007	1.8	12.8	<0.002	0.03	0.1	4.4	2	0.2	16	0.07	0.31	0.59	0.013	0.03	3.9	11	1.2	3.2	3	17.5
MJ-5-4880	2.3	0.9	0.0498	0.52	5.1	3.2	20.8	0.063	10.7	12.2	<0.002	0.26	0.27	8.4	3	1.2	75.3	0.26	0.09	8.58	0.139	0.03	14.6	53	9.1	8.7	23	179.5
MJ-5-4970	2.7	1.21	0.0556	0.37	4.71	2.3	27.2	0.057	1.2	18.6	<0.002	0.65	0.15	7.9	5	1	75.1	0.19	0.08	7.81	0.105	0.06	1.3	63	4.9	5.9	5	166
MJ-5-5286	4.4	0.65	0.0266	0.55	1.83	6.5	25.9	0.054	2.2	114	<0.002	0.31	0.19	10.9	3	2.9	32.7	0.33	0.65	10.35	0.241	0.17	3.1	83	7.3	9.2	5	153.5
MJ-6-1573	14.1	8	0.154	0.33	1.33	1.2	529	0.023	0.9	12.7	<0.002	0.06	0.67	37.3	1	0.6	169	0.09	<0.05	0.3	0.459	0.04	0.3	257	0.2	15	70	10.2
MJ-6-2532	19.2	3.22	0.0428	175.5	1.14	7	174.5	0.024	4.9	42.6	0.103	2.78	0.3	25.4	3	0.3	54.8	0.13	0.31	0.92	0.136	0.08	1.3	156	0.3	5.2	21	44.1
MJ-6-3218	0.7	0.71	0.0455	0.85	5.73	4	8.5	0.054	0.8	0.9	<0.002	0.01	0.15	1.6	<1	0.6	48.6	0.24	<0.05	2.5	0.081	<0.02	1.2	5	6	6	4	120
MJ-6-3374	5.8	1.05	0.0155	1.14	3.83	2.3	28	0.044	1	50.7	<0.002	0.01	0.1	6.7	<1	1.9	79.6	0.22	<0.05	5.12	0.151	0.12	1.4	63	0.9	3.7	7	140
MJ-6-4632	7.2	1.12	0.0392	0.5	1.8	5.8	36.3	0.045	0.8	127	<0.002	<0.01	0.13	10.4	<1	1.5	27.8	0.45	<0.05	7.49	0.262	0.15	1.3	96	1.7	5.1	5	122.5
MJ-6-4785	1	0.68	0.0452	0.57	4.86	1.8	12.3	0.035	0.9	3.7	<0.002	0.01	0.17	3	<1	0.4	45.5	0.13	0.06	1.42	0.058	0.03	0.7	22	2.1	3.4	4	72.6
MJ-6-5676	4.8	1.13	0.0099	0.6	3.43	2.5	33.6	0.017	0.9	57.5	<0.002	0.01	0.06	5.9	1	0.8	46	0.18	<0.05	2.29	0.102	0.11	1.9	56	1.3	2	5	68.4
MJ-6-6468	1.6	0.87	0.0252	1.2	4.65	1.3	26.4	0.019	1	12.9	<0.002	0.01	0.09	3.8	<1	0.4	70.5	0.07	<0.05	2.21	0.059	0.03	0.9	43	2	2.8	3	72.8
MJ-7-2947	2	0.49	0.0161	1.03	4.5	1.1	73.9	0.029	1.7	13.2	<0.002	3.16	0.11	4.3	50	0.9	54.9	0.1	0.4	4.08	0.067	<0.02	1.4	39	1.9	4.5	9	121
MJ-7-3018	1.6	0.46	0.0128	0.48	4.89	3.2	15.8	0.029	1.5	14.2	<0.002	0.01	0.12	3.8	<1	1.1	63.1	0.11	<0.05	3.59	0.076	0.04	2.3	35	3.8	3.1	4	80.5
MJ-9-2683	5.5	0.89	0.0203	0.56	4.77	2.9	37.1	0.054	1.1	34.5	<0.002	0.01	0.19	8.2	<1	2	64.2	0.21	0.06	5.92	0.184	0.12	1.8	71	3.4	7.5	7	150
MJ-9-3495	7.5	3.13	0.142	0.43	2.59	3.4	61.1	0.048	1	92.6	<0.002	<0.01	0.06	8.4	<1	1.2	62.8	0.33	<0.05	8.15	0.234	0.24	2.5	70	1.6	8.4	7	141
MJ-9-4130	3.6	4.31	0.463	1.16	1.13	3.8	45.4	0.019	1.7	13.6	<0.002	0.01	0.1	9.5	1	0.6	40.1	<0.05	0.57	1.89	0.035	0.04	5.5	74	2.3	16.9	6	24.7
MJ-9-5087	4.9	0.29	0.0066	1.71	3.23	2	133.5	0.015	57.7	12	0.002	7.82	0.13	2.8	20	0.5	29.5	0.09	3.8	1.45	0.031	0.03	0.9	118	1.2	5.1	9	58.1
MJ-9-6093	2.2	0.28	0.0084	0.64	3.5	2.9	9.9	0.018	7.6	42.6	<0.002	0.02	0.15	5.7	<1	1.1	43.1	0.17	<0.05	3	0.109	0.06	1.2	66	1.2	3.6	7	107.5
MJ-9-6450	20.5	7.05	0.0862	2.68	1.01	11.8	652	0.025	2.8	81.8	0.006	0.01	0.27	28.3	1	1.2	65.8	0.06	0.05	0.42	0.265	0.16	15.4	224	0.7	10.5	9	48.9

3. Photographs of Outokumpu drill core samples.

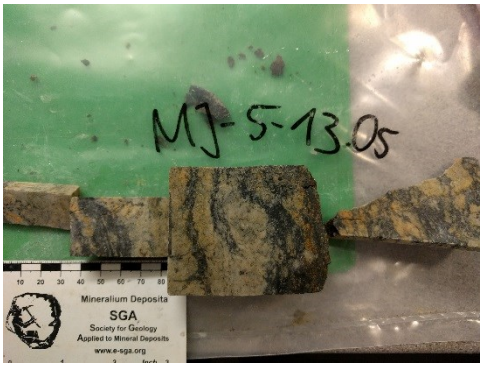


MJ-5-49.70
Mineralium Deposita


MJ-5-52.86
Mineralium Deposita


MJ-6 15.73
Mineralium Deposita
SGA
Society for Geology
Applied to Mineral Deposits


MJ-6-25.32
Mineralium Deposita
SGA
Society for Geology


MJ-6-32.18
Mineralium Deposita


MJ-6-3374


MJ-6-46.32
Mineralium Deposita


MJ-6-47.85


MJ-6-56.76


MJ-6-64.68
Mineralium Deposita


MJ-7-29.47
SGA
Society for Geology


Mineralium Deposita
SGA
Society for Geology
Applied to Mineral Deposits
www.e-sga.org
MJ-7-30.18


MJ-9
26.83


MJ-9 34.95
Mineralium Deposita


MJ-9 41.30
Mineralium Deposita


MJ-9 50.87
Mineralium Deposita
SGA


MJ-9 60.93
Mineralium Deposita


MJ-9 64.50